

Model-based design and operation of fuel cell systems

by

Sheila Mae Constantino Ang

A thesis submitted for the degree of Doctor of Philosophy of the University College London



Department of Chemical Engineering
University College London (UCL)
Torrington Place, London, WC1E 7JE, United Kingdom

I, Sheila Mae C. Ang, confirm that the work presented in this thesis is my own. Where information has been derived from other sources, I confirm that this has been indicated in the thesis.

Signature

Date

Acknowledgements

I would like to thank my supervisor, Dr. Dan Brett, for his guidance, advice and support. I cannot wish for a more insightful and friendlier supervisor.

I would also like to acknowledge the Philippine Department of Science and Technology for the scholarship.

Thanks to all of my friends in CAPE room and CCT office.

And finally, thanks to my parents, my sister Guen, and friends (especially to Nouri, Andrea, Georgette, Jacques, Ana, Matt, Mohammed, Jennifer and Sebastian) for support, love and encouragement throughout the course of my studies.

Abstract

Fuel cells are a promising technology for the production of electricity from hydrogen or other fuels with high efficiency and low emissions. They are suitable for stationary, transportation and portable applications. However, they are still more expensive than existing technologies and there are technical challenges that need to be overcome for their commercialisation. Therefore, accurate and efficient design methodologies for fuel cell systems design are becoming increasingly important.

Modelling and optimisation present a great potential to inform fuel cell systems design, which often results in savings in design cycle time and cost, and better design and operation. The purpose of this thesis is to investigate the applicability of model-based design approaches to fuel cell systems design when applied to a single-cell fuel cell, then a fuel cell stack and, ultimately, a system-level fuel cell system, such as a micro-cogeneration plant.

The development of mathematical models for a single-cell fuel cell, a stack and a micro-cogeneration system is presented in detail. The use of these models in model-based design is then illustrated. For instance, the effectiveness of a conventional humidification design is examined using the single-cell fuel cell model. The fuel cell stack model is used within a multi-objective optimisation framework to investigate how size trades for efficiency. Finally, the micro-cogeneration plant model is used to investigate the trade-off between fuel consumption and electrical power output, compare different micro-cogeneration operating strategies and examine the interaction between operating strategies and electricity network. Overall, when properly formulated and validated, modelling and optimisation are useful tools in fuel cell systems design as they provide means by which engineers can obtain valuable information about the behaviour of the system, make informed decisions, generate different design alternatives and identify good designs even before a prototype is fabricated.

Publications and presentations

Book chapter

S.M.C. Ang, D.J.L. Brett, E.S. Fraga (2011). Optimal design of fuel cell systems. Chapter in Fuel Cell Efficiency, Edited by A.E. Johnson and E.C. Williams, Nova Science Publishers, New York. ISBN: 978-1612096193

Journal articles

S.M.C. Ang, D.J.L. Brett, E.S. Fraga (2010). A multi-objective optimisation model for a general PEM fuel cell system. Journal of Power Sources 195, 2754-2763. ISSN: 03978-7753.

S.M.C. Ang, E.S. Fraga, N.P. Brandon, N.J. Samsatli and D.J.L. Brett (2011). Fuel cell systems optimisation - methods and strategies. International Journal of Hydrogen Energy 36, 22, 14678-14703. ISSN: 0360-3199.

S.M.C. Ang, D.J.L. Brett, I. Staffell, A.D. Hawkes, E.S. Fraga, N.J. Samsatli and N.P. Brandon (2012). Design of fuel cell micro-cogeneration systems through modelling and optimisation. Wiley Interdisciplinary Reviews Energy and Environment. Accepted.

S.M.C. Ang, D.J.L. Brett, E.S. Fraga (2010), A model for the multi-objective optimisation of a polymer electrolyte fuel cell micro-combined heat and power system, in S. Pierucci and G. Buzzi Ferraris (editors), Computer-Aided Chemical Engineering (Elsevier).

Research award

Runner-up, UCL Graduate School Research Poster Competition 2010 for the poster "Turning homes into power stations: optimal design of fuel cell micro-combined heat and power systems." URL: <http://www.grad.ucl.ac.uk/comp/2009-2010/poster/>

Conference refereed

S.M.C. Ang, D.J.L Brett, E.S. Fraga (2010), A model for the multi-objective optimisation of a polymer electrolyte fuel cell micro-combined heat and power system. ESCAPE 20.

Conference unrefereed

S.M.C. Ang, D.J.L Brett, E.S. Fraga. Optimal design of fuel cell systems. Postgraduate Symposium in Electrochemistry 2011.

S.M.C. Ang, D.J.L Brett, E.S. Fraga. Optimal design of a fuel cell micro-cogeneration plant. Supergen Fuel Cell Meeting 2011.

S.M.C. Ang, D.J.L Brett, E.S. Fraga. Turning homes into power stations: optimal design of fuel cell micro-combined heat and power systems. UKERC Annual Assembly and Summer School 2010.

S.M.C. Ang, D.J.L Brett, E.S. Fraga. Turning homes into power stations: optimal design of fuel cell micro-combined heat and power systems. CAPE PhD Poster Day 2010.

S.M.C. Ang, D.J.L Brett, E.S. Fraga. A model for the multi-objective optimisation of polymer electrolyte fuel cell systems. Electrochem 2009.

S.M.C. Ang, D.J.L Brett, E.S. Fraga. Multi-objective optimisation of a polymer electrolyte fuel cell micro-combined heat and power (PEFC/ μ CHP) system. CPSE Industrial Consortium 2009.

Contents

1	Introduction	23
1.1	Motivation for work	26
1.2	Thesis outline	26
2	Overview of fuel cell systems	30
2.1	Fuel cell basics	30
2.2	Fuel cell operation	34
2.3	Water and thermal management in PEFC	36
2.4	Fuel cell systems	39
2.4.1	Fuel cell stack	39
2.4.2	Fuel supply	41
2.4.3	Oxidant supply	42
2.4.4	Heat and water management	42
2.4.5	Power conditioning	43
2.4.6	Instrumentation and controls	43
2.4.7	Hybrid components	44
2.5	Fuel cell applications	44
2.5.1	Portable sector	45

2.5.2	Transportation market	46
2.5.3	Stationary sector	46
2.6	Conclusions	47
3	Fuel cell systems design	48
3.1	Fuel cell system design process	48
3.2	Requirements and objectives for design	52
3.3	Fuel cell modelling	57
3.3.1	Characteristics of fuel cell models	58
3.3.1.1	System boundary	58
3.3.1.2	Approach	59
3.3.1.3	State	60
3.3.1.4	Spatial dimension	61
3.3.1.5	Complexity/detail	62
3.4	Earlier reviews in fuel cell modelling	62
3.5	Review of fuel cell system modelling	63
3.5.1	Modelling of portable fuel cell systems	65
3.5.1.1	Portable DMFC systems	67
3.5.1.2	Portable SOFC systems	67
3.5.1.3	Portable hybrid systems	68
3.5.2	Modelling of transportation fuel cell systems	68
3.5.2.1	Fuel cell electric vehicles	69
3.5.2.2	Fuel cell hybrid vehicles	70
3.5.2.3	Fuel cell auxiliary power units	72

3.5.3	Modelling of stationary fuel cell systems	73
3.5.3.1	SOFC-based cogeneration plant	74
3.5.3.2	SOFC-gas turbine hybrid cogeneration plant	75
3.5.3.3	PEFC-based cogeneration plant	76
3.5.3.4	PEFC-gas turbine hybrid cogeneration plant	77
3.5.3.5	Other hybrid cogeneration plant based on PEFC	77
3.5.3.6	Cogeneration plant based on other types of fuel cell	78
3.6	System optimisation	78
3.7	Parametric study	85
3.8	Single-objective optimisation	86
3.8.1	Cost optimisation	87
3.8.2	System efficiency optimisation	89
3.9	Multi-objective optimisation	90
3.9.1	Methods	91
3.9.1.1	Generating methods	93
3.9.1.2	Preference-based methods	93
3.9.2	Multi-objective optimisation in fuel cell systems design	96
3.9.2.1	Bi-objective optimal design	96
3.9.2.2	Tri-objective optimal design	97
3.10	Conclusions	98
4	Modelling of a PEFC	100
4.1	Model Description	100
4.2	Assumptions	101

4.3	Governing equations	103
4.3.1	Mass Balance	103
4.3.2	Energy balance	107
4.3.3	Electrochemistry	107
4.4	Numerical method	110
4.5	Model simulation	112
4.6	Conclusions	116
5	Optimal design of a fuel cell stack	118
5.1	Introduction	118
5.2	Model formulation	121
5.2.1	Mass balances	123
5.2.2	Electrochemistry	125
5.2.3	System efficiency	126
5.2.4	Model validation	128
5.3	Case study: Trade-off between efficiency and size of stack	131
5.3.1	Multi-objective optimisation	131
5.3.2	Results and discussion	133
5.4	Conclusions	142
6	Introduction to the design of a fuel cell micro-cogeneration plant	144
6.1	Introduction	144
6.2	Micro-cogeneration	145
6.3	Classification	147
6.4	Technologies	148

6.5	Literature survey on micro-cogeneration	149
6.6	Criteria for the design of a micro-cogeneration plant	152
6.6.1	Size	152
6.6.2	Conversion efficiency	154
6.6.3	Heat-to-power ratio	155
6.6.4	Transient response	155
6.6.5	Reliability / availability / lifetime	156
6.7	Conclusions	156
7	Optimal design of a fuel cell micro-cogeneration plant	158
7.1	System description	159
7.2	Fuel processing subsystem	160
7.2.1	Fuel, air and water supplies	161
7.2.2	Steam reforming	162
7.2.3	Water gas shift	164
7.2.4	Preferential oxidation	165
7.2.5	Further fuel processing	167
7.3	Fuel cell subsystem	168
7.4	Thermal management subsystem	169
7.4.1	Afterburner	170
7.4.2	Phase change heat exchanger	171
7.4.3	Heat storage	172
7.5	Power management subsystem	173
7.6	System efficiencies	174

7.7	Case study: Trade-off between power output and fuel consumption of a fuel cell micro-cogeneration plant	177
7.7.1	Multi-objective optimisation	178
7.8	Results and discussion	179
7.9	Conclusions	181
8	Model application: investigation of the effectiveness of different fuel cell micro-cogeneration operating strategies	183
8.1	Energy demands	184
8.2	Transient demand characteristics of an individual dwelling	186
8.3	Operating modes	192
8.4	Network interaction	194
8.5	Impact on operational economics	200
8.6	Implications of energy demand variation	204
8.7	Conclusions	205
9	Conclusions and further work	207
9.1	Conclusions	207
9.2	Future directions	210

List of Figures

2.1	Illustration of fuel cell operation taking the hydrogen fuelled polymer electrolyte fuel cell as an example.	32
2.2	Illustration of the operating range of a fuel cell, showing the stack voltage, power, electrical efficiency and thermal efficiency.	36
2.3	Example of a fuel cell system for micro-cogeneration application showing the different equipment and interconnections.	40
2.4	Typical fuel cell applications for different fuel cell types.	45
3.1	A typical fuel cell system design process.	51
3.2	Summary and characterisation of fuel cell system models	65
3.3	Classification of multi-objective optimisation methods.	92
4.1	Schematic of the region considered in modelling.	102
4.2	Flowchart for the determination of the model solution.	112
4.3	Water and temperature profiles along the flow channels.	115
4.4	Partial pressures of oxygen and hydrogen along the flow channels.	116
4.5	Current distribution along the flow channels.	116
5.1	A general hydrogen-air PEFC system with a single-cell stack.	122

5.2	Simulation of the system for a base case: polarisation curve, power density, and system efficiency with respect to the current density at various operating pressures.	130
5.3	Pareto set at stack power output of 50 kW.	134
5.4	Comparison of the Pareto sets at different stack power outputs.	138
5.5	Optimal values of design objectives.	139
5.6	Optimal values of design variables.	140
5.7	Optimal values of the operating pressure with the upper bound increased to 10 atm.	141
5.8	Comparison of the Pareto sets at different stack power outputs with the upper bound on the pressure increased to 10 atm.	142
6.1	Efficiency of a centralised power generation and delivery.	145
6.2	The micro-cogeneration concept showing the import/export of electricity.	146
6.3	Energy consumption in the UK by end user 2000 to 2008.	147
6.4	Different micro-cogeneration technologies.	149
6.5	Illustration of a typical electrical and heat load for a UK dwelling.	154
7.1	Schematic of a fuel cell micro-cogeneration system.	159
7.2	Pareto set showing the trade-offs between net electrical power output and fuel consumption.	179
7.3	Values of the overall efficiency.	180
7.4	Values of electrical and thermal efficiencies.	181
8.1	Trends in the daily and 30-day rolling average heat and power demands for a single house from January and December.	187
8.2	The daily thermal vs. electrical demand values.	188

8.3	The daily electrical demand profile employed for simulation purposes.	189
8.4	Example of applying the considered operating strategies for a micro-cogeneration system to a daily electrical demand profile.	194
8.5	The import and export profiles for the considered operating strategies.	197
8.6	The heat profiles for the considered operating strategies.	199

List of Tables

2.1	Basic PEFC components.	34
2.2	Comparison of fuel cell with other power sources.	45
3.1	Characteristics of fuel cell models	58
3.2	Summary of optimisation studies performed on fuel cell systems.	80
3.3	Main features, merits and limitations of multi-objective optimisation methods.	95
4.1	Summary of the governing equations for the PEFC model.	108
4.2	Parametric constants used in the model.	113
5.1	Parametric constants in the model	127
5.2	Expressions for the physical parameters in the model	129
5.3	Comparison of the representative solutions in the Pareto set.	135
7.1	Heat capacities of gases.	175
7.2	Parametric constants in the PEFC micro-cogeneration system model.	176
8.1	General influences of transient heat and power demand variations upon the design of micro-cogeneration systems.	191
8.2	The electricity generation and utilisation characteristics of some micro-cogeneration operating modes.	196

8.3	The heat generation and utilisation characteristics of the considered micro-cogeneration operating modes.	201
8.4	Operating costs and carbon savings potential for different micro-cogeneration operating strategies.	203
8.5	Summary table for the comparison of the three considered operating strategies.	204

Nomenclature

A	Total active area of the MEA , cm^2
a	Heat transfer area per unit length, cm
a_k	Activity of water in stream k
$C_{p,i}$	Heat capacity of gas i , J (mol K)^{-1}
$C_{p,w}^l$	Heat capacity of liquid water, J (mol K)^{-1}
$C_{p,w}^v$	Heat capacity of water vapour, J (mol K)^{-1}
c_p	Specific heat constant of air, $\text{J K}^{-1}\text{kg}^{-1}$
c_w	Concentration of water in the membrane, mol cm^{-3}
$c_{w,k}$	Concentration of water at k interface of the membrane, mol cm^{-3}
D°	A parameter used in the expression for diffusion coefficient of water, $\text{cm}^2 \text{s}^{-1}$
D_w	Diffusion coefficient of water in the membrane, $\text{cm}^2 \text{s}^{-1}$
d	Channel height, cm
F	Faraday's constant, 96487 C eq^{-1}
f	Fraction of liquid water in the channel
$H_{w,k}^l$	Enthalpy of liquid water in k stream, J mol^{-1}
$H_{w,k}^v$	Enthalpy of water vapour in k stream, J mol^{-1}
h	Channel width, cm
I	Current density, A cm^{-2}
I°	Exchange current density for the oxygen reaction, A cm^{-2}
I_L	Limiting current density, A cm^{-2}

k_c	Evaporation and condensation rate constant, s^{-1}
K_p	Equilibrium constant for water gas shift reaction
L	Channel length, cm
LHV	Lower heating value of hydrogen, $2.4 \times 10^5 \text{ J mol}^{-1}$
M	Molar flow rate, mol s^{-1}
M_i	Molar flow rate of species i , mol s^{-1}
$M_{m,dry}$	Equivalent weight of a dry membrane, g mol^{-1}
$M_{w,k}^l$	Molar flow rate of liquid water in k channel, mol s^{-1}
$M_{w,k}^v$	Molar flow rate of water vapour in k channel, mol s^{-1}
m_{air}	Mass flow rate of air, kg s^{-1}
$N_{i,y,k}$	y -component of molar flux of species i in k channel, $\text{mol (s cm}^2)^{-1}$
$N_{w,y,k}^v$	y -component of molar flux of water vapour in k channel, $\text{mol (s cm}^2)^{-1}$
n_{cell}	Number of cells in a stack
n_d	Electro-osmotic drag coefficient (number of water molecules carried per proton)
P	System total pressure, atm
P_i	Partial pressure of component i , atm
P_{in}	Inlet air pressure to the compressor
$P_{w,k}^{sat}$	Vapour pressure of water in k channel, atm
p	Parameter for extent of steam reforming reaction
Q	Heat flow rate (J s^{-1})
q	Parameter for extent of steam reforming reaction
R	Gas constant, $8.314 \text{ J mol}^{-1} \text{ K}^{-1}$ or $82.057 \text{ cm}^3 \text{ atm mol}^{-1} \text{ K}^{-1}$
RH	Relative humidity
T	Temperature, K
T_a	Temperature of the anode stream, K
T_c	Temperature of the cathode stream, K
T_e	Entry air temperature, K
T_{ref}	Reference temperature (298 K)

T_s	Temperature of the solid phase, K
t_m	Thickness of the membrane, cm
U	Overall heat-transfer coefficient, J (s cm ² K)
V	Voltage, V
V_{oc}	Reversible/open-circuit cell voltage, V
V_{cell}	Effective cell voltage, V
W	Electrical power (W)
w	Parameter for extent of steam reforming reaction
x	Parameter for extent of steam reforming reaction
$x_{w,k}$	Mole fraction of water in k stream
y	Mole fraction of water vapour
z	Weighted sum of the objectives
z_i	A single objective

Greek symbols

α	Net water molecules per proton flux ratio
β	Amplification constant $\left(V (\text{cm}^2 \text{A}^{-1})^k \right)$
ΔH_{vap}	Enthalpy of water evaporation (J mol ⁻¹)
Δh_{rxn}	Enthalpy of reaction (J mol ⁻¹)
ξ	Extent of reaction (mol s ⁻¹)
η	System efficiency, %
η_c	Compressor connecting efficiency
η_{mt}	Motor efficiency
λ	Stoichiometric ratio
$\lambda_{\text{S/C}}$	Steam to carbon ratio
θ	Theoretical oxygen (mol s ⁻¹)
$\rho_{\text{m,dry}}$	Dry membrane density, g cm ⁻³
σ_m	Membrane conductivity, $\Omega^{-1} \text{cm}^{-1}$

χ	Excess air
ω	Weighting factor

Subscript

a	Anode
burn	Afterburner
CH ₄	Methane
CO	Carbon monoxide
CO ₂	Carbon dioxide
c	Cathode
comp	Compressor
del	Delivered (net)
H ₂	Hydrogen
hex	Heat exchanger
hs	Heat storage
hum	Humidifier
in	Inlet
inv	DC/AC inverter
k	Anode or cathode
m	Membrane
mt	Motor
N ₂	Nitrogen
O ₂	Oxygen
oc	Open circuit
out	Outlet
prox	Preferential oxidation reactor
prs	Parasitic
pump	Water pump

rec	Recovered
sr	Steam reformer
stack	Fuel cell stack
w	Water
wgs	Water gas shift reactor
x	Direction along the channel length, cm
y	y-direction
sat	Saturated
0	Initial condition

Superscript

k	Dimensionless power in the amplification term
l	Liquid
sat	Saturated
v	Vapour

Chapter 1

Introduction

Fuel cell systems are being developed for a wide variety of power generation applications. They have been demonstrated for transportation applications such as automobiles, buses, utility vehicles, scooters and bicycles. They are used for distributed power generation at a level of home, building, or community, in which case both power and heat generated by the fuel cells are utilised. They are also employed for portable applications, either as backup power generators or substitutes for batteries in various electronic devices and gadgets.

Fuel cells, however, are still more expensive than existing technologies. In addition, there are many challenges, technical and non-technical, that need to be overcome. The major technical issues include the following:

1. reduction in costs in all aspects of fuel cell production, materials, systems and applications as well as other components,
2. demonstration of fuel cell durability, reliability and availability,
3. choice and cost of fuel, and
4. improvement in performance.

The following non-technical issues also have to be addressed:

1. assessment of external costs (*e.g.*, disposal cost, impact on environment, safety and health, *etc.*)
2. socio-economic consequences of introducing new fuel cell technologies,
3. identification of barriers to commercial fuel cell development, and
4. availability of investment and venture capital to provide new fuel infrastructure and production facilities.

These are just few of the reasons why research and development on fuel cell systems are indispensable. Previous research efforts have successfully addressed some of the issues and barriers to fuel cell commercialisation, but more research is necessary to answer the remaining ones and produce fuel cell systems that are competitive enough to be commercialised.

This thesis illustrates the use of modelling and optimisation for fuel cell systems design by providing useful tools by which to effectively investigate, and ultimately overcome, some of the important technical issues.

Fuel cell systems design can be viewed as a decision-making process which involves identification of possible design alternatives and selection of the most suitable one. A good design represents a compromise of different requirements, also referred to as objectives or criteria. These objectives may include efficiency, size, fuel consumption, power output, durability, emissions, capital cost/investment, operating cost, savings, payback period, amongst others. A subset of these will be relevant for a particular application.

The use of modelling and optimisation in fuel cell systems design has received increasing interest. This has been motivated by the increased computational resources and the availability of new and effective methods for solving numerical problems. A mathematical model, which describes certain aspects of a fuel cell system and predicts its behaviour, may be a set of equations, algebraic or differential, or a computer-based

procedure or subroutine. This model may contain many alternative designs, thus criteria or objectives for comparing these alternatives must be included in the model. The model can be coupled with a numerical optimisation algorithm to generate better designs iteratively. A benefit of using this approach is a good design can be obtained with little or no need for physical fuel cell system prototype. This often leads to substantial savings in cost and design cycle time as well as better design and operation. However, an optimal design solution is only useful within the limitations of the model assumptions. The quality of an optimal design mainly depends on how well the model has been formulated. Many details are neglected because of modelling difficulties.

The contributions of this thesis include the following:

1. provides a comprehensive review of important techniques and applications of modelling and optimisation in fuel cell systems design,
2. examines the relative merits of existing fuel cell models,
3. identifies existing models for portable, stationary and transportation applications,
4. characterises existing models according to approach, state, system boundary, spatial dimension, and complexity or detail,
5. summarises model-based design approaches relevant to fuel cell systems design, such as parametric study, single-objective optimisation and multi-objective optimisation,
6. explores important criteria crucial for the design of a fuel cell system,
7. presents a two-dimensional, non-isothermal, multi-phase mass and heat transfer model of a single-cell PEFC and illustrates the use of the model to evaluate the effectiveness of a conventional humidification design,
8. extends the single-cell model to a fuel cell stack and subsequently use the fuel cell stack model within a multi-objective optimisation framework to investigate the trade-off between efficiency and size,

9. develops a system-level model for a PEFC micro-cogeneration system by combining the fuel cell stack model with the model for fuel processing subsystem, thermal management subsystem and power management subsystem, and
10. demonstrates the use of the fuel cell micro-cogeneration model to investigate the trade-off between fuel consumption and electrical power output, evaluate the effectiveness of different operating strategies, examine the interaction between different operating strategies and the electricity network, obtain estimates of the daily savings, size of the thermal store, efficiencies (electrical, thermal and overall), heat-to-power ratio, amongst others.

1.1 Motivation for work

There is a great opportunity for modelling and optimisation to be used to inform system design. One clear motivation for this work is to make use of the available and suitable techniques in order to obtain accurate and detailed designs based on representative models of the components of a fuel cell system and their interactions. If successful, this approach could result in significant savings by reducing the need for experiments and extended pilot plant trials. If the design methodology is accurate enough one could obtain designs that may be uncommon and unexpected with greater performance over traditional designs. Certainly, some improvement can be expected by optimising the design and operation of fuel cell systems. There are also advantages to be gained by improving the speed of the design process.

1.2 Thesis outline

Chapter 2 For the reader who is not familiar with fuel cells and fuel cell systems, an overview of the fundamental principles of fuel cells and fuel cell systems is provided. Here, the basics of a fuel cell, its operation, and water and thermal

management are discussed. The fuel cell stack is the heart of a fuel cell system but a significant amount of auxiliary components are needed for the fuel cell to function as a complete system. Thus, this chapter devotes a section for the discussion of the different equipment and interconnections found in a fuel cell system. The last section explores the different applications of fuel cell systems in the portable, transportation and stationary sectors.

Chapter 3 This chapter examines the role of modelling and optimisation in the design of fuel cell systems. It considers a typical fuel cell system design process and discusses how modelling and optimisation are used to generate different design alternatives and identify good designs. Prior to the design, a clear understanding of the requirements and objectives is crucial. Thus, some examples of application-specific criteria and design variations amongst applications are discussed. This chapter also presents a literature review of fuel cell system modelling. The existing models in the literature are categorised by approach, state, system boundary, spatial dimension, and complexity or detail. The remaining sections in this chapter deal with the different model-based design approaches, such as parametric study, single-objective optimisation and multi-objective optimisation, relevant to fuel cell systems design.

Chapter 4 For the rest of this thesis, the focus is on modelling of fuel cells; several examples on how these models can be used to obtain valuable system information, make informed predictions, and improve the design and operation of the system are presented. This chapter presents a model for a single-cell PEFC, which is a two-dimensional, nonisothermal, multi-phase mass and heat transfer model. The model is described and the assumptions in modelling are considered. The detailed formulation of the governing equations (*i.e.*, the mass balance, energy balance and electrochemical equations) and the numerical method used to solve the model are then discussed. For a PEFC, proper water and heat management is crucial for achieving a high power density and high energy efficiency performance.

Thus, an example that demonstrates the use of the model in obtaining important information about an appropriate approach to water and heat management is presented.

Chapter 5 The model for a single-cell PEFC presented in Chapter 4 is extended to a fuel cell stack, and in this chapter an optimisation model for a PEFC stack suitable for multi-objective optimisation is presented. In principle, the design of fuel cell systems inherently involves simultaneous optimisation of two or more conflicting objectives. Achieving an optimum for one objective often requires a compromise on two or more other objectives. For example, in the design of a fuel cell stack, there is a trade-off between efficiency and size, *i.e.*, a more efficient stack is bigger and vice versa. Information about the trade-off between these two objectives can inform design engineers in making their design decisions rationally and quantitatively. For example, in the current consumer demographic size and portability may be the deciding factors for mobile users, whereas other users may value operating costs more than portability.

Chapter 6 Micro-cogeneration is one of the early entry points of fuel cell technology into the commercial market. Fuel cells are promising for residential micro-cogeneration because of their high electrical efficiency, low emissions and low heat-to-power ratio that is well suited for residential applications. This chapter serves as an introduction to the modelling and optimisation of fuel micro-cogeneration system, which is the focus of the remaining chapters in this thesis. It discusses the context for interest in fuel cell micro-cogeneration systems, the classification and the technologies. It also reviews the current state of the art of the technology. Finally, this chapter examines the important criteria relevant to micro-cogeneration system design.

Chapter 7 This chapter presents a system-level mathematical model for a PEFC micro-cogeneration system. The fuel cell stack model developed in Chapter 5

is combined with the mathematical models for subsystems for fuel processing, thermal management and power management in such a way that the system will function as a residential heat and power generator. Similar to the design problem encountered in Chapter 5, the design of micro-cogeneration systems naturally involves conflicting objectives. For example, there is a trade-off between the net electrical power output and the fuel consumption at a given thermal power rating; both of these objectives are crucial in assessing the economic benefits of the technology. The last section of this chapter presents a case study that illustrates the use of the fuel cell micro-cogeneration model in generating different design alternatives that trade off fuel consumption for electrical power output.

Chapter 8 This chapter gives further examples of the application of the fuel cell micro-cogeneration model developed in Chapter 7 in informing system design and operation. The model can provide design engineers information about the relative benefits of three of the various operating strategies: constant-output mode, restricted-running time mode and continuous-output mode. Choosing an appropriate operating strategy depends on the energy consumption pattern of a household, and so this chapter explores the key characteristics of the electrical and thermal demands of UK dwellings. This chapter also considers the interaction between the considered operating strategies and the electricity network.

Chapter 9 In this last chapter, a summary of the work carried out in this thesis and the conclusions drawn from the results of the example problems are presented. In the last section, some of the areas for future work are explored.

Chapter 2

Overview of fuel cell systems

Fuel cell systems are a promising technology for a wide range of power generation applications. They have been, and are being developed for portable, transportation and stationary applications. However, fuel cells are still more expensive than the existing technologies and there are technical challenges that need to be overcome for their commercialisation.

There is a great opportunity for modelling and optimisation to be used to inform system design, which often results in savings in design cycle time and cost, and better design and operation. Modelling and optimisation require understanding of the system, and so this chapter discusses the basic principles of fuel cells and fuel cell systems.

2.1 Fuel cell basics

Fuel cells are electrochemical devices that convert the chemical energy of a fuel directly into electricity (and heat) without involving the process of combustion. A simplistic view of a fuel cell is that it is a cross between a battery (chemical energy converted directly into electrical energy) and a heat engine (a continuously fuelled air breathing device); this is why fuel cells are sometimes referred to as electrochemical engines. There are a number of fuel cell technologies with very different designs, each suited to

different applications. However, they all share the characteristics of high efficiency, no moving parts, quiet operation, and low or zero emissions at the point of use. In addition, modular stack design means that there are no technical limitations on minimum capacity, which is a problem for mechanical heat engines.

Several types of fuel cells are under development. The classification is primarily by the kind of electrolyte [1], which determines the chemical reaction that takes place in the cell, the catalyst required, the operating temperature range, and the fuel required. Among the most promising types are alkaline fuel cells (AFC), proton exchange membrane fuel cells (PEFC), molten carbonate fuel cells (MCFC) and solid oxide fuel cells. Although the optimal design approach discussed in this thesis may be applicable to all fuel cell types, this thesis specifically considers the optimal design of PEFC systems. For certain applications, the PEFC is favoured over other types of fuel cell for the following reasons: their high power density means they are lighter and smaller compared to other fuel cells, low operating temperature allows fast start-up and immediate response in power demand, and use of a solid polymer simplifies assembly and handling [1]. All the hydrogen fuelled buses and cars on the market by major companies are powered by PEFC and 90% of fuel cell research and development work involves the PEFC [2].

A PEFC consists of a negatively charged electrode (anode), a positively charged electrode (cathode), and a polymer electrolyte membrane made of persulfonic acid groups with a Teflon backbone. Both the anode and cathode contain a catalyst to speed up the electrochemical processes, as shown in Figure 2.1. Hydrogen fuel is channeled to the anode wherein the catalyst separates the hydrogen's negatively charged electrons from the positively charged protons. The membrane allows the positively charged protons to pass through the cathode, but not the negatively charged electrons. The electrons must flow around the membrane through an external circuit. This flows of electrons forms an electric current. At the cathode, the negatively charged electrons and positively charged hydrogen ions (protons) combine with oxygen to form water and heat.

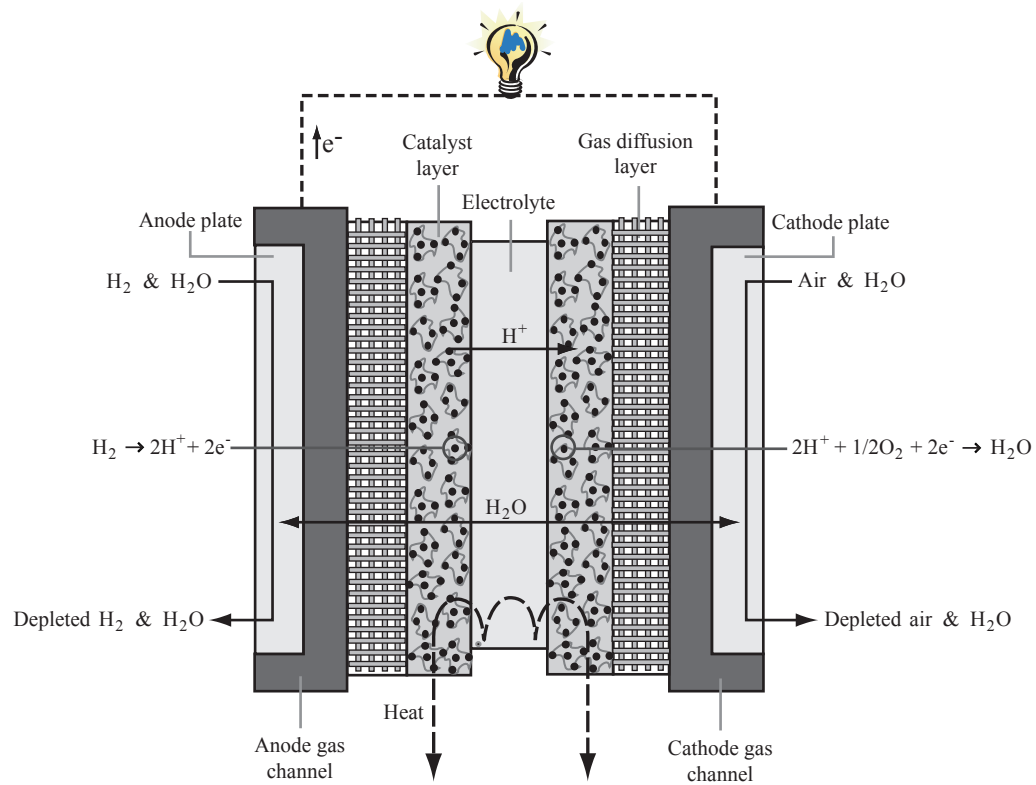
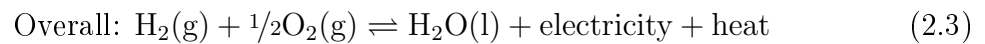
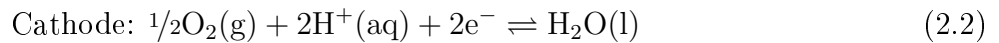


Figure 2.1: Illustration of fuel cell operation taking the hydrogen fuelled polymer electrolyte fuel cell (PEFC) as an example.

A typical PEFC has the following reactions:



A fuel cell produces power as long as the reactants – fuel and oxidant – are supplied. In theory, any substance that is capable of chemical oxidation can be used as fuel for the anode of a fuel cell. Hydrogen is the main choice for most applications because it is highly reactive with a suitable catalyst, can be produced from wide range of energy sources, and is high in energy density. Conversely, any substance that can be reduced can be used as oxidant. Oxygen is most commonly used for this purpose because it is economically available in air. The reactants are transported by diffusion and/or

convection to the catalysed electrode surfaces where the electrochemical reactions take place. The water and waste heat generated by the fuel cell must be continuously removed and may present critical issues for PEFCs.

The amount of power produced by a fuel cell depends on several factors, including the type of fuel cell, the fuel used, the cell size, the temperature and pressure at which it operates, *etc.* The current output is proportional to the active area of the individual cells, and the voltage is proportional to the number of cells connected together. As with solar photovoltaic cells and batteries, a single fuel cell produces voltage barely enough for even the smallest applications (< 1 V), so individual cells are connected in series to form a *stack*. A basic PEFC stack consists of a proton exchange membrane (PEM), catalyst and gas diffusion layers, flow field plates, gaskets and end plates as shown in Table 2.1. The actual fuel cell layers are the PEM, gas diffusion and catalyst layers. These layers are "sandwiched" together using various processes, and are collectively referred to as the membrane electrode assembly (MEA). A stack with many cells has MEAs sandwiched between bipolar flow field plates and only one set of end plates.

Table 2.1: Basic PEFC components.

Component	Purpose	Common types
Proton exchange membrane	Enables hydrogen protons to travel from the anode to the cathode	Persulfonic acid membrane (Nafion 112, 115, 117)
Catalyst layers	Breaks the fuel into protons and electrons. The protons combine with the oxidant to form water at the fuel cell cathode. The electrons travel to the load.	Platinum/carbon catalyst
Gas diffusion layers	Allow fuel/oxidant to travel through the porous layer, whilst collecting electrons	Carbon cloth or Toray paper
Flow field plates	Distributes the fuel and oxidant to the gas diffusion layer	Graphite, stainless steel
Gaskets	Prevent fuel leakage, and helps to distribute pressure evenly	Silicon, Teflon
End plates	Holds stack layers in place	Stainless steel, polyethylene, PVC

2.2 Fuel cell operation

Figure 2.2(a) illustrates the voltage and power *vs.* current curve for a generic fuel cell. An increase in current density (current per unit area of each cell) results in a decrease in operating voltage due to internal losses in the system. Power output initially increases and reaches a maximum at point 'D'. After which, the decreasing voltage and increasing losses in the system results in loss of electrical power output, although the heat generated continues to increase. The nominal operating point is around point 'C', which is typically $2/3$ to $3/4$ of the open circuit voltage of the cell. The point of operation is a trade-off between electrical efficiency and capital cost [3]; for a micro-cogeneration system, the requirement to supply the heat load is also a factor in determining the operating point.

Considering the whole fuel cell system, Figure 2.2(b) shows how the electrical and

thermal efficiency varies with the electrical load. In contrast to heat engines which have a maximum efficiency at their nominal operating point, fuel cells are known to have excellent 'turn-down' performance, *i.e.* reducing the electrical load results in higher electrical efficiency. However, since there are components that require electrical supply (*e.g.* sensors, actuators, control system), and their load is constant regardless of the power delivered by the fuel cell, this parasitic load degrades the system efficiency at low electrical load. There is a point 'B' where the parasitic load equals the power delivered by the fuel cell and the system therefore has 'zero efficiency'. In a similar sense, SOFCs have a lower operational point below which the stack is no longer thermally self-sustaining and begins to cool. There is therefore a practical lower limit below which the system cannot operate, typically of the order of 20% of the nominal operating point.

It can be seen from Figure 2.2(b) that as the electrical load on the fuel cell increases, the thermal efficiency increases and the electrical efficiency decreases. The way in which the heat-to-power ratio of the fuel cell varies with electrical load will depend very much on the system design, but will generally tend to increase when subjected to heavy electrical loading. However, it should be remembered that the heat-to-power ratio of the system can also be controlled at any fuel cell operating point by varying the fuel utilisation and the amount of heat generated in an auxiliary afterburner.

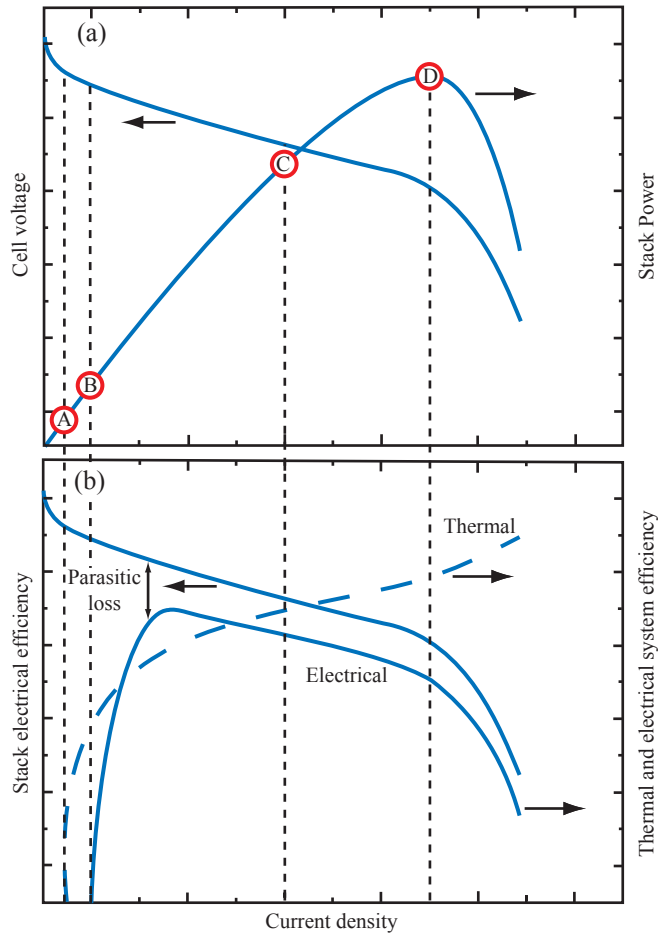


Figure 2.2: Illustration of the operating range of a fuel cell, showing (a) stack voltage and power and (b) electrical and thermal efficiency. Labeled operating points are described in the text.

2.3 Water and thermal management in PEFC

Proper membrane hydration is important at all times of operation to prevent high ionic resistance that can potentially result in failure of the membrane. There must be a sufficient water in the polymer electrolyte membrane. Proton conductivity is directly proportional to the water content. However, there must not be so much water that the electrodes that are bonded to the electrolyte flood, blocking the pores in the electrodes or the gas diffusion layer. A balance is, therefore, needed, which takes an effort to achieve.

Maintaining water balance in the cells requires maintaining optimal conditions on both

the anode and cathode sides. Determining these optimal conditions requires understanding of the physical processes that occur inside the fuel cell.

It is important to consider the following issues in water management:

1. During the operation of the cell, the H^+ ions moving from the anode to the cathode pull water molecules with them. This process is called electro-osmotic drag. Typically, between one and five water molecules are dragged for each proton. This means that especially at high current densities, the anode side of the electrolyte can become dried out even if the cathode is well hydrated.
2. The air has a drying effect at high temperatures. At temperatures of over approximately around $60\text{ }^\circ\text{C}$, the air will always dry out the electrodes faster than the water is produced by the H_2/O_2 reaction. One common way to solve this is to humidify the air, the hydrogen, or both, before they enter the fuel cell. This may seem contrary to intuition, as it effectively adds a by-product to the inputs in the process, and there cannot be many processes where this is done. However, for most cases, it greatly improves the fuel cell performance.
3. The water balance in the electrolyte must be correct throughout the cell. In actual operation, some parts may be just right, others too dry, and others flooded. To illustrate, consider the air as it passes through the fuel cell. It may enter the cell quite dry, but by the time it has passed over some of the electrodes it may be about right. However, by the time it has reached the exit it may so saturated that it cannot dry off any more excess water. This issue is more pronounced when designing larger cells and stacks.

Similar to any other physical energy conversion device, fuel cells are not 100% efficient. The amount of fuel energy that cannot be converted to useful electrical energy has to be rejected as heat. The operating temperature of PEFCs is between 60 to 100 $^\circ\text{C}$ compared to that of an internal combustion engines which ranges from 200 to 400

°C. It is also necessary that all the waste heat in the fuel cell system be removed by the radiator as opposed to the internal combustion engine where some of the heat is removed by the exhaust gases. Heat rejection is indeed far more difficult compared to that of an conventional internal combustion engine. This problem may translate into either large heat exchange equipment or large parasitic loads like a radiator fan power. The three most commonly used approaches are listed below:

1. Cooling using cathode air supply

This is the simplest of all methods of cooling a fuel cell. This method, however, can only be used for systems of power up to about 100 W_e . This is usually done by using purely convected air to cool the cell and provide sufficient air flow to evaporate the water.

2. Separate reactant and cooling air

This method is the highly suggested way of cooling cells in the range from about 100 to 1000 W_e . This is implemented by making extra channels in the bipolar plates through which cooling air can be blown. Alternatively, separate cooling plates can be added, through which air is blown. Using separate cooling air works for fuel cell between 100 W_e and 1 kW_e or so, but for larger cells this becomes impractical and water cooling is preferred.

3. Water cooling of PEFCs

As a rule of thumb, operations above 5 kW_e will be water cooled, those below 2 kW_e will be air cooled, with the decision for cells in between being a matter of judgment. One consideration will be what is to be done with the heat. If the heat is to be just lost to the atmosphere then the bias will be towards air cooling. On the other hand, if the heat is to be recovered (e.g. in a small domestic CHP system), then water cooling becomes much more effective.

2.4 Fuel cell systems

The fuel cell stack represents the main and most expensive component of the entire system. However, a significant amount of auxiliary equipment, also referred to as *balance-of-plant*, is required to operate the stack and function as a system. Figure 2.3 presents an example of the different equipment and interconnections found in a fuel cell system for micro-cogeneration application. The precise configuration will depend to a large extent on the type of fuel cell technology used, but in general a typical fuel cell system requires several subsystems: fuel cell stack, fuel supply, oxidant supply, water management, heat management, power conditioning, instrumentation and controls, and in some cases, hybrid components.

2.4.1 Fuel cell stack

A fuel cell stack is the heart of a fuel cell system. A typical fuel cell stack may contain hundreds of fuel cells. A fuel cell is an electrochemical engine that converts chemical potential energy of a fuel into electric power. The classification of fuel cells is primarily by the type of electrolyte used. The electrolyte determines the types of reaction that take place in the cell, the types of catalyst required, the temperature range in which the cell operates and the fuel required. Several types of fuel cell – each with its own advantages, limitations and potential applications – are presently under development. Amongst the most promising types are the direct methanol (DMFC), molten carbonate (MCFC), phosphoric acid (PAFC), polymer electrolyte (PEFC), and solid oxide (SOFC) fuel cell.

A single fuel cell is an inherently low voltage device, having an output voltage of typically less than 1 V. It produces barely enough electricity for even the smallest application. To increase the amount of electricity generated, individual cells are combined in series, into what is referred to as a stack. A stack, however, is not useful without the supporting components necessary to operate the stack and deliver electrical power.

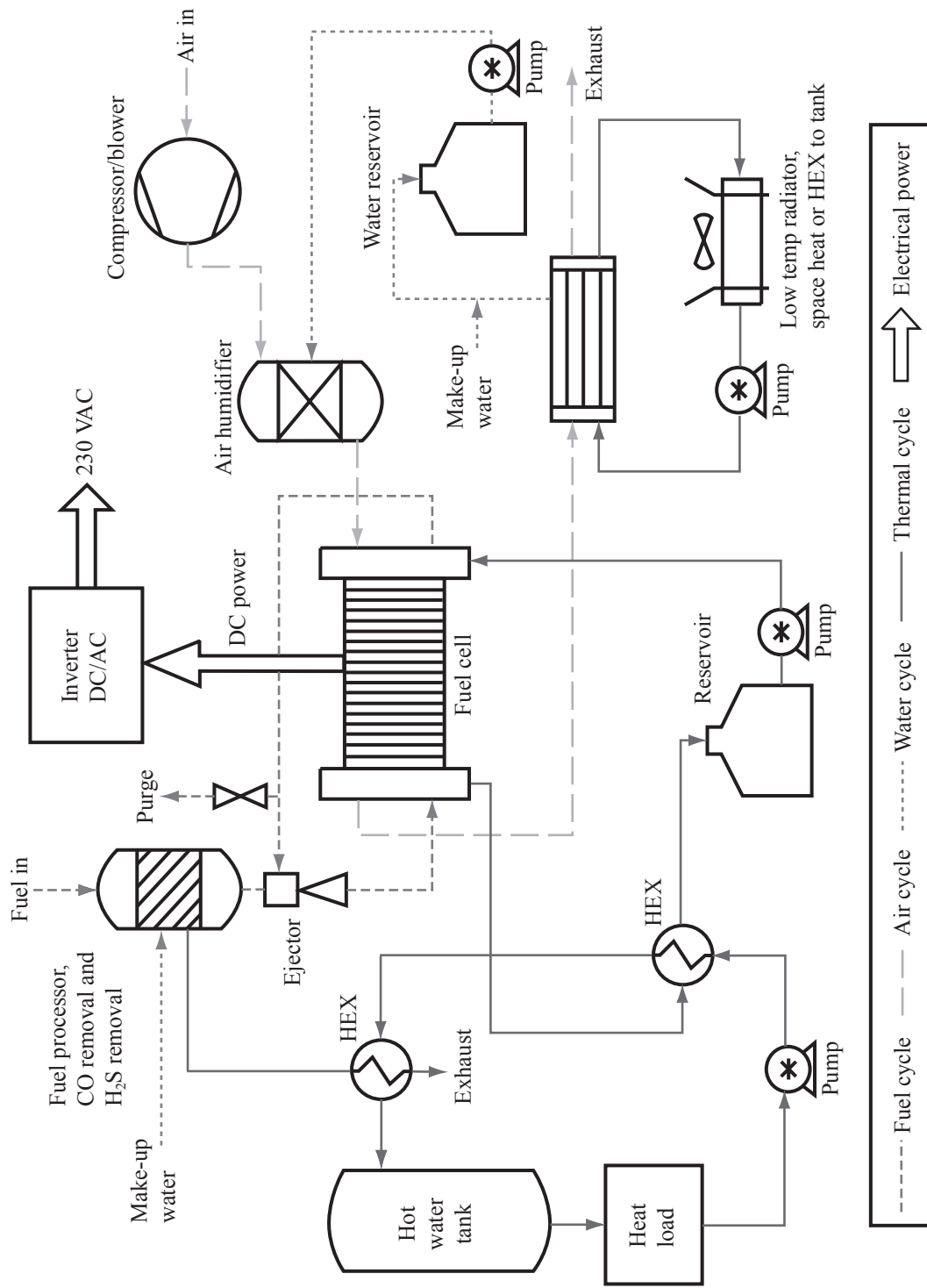


Figure 2-3: Example of a fuel cell system for micro-generation application showing the different equipment and interconnections.

2.4.2 Fuel supply

In theory, any substance that is capable of chemical oxidation can be used as fuel for the anode of a fuel cell. Hydrogen is the best choice for most fuel cell types because of its high reactivity with a suitable catalyst, its high energy density, and the fact that only water is generated at the point of use. Although hydrogen is the most abundant element on Earth, it is not often present in its molecular form, but is typically found in chemical compounds, such as water and hydrocarbons. For fuel cell systems, H₂-rich gas may be produced from other fuels and then stored as part of the system. However, hydrogen storage requires a lot of space even when hydrogen is compressed to very high pressures or even liquefied.

By making hydrogen generation part of a fuel cell system, conventional hydrocarbon fuels (such as methanol for portable power, natural gas for stationary applications, and gasoline for transportation) may be used. There are several processes for generating hydrogen from hydrocarbon fuels, such as steam reforming, partial oxidation, and autothermal reforming, which is a combination of steam reforming and partial oxidation. These processes, however, produce carbon monoxide as a by-product. Low temperature fuel cells that rely on precious metal electrocatalysts (e.g., platinum) such as PEFC and PAFC are sensitive to CO [4]. Therefore, additional processes must be employed for these types of fuel cell to ensure that hydrogen is pure enough to avoid poisoning (typically <10 ppm CO for PEFC) [5]. The water gas shift reaction [6] reduces the content of CO in the gas produced by the fuel processor. Preferential oxidation [7], methanation [8] or membrane separation [9] further minimises the CO content in the reformat gas. Desulfurisation [10] removes the sulphur compounds present in fuel.

There are fuel cells, however, that do not need an external reformer to convert hydrocarbon fuels to hydrogen. For example, the DMFC is powered by pure methanol, which is mixed with water and fed directly into the anode of the fuel cell. Also, high temperature fuel cells like the SOFC and MCFC convert fuels to hydrogen within the fuel cell via internal reforming [11], which is made possible by the high temperature at

which they operate.

2.4.3 Oxidant supply

In principle, any substance that can be reduced can be used as an oxidant. Oxygen is most commonly used for this purpose because it is economically available in air. For low-pressure systems, air is typically supplied by a fan or a blower, whereas an air compressor may be used for pressurised systems. In any case, a fan, a blower, or a compressor requires electrical power and thus represents power loss or *parasitic load*. For applications that require very low power, e.g., low power portable systems, it is possible to design and operate the fuel cells with passive air supply [12]. In these cases, the cathode is directly exposed to the atmosphere and the supply of oxygen relies only on natural convection due to concentration gradients.

Pure oxygen systems are only used where air is not available, such as in submarines or space applications, due to the added size and weight of oxygen storage and the associated safety concerns. The supply of oxygen to the fuel cells only requires a pressure regulator since stored oxygen is already under pressure.

2.4.4 Heat and water management

Water and heat are the by-products of fuel cell operation and the system must include the means for their removal. The water may be drained from the system whilst the heat may be discarded to the surroundings. However, both water and heat from the fuel cell stack may be partially reused. Water and heat management may be integrated into a single subsystem, in which case the water removes the heat from the stack and the resulting hot water is used for preheating and humidifying the reactant gases, or to generate steam for the reforming and shift reactions.

In some cases, an afterburner is employed, where combustion of unreacted fuel takes place to obtain additional heat. The heat from high temperature combustion gases

leaving the afterburner may be extracted using a phase-change heat exchanger. The majority of the heat recovered comes from the cooling of the exhaust gases and from the condensation of water vapour therein. For a stationary fuel cell system, a hot water tank is usually employed to store the heat recovered from the system.

2.4.5 Power conditioning

The electricity produced by the stack goes through power conditioning where it is modified to match the load requirements in terms of voltage, power quantity and transients. Also, the fuel cells generate direct current (DC), but some loads or applications require alternating current (AC). A DC/AC converter is included in the power conditioning subsystem for this purpose. Voltage regulation is one of the most important functions of this subsystem because a fuel cell stack has a tendency for voltage swing [13], which few loads can tolerate. The fuel cell system must also provide for its electrically powered components, such as pumps, fans, blowers, instruments, etc., at the correct voltage and current. Furthermore, in hybrid systems the fuel cell is coupled with a battery or a supercapacitor for startup or peaking. The power from the battery or supercapacitor also needs to be conditioned to suit the load requirements. The fuel cell can also recharge the battery or supercapacitor. Finally, the power management subsystem delivers the power from the fuel cell system to the user. The configuration and characteristics of this subsystem depend on the load requirements, which vary with application.

2.4.6 Instrumentation and controls

This subsystem implements a strategy to control the system operating parameters, e.g., flow rates, temperature, pressure, etc. It also communicates with the load and other electrical components of a system. It is typically composed of sensors, actuators, controllers, processors, etc.

2.4.7 Hybrid components

In some situations, another power source is combined with the fuel cell, forming a hybrid system. Hybridisation seeks to combine the desirable features and minimise the disadvantages of the coupled power sources. For example, a battery can be used to accommodate peak demands and load transients, whilst the fuel cell delivers the energy stored in the fuel [14–18]. Supercapacitors have also been suggested as an auxiliary power source that can be combined with a fuel cell system [10]. A supercapacitor is an electrochemical energy storage device like a battery, but has greater power density and requires less maintenance. For transportation applications, in particular, the fuel cell has the advantage of being a range extender, whilst a battery or supercapacitor is important in recovering the braking energy, providing startup power and for load following [16–18]. The fuel cell stack can also be combined with a heat engine, such as a gas turbine to generate additional power [19–25]. This is preferable because the temperature of the streams exiting a high temperature fuel cell stack and afterburner is suitable for the inlet temperature of the turbine. Moreover, fuel cell stacks of different types can also be hybridised [26]. Finally, coupling a fuel cell stack with renewable power sources [15, 27] can further take advantage of the fuel cell technology.

There are many ways the subsystems and their components, and the flows between them can be arranged. There are also many ways of designing and operating them. In any event, the goal is to have a system that meets the design requirements and represents a trade-off amongst the different design objectives. The set of objectives and constraints depend on the intended application of the fuel cell system, namely portable, stationary and transportation.

2.5 Fuel cell applications

Fuel cells may be used in applications with a wide range of power needs because of their flexibility in sizes. Their potential application ranges from systems of a few watts

to megawatts; they can power almost every energy utilising plant and/or device, from houses to cars to mobile phones [2,28]. For instance, fuel cells are particularly useful for applications that are energy-limited, such as portable devices which require constant recharging. Table 2.2 compares the weight, energy, and volume of batteries to a typical PEFC. As indicated in Table 2.2, the fuel cell system can provide a similar energy output to batteries with a much smaller system weight and volume.

Table 2.2: Comparison of fuel cell with other power sources [28].

	Weight (lb)	Energy (Wh)	Volume (L)
Fuel cell	9.5	2190	4.0
Zinc-air cell	18.5	2620	9.0
Other battery types	24	2200	9.5

Future markets for fuel cells include the portable, transportation and stationary sectors.

Figure 2.4 illustrates some typical fuel cell applications for different fuel cell types.

Typical applications	Portable electronics equipment			Cars, boats and domestic micro-CHP			Distributed power generation, CHP and buses		
Main advantages	Higher energy density than batteries, faster recharging			Potential for zero emissions, higher efficiency,			Higher efficiency, less pollution, quiet operation		
Power (W)	1	10	100	1K	10K	100K	1M	10M	
Application range									

Figure 2.4: Typical fuel cell applications for different fuel cell types.

2.5.1 Portable sector

One of the major future markets for fuel cells is the portable sector. There are numerous portable devices that would use fuel cells in order to power the device for longer amounts

of time. Some of these devices include laptops, cell phones, video recorders, ipods, *etc.* Fuel cells will power a device as long as there is fuel supplied to it. The current trend in electronics is the convergence of devices, and the limiting factor of these devices is the amount of power required. Therefore, power devices that can supply greater power for a longer period of time will allow the development of new, multifunctional devices. The military also has a need for high power, long-term devices for soldier's equipment. Fuel cells can be manufactured with greater power and less weight for military applications. Other military advantages include silent operation and low heat signatures.

2.5.2 Transportation market

The transportation market will benefit from fuel cells because fossil fuels will continue to become scarce, and because of this, there will be inevitable price increases. Legislation is becoming stricter about controlling environmental emissions. There are certain parts of countries that are passing laws to further reduce emissions and to sell a certain number of zero emission vehicles annually. Fuel cell vehicles allow a new range of power use in smaller vehicles and have the ability to be more fuel efficient than vehicles that are powered by other fuels.

2.5.3 Stationary sector

Large stationary fuel cells can produce enough electricity to power a house or business. These fuel cells may also make enough power to sell back to the grid. This fuel cell type is especially advantageous for business and residences where no electricity is available. Fuel cell generators are also more reliable than other generator types. This can benefit companies by saving money when power goes down for a short time.

2.6 Conclusions

Fuel cells, electrochemical engines that convert chemical potential into electric power, allow production of electrical energy from hydrogen or other fuels with high efficiency and low emission. This technology is promising in the area of stationary, transportation and portable applications. Modelling and optimisation offer a great potential to inform fuel cell system design, which often results in savings in design cycle time and cost, and better design and operation. This chapter covered the fundamental principles of fuel cells and fuel cell systems, their operation and applications. A good understanding of these concepts are essential in appropriately designing fuel cell systems, which is the focus of the following chapters.

Chapter 3

Fuel cell systems design

This chapter examines the role of modelling and optimisation in the design of fuel cell systems. It discusses a typical fuel cell system design process and how modelling and optimisation are used to generate design alternatives and identify good designs. A fuel cell system model may contain many different design alternatives, and criteria for comparing them are necessary. Each application has its own specific set of design criteria and identifying the critical ones and those that can be compromised is very important, and so some examples of application-specific criteria and design variations amongst applications are discussed. Furthermore, the existing models for different fuel cell systems applications, namely portable, stationary and transportation, are identified and characterised by approach, state, system boundary, spatial dimension, and complexity or detail. These models are used for model-based design approaches such as parametric study, single-objective optimisation and multi-objective optimisation; a summary of the existing studies is provided.

3.1 Fuel cell system design process

The design of a fuel cell system is a decision-making process which involves the identification of possible design alternatives and the selection of the most suitable one. A good

design is one that meets the design requirements and represents a trade-off amongst the different design objectives. For a fuel cell system, the requirements and objectives may include efficiency, size and weight, power output, emissions, quick startup and fast response to load changes, lifetime, noise level and operability in extreme weather conditions. A subset of these will be relevant for each particular application.

The use of modelling and computer-based optimisation in fuel cell systems design is receiving increasing interest. This has been motivated by the increase in computational resources and the availability of new and effective methods for solving numerical problems. A benefit of this approach is that it often leads to substantial savings in cost and design cycle time, as well as better design and operation. However, an optimal design solution is only useful within the limitations of the model. The quality of an optimal design mainly depends on how well the model has been formulated.

Figure 3.1 shows the role of modelling and optimisation in a typical fuel cell system design process. The process starts by identifying a set of design objectives and constraints, which mainly depend on the intended application of the fuel cell system. In this paper, the term “criterion” will be used to refer to either a requirement¹ or an objective². A criterion may be critical or irrelevant for a particular application. Identifying the crucial ones and those that can be compromised without adversely affecting the design is very important. Some application-specific criteria are discussed in Section 3.2.

Modelling is performed to capture the aspects of a fuel cell system that are of interest to the designer. Knowledge of fuel cell phenomena, such as electrochemical, thermodynamic and transport processes, material properties, and various interactions are useful in formulating a model. A mathematical model, which describes certain aspects of a fuel cell system and predicts its behaviour, may be a set of equations, algebraic or differential, or a computer-based procedure or subroutine. The model may contain many different design alternatives, which can be obtained by changing the variables, param-

¹In this paper, “constraint” and “requirement” are used interchangeably.

²In some optimisation works, a “criterion” is synonymously used with an “objective”.

eters, conditions, or constraints. The criteria defined in the previous step provide the basis for comparison of the different design alternatives.

The model can then be coupled with a numerical optimisation algorithm to generate better designs iteratively. This may result in a single or multiple optimal solutions. Modelling and optimisation aid the designer in shortlisting candidate designs for further consideration. Optimisation, however, does not always generate a good design suitable for fabrication. In this case, iteration of the previous steps is necessary to verify that appropriate fuel cell phenomena are captured in the model and correct governing equations are used, examine the validity of the assumptions used in modelling, and if necessary, adjust or modify the design requirements and objectives.

The designer then evaluates the design solutions generated from optimisation and selects one or more alternatives that can be fabricated, guided by the knowledge of the trade-offs amongst the objectives, in addition to own experience and other considerations that could not be included in the optimisation problem. Tests and diagnostics (e.g., model validation against experiments) are carried out to determine what else can be further improved in the existing design, verify the assumptions and validate the models. The final design may either result in a final prototype or an iteration of an existing design for further improvement.

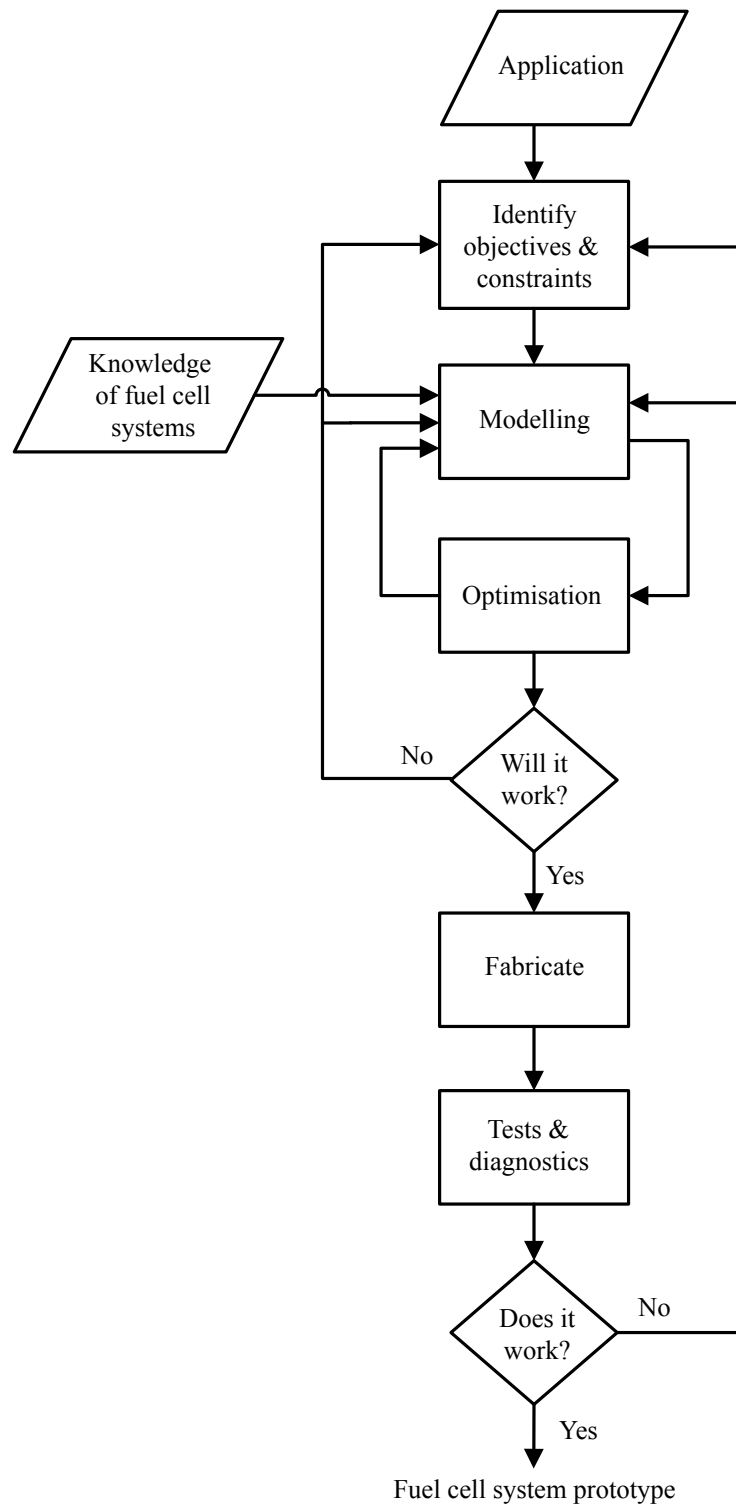


Figure 3.1: A typical fuel cell system design process [29–31].

3.2 Requirements and objectives for design

Each application has its specific set of requirements and objectives for design. For a fuel cell system, the criteria may include efficiency, size and weight, power output, emissions, ability for quick startup and fast response to load changes, lifetime, noise level and ability to function in extreme weather conditions. A criterion may be critical or irrelevant for a particular application. Identifying the crucial ones, and those that can be neglected without adversely affecting the design, is very important. The choice should be guided by knowledge and expertise related to the system and application.

A requirement, also referred to as a constraint, establishes the validity of a design. An objective, on the other hand, drives the search for optimal design. An example design problem may be to obtain the highest possible efficiency with the system size not exceeding a specified value. In this case, the efficiency is an objective and the size is a constraint. The objectives and constraints may switch roles in different scenarios to capture an intended design purpose. For example, minimising the size whilst imposing a lowest possible value for the efficiency is another design problem where the objective is the size and the constraint is the efficiency. In all cases, however, satisfying the constraints is more important than finding an optimum (i.e., minimum or maximum) value for an objective. A valid design satisfies all constraints. An optimal design is the *most desirable* amongst the valid designs.

The potential conflict between objectives adds another dimension to the design problem. In the example above, efficiency and size are conflicting objectives, i.e., higher efficiency typically requires a larger system and vice versa [3]. Efficiency and size do not only conflict with each other but they may also affect other objectives such as cost, emissions and lifetime. A good design, therefore, is one that satisfies the design requirements and represents a trade-off amongst the different design objectives.

Some examples of application-specific criteria and corresponding design variations amongst the applications are discussed below:

1. Efficiency

Efficiency is critical for portable, stationary and transportation applications. Efficiency directly translates into cost of fuel, and if present, size and capital cost of a hydrogen generating device and hydrogen storage. Since efficiency can be traded with size [3] and capital cost, optimisation is necessary to achieve a balance between the objectives.

2. Size and weight

Size and weight are critical for transportation applications. They are important but not critical for stationary applications. For portable applications, the size and weight of the fuel cell system should be comparable with the size and weight of the technology that it replaces, e.g., a battery.

The presently high weight and volume of hydrogen storage is one of the main challenges for commercialisation of fuel cell systems. For example, for transportation applications, this results in an inadequate vehicle range compared with conventional engines fuelled by petroleum. Design alternatives to improve vehicle range compromise other objectives. For instance, on-board reformation of fuels such as gasoline results in increased emissions of CO₂. Another option is to store hydrogen in metal hydrides or use a portable hydrogen-generating device (e.g., portable electrolyzers). However, this increases the cost of the system.

3. Electrical power output

Portable power systems with power output below 100 W_e are classified as battery replacements, whilst those with power output up to 1 kW_e are categorised as portable power generators.

As an indicator of electrical power requirements, passenger vehicles require power of the order of 50 kW_e; buses typically require about 250 kW_e or more; and scooters and bicycles require up to 3 kW_e and 1 kW_e, respectively.

For stationary applications, fuel cell systems with 1–10 kW_e power output can be used for individual homes, trailers and recreational vehicles. For larger homes, groups of homes, and small commercial premises, a fuel cell system with 10–50 kW_e power output is typically required. Small communities, office buildings, hospitals, hotels, military bases, etc. need 50–250 kW_e or higher.

For hybrid fuel cell systems, one of the important problems is the design of a power management strategy that controls the power flow between the power sources (i.e., fuel cell and battery or supercapacitor) for various modes of operation to achieve certain design objectives whilst taking into account the system constraints. A proper power management strategy is crucial for better system efficiency and durability, and directly affects the other design criteria.

4. Emissions

A fuel cell system run on hydrogen does not produce any emissions at the point of use. The only by-product is pure water which leaves the system as liquid and vapour. If another fuel, e.g., methanol, gasoline, or natural gas, is used and reformed to produce hydrogen, the system generates emissions in the reforming process. However, these emissions are in general still much lower than the emissions from an internal combustion engine or centralised power plant due to the high efficiency of the fuel cell.

Moreover, the entire life cycle should be considered when analysing the emissions of a fuel cell system. If hydrogen, produced from other fuel, is used as the fuel to the fuel cell, the emissions resulting from the reforming process should be taken into account regardless of whether the hydrogen generation takes place in a refinery, at the refuelling station, or on the vehicle. Hydrogen production from water using renewable energy sources does not generate any emissions, hence takes full advantage of the fuel cell technology.

5. Agility

An agile fuel-cell system is one that can start up quickly and respond quickly to load changes. Transportation fuel cell systems are expected to have a very short startup time, i.e., a fraction of a minute. The startup time for most portable and stationary fuel cell systems is less critical. Stationary fuel cell systems are often operated at constant load for extended periods to avoid efficiency losses associated with startup and shutdown.

The presence of energy storage, such as a battery or a supercapacitor, results in quick startup and response to load changes. However, the disadvantages of having the battery or supercapacitor are extra cost, weight and volume.

6. Lifetime and durability

The average lifetime of a vehicle is 10 to 12 years. However, the actual operating time is only about 3,000 to 5,000 hours or 100,000 miles. Thus, an automotive fuel cell system is expected to have a similar lifetime. Fuel cell systems for buses and trucks are anticipated to have longer operating lifetime ($\sim 150,000$ miles). A vehicle's highly intermittent operation, i.e., many startups and shutdowns, as well as the high dynamic load, poses an extra challenge for fuel cell durability.

Stationary fuel cell systems are expected to operate for 40,000 to 80,000 hours (5 to 10 years). The effect of real-life conditions such as impurities in fuel and oxidant can reduce the system's operating life.

Portable fuel cell systems may operate up to 2,000 hours. For the same weight and volume, fuel cells can achieve much longer lifetimes than the traditional Li-ion battery [32].

The lifetime of a fuel cell system is primarily determined by its durability, which is often evaluated in terms of platinum catalyst degradation, carbon catalyst support corrosion, membrane chemical attack and ageing of specific components. Durability affects other design criteria such as efficiency and cost. Also, system models that do not incorporate degradation tend to overpredict performance.

7. Noise levels

The acceptable noise level for stationary applications is low. This criterion is especially important when the fuel cell system is to be installed indoors. Although a fuel cell does not produce any noise, noise may be generated by the air and fluid handling devices. For transportation and portable applications, a low noise requirement is important but not critical.

8. Operability in extreme conditions

The ability to survive and operate in harsh weather conditions has an enormous impact on the design of the system. For transportation applications, the fuel cell system must be designed to start quickly even in extremely cold climate (which can be as low as -40°C). The presence of water in the system makes the fuel cell system susceptible to freezing if used in a cold environment. Also, the system must be sized for effective heat rejection even in exceptionally hot weather (32 to 40°C). The same applies for stationary fuel cell systems, but becomes irrelevant when the system is to be installed indoors. Similarly, this criterion is important but not critical for portable applications.

9. Cost

Perhaps the overriding design criterion is cost. However, cost is not always a practical choice as a design criterion because it can be very difficult to quantify. In addition, although the design with the lowest cost is usually the preferred choice, it does not necessarily mean that the design with the lowest cost must be implemented. Careful consideration of the other criteria such as lifetime, emissions, size and weight, etc. is important.

The total cost of a fuel cell system is the aggregate of capital cost, fuel production cost, operating cost, maintenance and repair cost, emissions cost and disposal cost. The cost must compete with that of the technologies that the fuel cell systems replace, e.g., batteries for portable fuel cell systems, internal combustion engine

for transportation fuel cell systems, and grid electricity and condensing boilers for stationary fuel cell systems.

In some cases, *return on investment* is used as a criterion instead of the the total cost. An example is the payback time, which is the ratio between the capital cost and annual savings in operating cost, and measures the number of years it takes for an investment to pay back. Although payback time serves as a quick reference, it does not consider the time value of money (i.e., interest earned over a period of time), inflation and changes in prices of fuel and electricity. Alternative criteria of return that take into account the time value of money are net present value and internal rate of return.

3.3 Fuel cell modelling

Modelling and optimisation are useful tools because they often result in substantial savings in design cost and cycle time and better system design and operation. Fuel cell models allow one to explore the many interacting and complex phenomena, such as coupled electrochemical, thermodynamic and transport processes, which are expensive and time-consuming to study experimentally. If formulated properly, fuel cell models provide insight into the performance of a fuel cell system and how the performance can be influenced. Modelling enables the analysis of feasibility, reliability, profitability and safety in the design phase to ensure that a design works under a wide range of conditions, even before a prototype is fabricated and tested.

However, poor modelling and strict requirements can make the design iteration loop shown in Figure 3.1 long and recurrent. A good model should be robust, accurate and able to provide meaningful solutions to fuel cell problems quickly [28]. A robust model is able to predict fuel cell performance over a wide range of operating conditions. Accuracy, on the other hand, can be attributed to using reasonable assumptions and correct input parameters such as physical and chemical properties, to the proper

identification of the physical phenomena and to using the correct governing equations. However, improving robustness and accuracy often involves a sacrifice in computational efficiency. A good model should exhibit a balance between robustness and accuracy and computational efficiency.

3.3.1 Characteristics of fuel cell models

Many fuel cell models with different complexity, level of detail and scope have been presented in the literature. These models can be characterised by approach, state, system boundary, spatial dimension and complexity or detail (Table 3.1).

Table 3.1: Characteristics of fuel cell models

Category	Level
System boundary	Cell, stack, system
Approach	Empirical, semi-empirical, mechanistic
State	Steady, dynamics
Spatial dimension	Lumped, 1-D, 2-D, 3-D
Complexity/detail	Electrochemistry, transport processes, thermodynamics, catalysis, fluid dynamics

3.3.1.1 System boundary

The system boundary defines the area of interest in the model. It may range from: the cell-level (which includes models that considered specific components of a fuel cell such as the membrane or the electrodes, or an entire fuel cell), to the stack-level with individual fuel cells assembled in a stack, and finally to the system-level consisting of a fuel cell stack and auxiliary components or balance-of-plant.

Cell-level models enable an understanding of local behaviour of fuel cell phenomena. They serve as building blocks for understanding and modelling of stacks and systems. Cell-level and stack-level models in the literature have been thoroughly surveyed [33–47]. For this reason, this chapter only reviews system-level fuel cell models.

System-level models are used to study specific applications of fuel cells. Different applications are made up of different components or subsystems arranged and operated differently. The aim is the same, however, for any application: to design and operate the system so as to meet the design requirements and obtain a compromise amongst the different design objectives. Individual components may behave differently when operated as part of a system. This is why it is preferable to carry out optimisation using a system-level model. A system-level model allows understanding of the interactions between components and enables determination of the response of the system as a whole. The interaction between the different components poses a challenge in optimisation.

3.3.1.2 Approach

Fuel cell modelling approaches can either be mechanistic, empirical or semi-empirical. Mechanistic models, also known as theoretical models or physics-based models, are derived from the physics and the electrochemistry governing the fuel cell phenomena of interest. They provide a detailed and complex account of the phenomena in the fuel cells. They are typically represented by a mixture of partial differential and algebraic equations. They are useful for the investigation of localised phenomena, for example, at a pore level, or a single three-phase boundary. However, they are rarely employed for high system-level simulations because their solution requires long computational times. Also, their development is laborious and their validation may be difficult. For these reasons, mechanistic modelling is usually performed on one aspect or region of the fuel cell only.

Empirical models, also called analytical models, are used when the physical phenomena are difficult to model or are not well understood. Empirical models are developed based on experimental data and are represented as a correlation between input and output. Their advantages over mechanistic models are that they are much simpler and have smaller computational requirements. They are useful for making quick predictions and provide a fast start into fuel cell modelling. However, empirical models are only

approximate and do not provide a sufficient understanding of fuel cell phenomena. Also, they are limited to a narrow range of operating conditions and cannot accurately predict the fuel cell performance beyond the conditions for which they were developed. Furthermore, the relationships are only applicable to a specific fuel cell stack. The coefficients in the equations need to be re-evaluated so they can be used for different fuel cell stacks. An example of an empirical model that is commonly cited is the one formulated for the Ballard PEFC, which shows the dependence of voltage on current, temperature and partial pressures of hydrogen and oxygen [48–52].

Semi-empirical modelling combines theoretically derived differential and algebraic equations with empirically determined relationships. They contain more details than empirical models but solve more quickly than mechanistic models. The majority of the system-level fuel cell models presented in the literature are semi-empirical models [10, 18–27, 48–69].

3.3.1.3 State

The state of the model, either steady-state or dynamic (transient), is determined by the intended use of the model.

Steady-state models are often used to size a component or equipment, perform parametric studies and calculate the amount of materials required (e.g. reactant flow rates, catalyst loading). These models are also employed to simulate the behaviour of laboratory fuel cell setups, which are normally run at steady-state. The same applies for fuel cell systems used for stationary applications. These systems are typically operated at steady-state to avoid intermittent operation which leads to efficiency losses during startup and shutdown.

Although there is a considerable body of work on steady-state system-level fuel cell modelling [12, 14–16, 19–27, 48, 51, 53–58, 60–73], only a few dynamic models are available [10, 17, 18, 50, 52, 59, 74–76]. Dynamic models are required to model important transients such as startup, shutdown and load changes. These models include time derivatives in

their formulation. Dynamic models are also employed for investigation of fuel cell system degradation. For example, the thermal stress associated with load and thermal cycling that may contribute to cell failure. Dynamic models can be used to track changes of these phenomena with time. In addition, dynamic models are prerequisites for control systems design. A control system automatically regulates the response of the system and keeps it at the desired value by manipulating some variables such as temperature, flow rate or composition of reactant streams.

3.3.1.4 Spatial dimension

In the early stage of modelling, lumped models or zero-dimensional models are advantageous because of their simplicity and low computational time. They are also suitable for initial systems optimisation. In the literature, the majority of the system-level fuel cell models are lumped models [10, 12, 14–27, 48–58, 60–68, 70, 72, 73, 76, 77].

However, when modelling phenomena such as mass and heat transport, it is preferable to consider at least one spatial dimension. Spatially-distributed models are comprehensive and provide a great deal of information. If properly formulated, they provide means for intricate analysis of many difficult performance aspects of a fuel cell system. They can be used to generate flow patterns, temperature and current density distribution, etc. However, distributed models may be complex and require long computational times. They are composed of partial differential equations which are commonly solved using numerical methods such as finite difference, finite volume, or finite element. Commercial software for solving distributed models is becoming increasingly available [78–80]. However, caution needs to be exercised in selecting such software to ensure that the underlying assumptions are consistent with the problem at hand. The solutions of distributed models require specifications of boundary conditions such as flow rates and conditions at the inlet and at the outside walls.

3.3.1.5 Complexity/detail

Coupled processes such as mass and heat transfer, electrochemistry, thermodynamics, catalysis and fluid dynamics, occur simultaneously during the operation of fuel cells. In practice, however, a model is not expected to describe all of these phenomena. The level of detail depends on the purpose of the model. The purpose of the model must be well understood to avoid adding complexity that might be unnecessary. The model should be simple enough to allow for repeated calculations, but sufficiently complex to differentiate between alternative designs [3].

In general, the following equations (or their combination) are able to describe any phenomena in a fuel cell system [69]:

1. conservation laws of mass (total and component), momentum, electric charge, and energy;
2. constitutive equations for various fluxes;
3. kinetic relations for reactions;
4. thermodynamic relationships; and
5. auxiliary or supporting relationships.

3.4 Earlier reviews in fuel cell modelling

Amongst the different types of fuel cells, PEFC and SOFC are the most well-studied. There are numerous reviews available on modelling of these two types of fuel cell. Reviews of modelling of fuel cells other than PEFC and SOFC are not available to date, which may be due to the relatively low number of modelling studies performed on such types of fuel cell.

An overview of PEFC models and comparison of different approaches to PEFC modelling appear in Refs. [34,35]. Many reviews have focused on specific aspects of PEFC

modelling. The reviews performed by Djilali [37] and Gurau and Mann [38] have considered computational fluid dynamics (CFD) modelling; the former has discussed the challenges and opportunities in CFD modelling, whilst the latter have examined multiphase CFD models. Several reviews have focused on modelling studies related to water management, summaries of which are given in Refs. [41, 45]. A more specific discussion of water management in PEFCs can be found in Ref. [43], in which the transport of water within the gas diffusion layer has been considered. The models for heat and mass transport in PEFC have been surveyed in Refs. [36, 44]. A summary of studies that have employed modelling to investigate the impact of contamination on the performance of PEFC is provided in Ref. [81].

With regard to SOFC modelling, a summary of existing models and a commentary on the present status of modelling efforts can be found in Ref. [42]. Ref. [33] covers the dynamic modelling studies performed on SOFCs. A discussion of challenges and opportunities for thermal management of SOFCs and PEFCs and the use of modelling to overcome some technical limitations are given in [46]. Considering only a specific type of SOFC, Ref. [47] discusses the research activities, the design issues, and the role of modelling in the design of micro-tubular SOFC. A review of impedance modelling and validation in SOFC diagnostic is given in Ref. [40].

3.5 Review of fuel cell system modelling

This section reviews the existing system-level fuel cell models. System-level models are used to study specific applications of fuel cells such as portable, transportation and stationary. Different applications are composed of different components or subsystems arranged and operated differently. The functions of the different subsystems are discussed in Section 2.4. It is preferable to perform optimisation using a system-level model because individual components behave differently when operated as part of a system. Readers who are interested in cell-level and stack-level modelling are referred

to the available reviews [33–47].

Figure 3.2 presents a systematic overview of the existing fuel cell system models. The models are identified as either for a portable, stationary, or transportation fuel cell system. The type of fuel cell, spatial dimension and state are also indicated. It can be concluded from Figure 3.2 that most of the system-level fuel cell models are lumped, steady state and based on either PEFC or SOFC. Although not shown in the diagram, the majority of these models are semi-empirical.

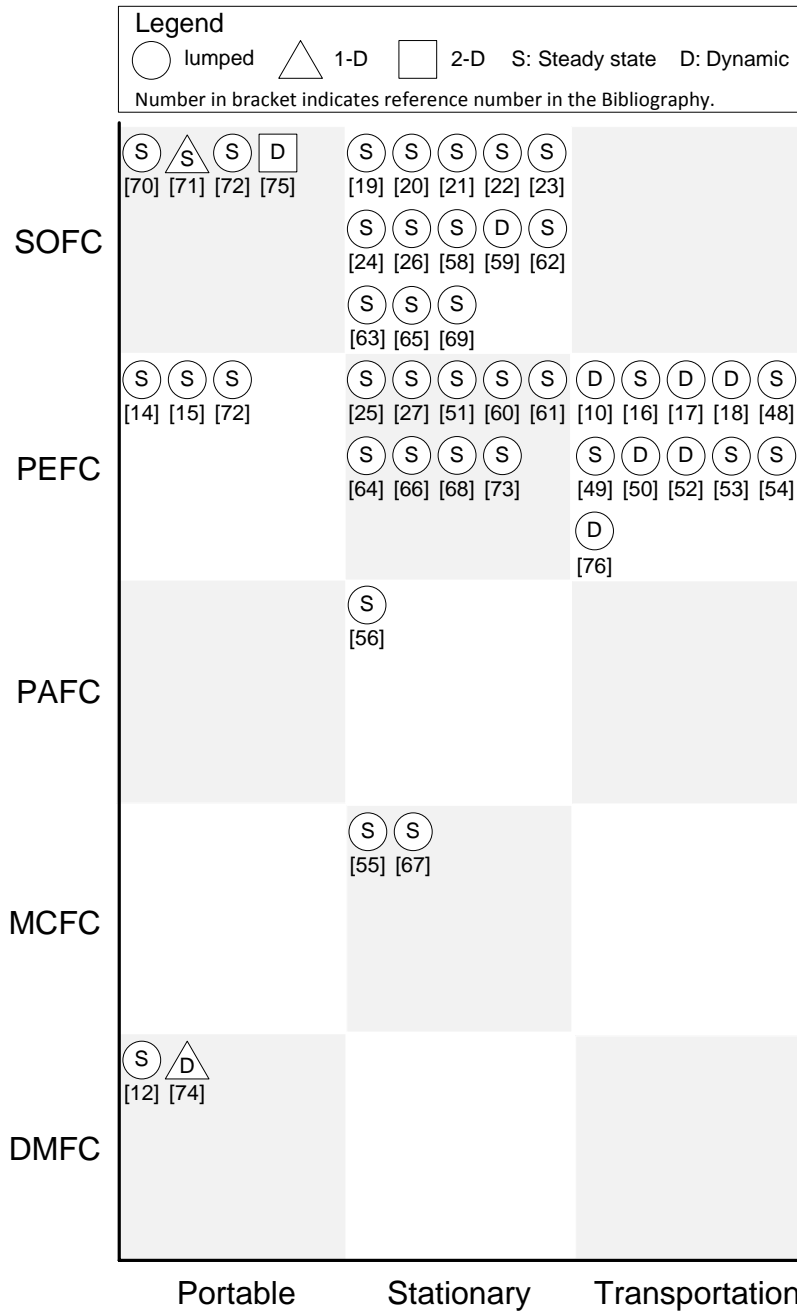


Figure 3.2: Summary and characterisation of fuel cell system models

3.5.1 Modelling of portable fuel cell systems

Portable power systems are small grid-independent power devices with electrical output ranging from a few watts to roughly 1 kW [82]. They are either used as micropower in consumer electronic devices or as backup power when regular power systems fail.

Portable power systems with electrical output below 100 W_e are classified as battery replacements, whilst those with electrical output up to 1 kW_e are categorised as portable power generators [2].

Fuel cell based systems are emerging alternatives to technologies used in backup power systems due to their high power density, high reliability and low emissions [14]. Traditional portable power systems include lead-acid battery systems and engine-generator sets, or combination of both [83]. Compared with batteries and generators, fuel cells provide longer continuous runtime and better durability in extreme environmental conditions [84]. They are also quieter and emit less pollutants. However, the high capital cost of fuel cells is one of the primary drawbacks.

Figure 3.2 shows the modelling studies that have been performed for portable fuel cell systems based on PEFC, DMFC and SOFC. PEFC is attractive for portable applications because it operates at low temperature, responds relatively quickly to load changes and is compact and lightweight. DMFC, in principle, is a subcategory of PEFC in which methanol is used as the fuel. Although it has a lower efficiency compared to PEFC, it is favoured over PEFC due to the ease of transport and storage of methanol, and the lack of complex steam reforming processes. Also, for portable applications such as laptops, PDAs and mobile phones, power density is more important than efficiency. DMFC operates at low temperature, has low weight, and has a higher higher density compared to a traditional Li-ion battery. There is also some interest in using SOFCs for portable applications because of the possibility of using a wide variety of fuels such as ammonia, propane or butane. SOFC can reform hydrocarbon fuels internally, which makes it more attractive than PEFC. To produce H_2 , PEFC requires partial oxidation where CO is generated as a by-product. However, SOFCs operate at high temperature and can take several hours to be heated up to the desired operating temperature.

3.5.1.1 Portable DMFC systems

Yeh and Chen [12] have analysed the performance of a passive DMFC system using a lumped semi-empirical steady-state model based on mass transport and electrochemical reaction kinetics. The model was used to perform a parametric study to analyse the effects of various variables such as catalyst loading, catalyst layer thickness, electrolyte membrane thickness and methanol concentration on power density. Amongst the considered variables, the cathode catalyst loading and cathode catalyst layer thickness are the most important.

Alotto et al. [74], on the other hand, have presented a 1-D mechanistic model of a DMFC system for low-power applications. The steady-state and dynamic models are both discussed in their paper. The model accounts for electrochemical reaction, electronic and protonic conduction, methanol crossover through the electrolyte membrane, diffusion of reactants through the substrates and electric current generation. The model was used to minimise both the methanol crossover and the duration between two consecutive fuel charges.

3.5.1.2 Portable SOFC systems

A 1-D semi-empirical steady-state model of a SOFC-based portable power generation device fuelled by ammonia and butane was proposed by Chachuat et al. [71]. The system consists of a fuel processing reactor, a SOFC stack and two burners. Hydrogen is produced from ammonia decomposition, whilst butane is catalytically oxidised to produce heat and maintain the stack at a sufficiently high temperature. The model, which is composed of partial differential equations, is implemented in DAEPACK [85]. Using the model, a parametric study was performed to analyse the effect of the heat loss coefficient, exchange current density and electrolyte thickness on power density and efficiency.

3.5.1.3 Portable hybrid systems

Recently, models for hybrid portable fuel cell systems have been reported in the literature [14, 15]. A common design problem is the proper sizing of the different elements comprising the system. Using a lumped semi-empirical steady-state model, Vasallo et al. [14] have developed a methodology for sizing a hybrid backup power to obtain the minimum lifecycle cost. The backup power system is composed of a PEFC stack, a battery bank and power electronic devices. The methodology was coupled with an existing sizing tool for hybrid systems, called HOMER [86]. In order to carry out sizing, data such as the load profile and backup time must be specified. The load profile, which is usually taken as the average of electrical power values over a given time interval (e.g., hourly), represents the load fluctuations and help establish the required operating reserve to ensure that the system has enough energy capacity to support the demand. The backup time, on the other hand, denotes the maximum time that the backup power must supply the load during interruption of the regular power supply. As a practical application, sizing of backup power for a telecommunication system was illustrated.

Lagorse et al. [15] have dealt with a similar design problem but a different system by developing a lumped semi-empirical steady-state model of a hybrid system composed of photovoltaic (PV) cells, a battery and a PEFC stack as a stand-alone power source for street lighting. The model was implemented in the SIMPLORER software [87] and was used to obtain the configuration that results in minimum cost by proper sizing of the different components of the system.

3.5.2 Modelling of transportation fuel cell systems

The power generated by fuel cells can be used for vehicle propulsion [10, 16, 17, 49, 50, 76] and operation of electrical accessories [48, 52, 70, 75]. The advantages of fuel cell vehicles include high efficiency [10, 16, 18, 49, 50, 52], low operating noise [10, 18, 52], little or no

emissions from H_2 or H_2 -rich reformer gases and air [16, 18, 49, 50, 76] and long vehicle range [10]. However, the high cost of the fuel cells [17, 49, 76, 88, 89], durability concerns [89], and bulky fuel storage [10, 18, 53, 88, 89] are amongst the major obstacles for commercialisation. The PEFC is considered to be the primary candidate for automotive applications because it operates at low temperature, therefore allowing fast startup [50], and achieves high power density. However, it requires on-board stored H_2 or H_2 -rich gases generated on-board from liquid fuels such as methanol, gasoline or diesel [18].

Recently, modelling of hybrid fuel cell vehicles has also been reported [10, 16–18]. In these systems, the fuel cell stack is equipped with energy storage devices such as batteries and supercapacitors. The fuel cell has the advantage of being a range extender, whilst a battery or supercapacitor is important in recovering the braking energy, providing startup power and following the load.

Another transportation application is that of auxiliary power units [48, 52, 70, 75], where another engine is used for propulsion and the fuel cell system is used either to run a portion or all of the vehicle electrical system. This is particularly appealing for trucks and buses as it allows operation of an air conditioning or refrigeration unit whilst the vehicle is not moving without the need to run the main engine.

Although there are different fuel cell technologies available, only PEFCs and SOFCs are considered for transportation applications because of their solid electrolyte [76]. Figure 3.2 indicates that almost all of the modelling studies performed on transportation fuel cell systems are based on PEFC.

3.5.2.1 Fuel cell electric vehicles

Modelling studies that have considered fuel cells solely for vehicle propulsion include Jemei et al. [76], Maxoulis et al. [50] and Xue and Dong [49]. Jemei et al. [76] have proposed a lumped empirical model of an automotive PEFC system using neural networks. Both the steady-state and dynamic formulations of the model are presented in their paper. The gas flow rates, air humidity level, stack temperature and current

density are the inputs for the model, whilst the stack voltage is the output. However, the experimental data from which the neural network model was built were taken from a low-power PEFC stack (500 W_e). The suitability of the model at higher stack output, e.g., ~50 kW_e for automotive applications, still needs to be established. Also, the behaviour of the system with auxiliary components may be different from the behaviour of the stack alone. Furthermore, a drive cycle and the automotive environment such as propulsion and other electrical loads must also be considered.

The effect of temperature variation during a driving cycle was considered by Maxoulis et al. [50] using a lumped semi-empirical dynamic model implemented in the ADVISOR vehicle simulation program [90]. ADVISOR is a software package that allows investigation of fuel cell operation in driving cycles. However, some details have been sacrificed by assuming enough hydration of the PEFC electrolyte membrane under all operating conditions and constant species concentration during simulation. Another limitation is that it requires input such as the required power to meet the propulsion and auxiliary component loads, which is very difficult to specify, and preferably could have been an output of the calculation.

Xue and Dong [49], on the other hand, have modelled a fuel cell propulsion system for a bus. The system is composed of PEFC stacks and modules for hydrogen supply, air supply, cooling and control. The electrochemical model is based on an empirical model of the Ballard Mark V PEFC; the coefficients of which were evaluated using experimental data. The lumped semi-empirical steady-state model for the entire system was used to analyse the power output, efficiency and capital cost.

3.5.2.2 Fuel cell hybrid vehicles

There are several modelling studies on fuel cell hybrid vehicles. Some of the models were used to determine the *degree of hybridisation*, which is the relative size between the fuel cell and the battery or supercapacitor [10,17]. For example, Wu and Gao [10] have used a lumped semi-empirical dynamic model to determine the number of fuel

cell units and supercapacitor units in a hybrid automobile power train consisting of a PEFC stack, a supercapacitor bank, a DC/DC converter, an inverter, an AC motor and a transmitter. Kim et al. [17], on the other hand, have employed a lumped empirical dynamic model to size the fuel cell and the battery of a hybrid mini-bus power train composed of a PEFC stack, a battery bank, a DC/DC converter, and equipment for fuel and air supply and heat and water management. Although both studies have sized the components comprising the hybrid system, the objective of the former was to obtain the lowest total cost whilst the aim of the latter was to achieve the highest system efficiency.

The effect of the size of the other components on the performance of the system has also been a subject of interest. For instance, Kim and Peng [16] have investigated the effect of the number of fuel cells and the compressor diameter on the efficiency of a fuel cell/battery hybrid system using a lumped empirical steady-state model. The system consists of a PEFC stack, a battery, a compressor, cooling/heating devices and equipment for water management. The electrochemical model is based on an empirical voltage-current data set gathered from a test bench, whilst the battery model is built using the SAFT Li-ion battery test data.

In some studies, a power management strategy has been formulated using a model for a hybrid system [16,18]. Schell et al. [18], for example, have employed a lumped semi-empirical dynamic model to formulate a power management strategy for a hybrid vehicle propulsion system consisting of a PEFC stack, a Li-ion battery bank, and a peak traction system. The model was implemented in MATLAB/Simulink environment [91]. In this study, the fuel processing subsystem was not considered because it was assumed that the system has sufficient hydrogen supply at all times and the dynamics associated with the fuel processing system does not influence the vehicle performance significantly. In a different study, Kim and Peng [16] have considered the effect of power management strategy and component sizing on a vehicle's fuel economy. They have reported that the two factors are interacting, i.e., each set of components' sizes requires a different

power management strategy to achieve minimum fuel consumption.

3.5.2.3 Fuel cell auxiliary power units

Fuel cell systems have also been modelled as auxiliary power units in vehicles [48, 52, 70, 75]. Mazumder et al. [75] have developed a mechanistic, 2-D, dynamic model for a SOFC-based power conditioning system for vehicular auxiliary power units (APUs). The system comprises of a planar SOFC, balance-of-plant, power electronic subsystem, and application load. The model was implemented in MATLAB/Simulink [91] with SimPowerSystem [92] and gPROMS [93] with gO:Simulink [94]. The model accepts system inputs such as flow rates, compositions and temperatures of reactant streams, cell geometric parameters and cell current; and computes the spatial distribution of fuel cell properties such as temperature, fuel utilisation and stack voltage with respect to time. A simplified model for fast simulation was derived from the detailed model by transforming the model of the power electronic subsystem from a switching model to an averaged model [95], using polynomial-approximation for the high-order equations for balance-of-plant, and reducing the spatio-temporal SOFC model from two dimensions to one dimension. This resulted in lower computational time at the expense of lower accuracy.

Baratto and Diwekar [70] have also modelled an auxiliary power unit based on SOFC. The model was implemented in Aspen Plus [96], and was used to carry out a sensitivity analysis to identify the design variables for optimisation. The sensitivity of the different design objectives to various design variables was quantified using the Partial Correlation Coefficient calculated on Ranks [97]. The design objectives are efficiency, cost, and impact on the environment and health. The design variables are diesel intake, system pressure, cathode stoichiometric ratio, air preheating temperature, reformer temperature, fuel utilisation in the fuel cell, steam/diesel ratio, SOFC temperature, and steam temperature. The result indicates that air pressure and diesel intake are the variables that have the most influence on the objectives. The only objective that is not

significantly influenced by the diesel intake is the system efficiency.

Some investigators have modelled fuel cell-based APUs for shipboard applications. For example, Tsourapas et al. [52] have developed a lumped semi-empirical dynamic model of an APU made up of a catalytic partial oxidation reformer, a PEFC stack and a catalytic burner, which are integrated in a combined heat and power generation plant. The model was used to analyse the open-loop dynamics of the system, and design a controller that mitigates H₂ starvation and regulates reactor temperatures. Similarly, Frangopoulos and Nakos [48] have investigated the performance of a PEFC-based APU for merchant ship application using a lumped semi-empirical steady-state model. The system consists of a PEFC stack, and subsystems for air compression, hydrogen supply and cooling. Mass and energy balances are used to model the system. The electrochemical model is based on an existing empirical model for the Ballard Mark V stack. A parametric study was performed to analyse the effect of operating temperature and current density on cell and system efficiencies, power density, rate of H₂ consumption and rate of heat rejection by the cooling system.

3.5.3 Modelling of stationary fuel cell systems

Cogeneration or combined heat and power (CHP) is the simultaneous generation of heat and power in a single, integrated system. The principle of CHP is to recover and make use of the waste heat that is typically rejected in a conventional power plant, thereby achieving higher overall efficiency [25, 55, 57, 67, 68, 98]. In addition, CHP generates electricity close to the point of use. Thus, electrical transmission and distribution losses are reduced [57, 68, 98]. CHP technology presents a potential decrease in demand for grid electricity and heating systems based on fossil fuels [68, 98], possible reduction in carbon emissions [57, 65, 67, 98, 99], and cost savings in the long run [56, 98, 100, 101].

Micro-cogeneration or micro-CHP is a subset of cogeneration systems having power output of less than 5 kW_e for residential and small commercial applications [102, 103].

Mini-cogeneration or mini-CHP, on the other hand, is a type of cogeneration installation with power output of more than 5 kW_e but less than 500 kW_e for use in a building or medium-sized business [104].

There are several different CHP technologies including reciprocating engines (e.g., internal combustion engine and Stirling engine), turbines (e.g., gas turbine, steam turbines, and micro-turbines) and fuel cells. All of them consume fuel to produce heat and electricity simultaneously. In the case of engines and turbines, a generator is driven to produce electricity. A fuel cell, on the other hand, generates DC electric power by consuming fuel within the electrochemical cells. Amongst the candidates for CHP applications, fuel cells have the highest electrical efficiency and lowest emissions [98, 104]. Currently, the low temperature PEFC and the high temperature SOFC are the ones most commonly deployed for CHP applications. However, CHP based on MCFC and PAFC have also been reported in the literature.

In Figure 3.2, the models for stationary fuel cell systems are characterised as lumped, semi-empirical and steady-state, except for the model presented in Ref. [59], which is lumped, semi-empirical and dynamic.

3.5.3.1 SOFC-based cogeneration plant

A techno-economic model for a residential grid-connected micro-CHP plant was presented by Hawkes et al. [58]. The system consists of an intermediate-temperature direct internal reforming SOFC stack, power electronics module and a supplementary boiler. The model was used to analyse the annual total cost of meeting given electricity and heat demand profiles.

Palazzi et al. [62] have developed a thermo-economic model for a residential grid-connected micro-CHP plant composed of a fuel processing subsystem, a SOFC stack and post-combustion subsystem. Formulating the model as a mixed integer nonlinear programming problem (MINLP), different fuel processing options, represented as

integer variables, can be selected based on system efficiency and specific investment cost.

The cogeneration plant considered by Riensche et al. [65] consists of a turbo-expander for natural gas, a SOFC stack, its ancillaries, and CO₂ compression. The model simulates the mass flow of components and conditions and calculates the energy demand or energy production.

The model presented by Perdikaris et al. [63] is for a SOFC cogeneration plant integrated with coal hydrogasification. The seven major subsections are hydrogasification with carbonation/reforming, gas recycling/ejector/calcliner, SOFC stack, heat pipes and gas cleaning. The model was used in a parametric study to investigate the effect of sorbent ratio on carbonation conversion, calcination heat duty, fuel utilisation factor in SOFC and overall electrical efficiency of the cycle.

3.5.3.2 SOFC-gas turbine hybrid cogeneration plant

SOFC can be combined with gas turbines to generate additional power. This is promising because the temperature of the streams exiting a SOFC stack and afterburner is suitable for the inlet temperature of the turbine.

Several models have been presented for a SOFC/gas turbine hybrid plant each with a different configuration [19, 21–24]. The system proposed by Burer et al. [19] is composed of a SOFC/gas turbine combined cycle, a compression heat pump, a compression/absorption chiller and a gas boiler. The model can be used to approximate the annual total cost of power generation, heating and cooling and the annual CO₂ emissions. The hybrid plant modelled by Calise et al. [21] comprises of an internal reforming SOFC stack, a radial gas turbine, centrifugal compressors and plate-fin heat exchangers. The model calculates the energy, entropy and exergy flow rates of the streams and estimates capital cost of each component.

A SOFC stack, gas turbine, double pipe heat exchanger and compressor comprise the

SOFC/gas turbine hybrid modelled by Koyama and Kraines [22]. The model can be used to solve for the cost of electricity generation and the rate of CO₂ emissions for a given electricity demand. The hybrid plant of Yi et al. [23] is composed of an internal-reforming tubular SOFC, an intercooled gas turbine, a humidifier and other auxiliary components. The model was implemented in Advanced Power System Analysis Tool (APSAT) simulation software [105] and can be used to analyse the system efficiency. Zhao et al. [24] have modelled a hybrid system made up of a SOFC stack, a gas turbine, heat exchangers and air compressor. The model can be used to investigate the system efficiency and the power output of the system.

3.5.3.3 PEFC-based cogeneration plant

A model of a CHP plant based on PEFC is presented by Godat and Marechal [51]. The plant consists of three subsystems: a fuel processing subsystem which includes a steam reformer, a water gas shift reactor and a preferential oxidation reactor, a PEFC subsystem and a post-combustion subsystem. The model can be used to analyse the behaviour of efficiency with respect to steam-to-carbon ratio, steam reformer temperature, PEFC temperature and fuel utilisation.

Oyarzabal et al. [61] have developed a thermodynamic, geometric and economic models of a PEFC cogeneration system. The system is composed of a PEFC stack, fuel and air compressors, an exhaust expander, a steam reformer, a shift reactor, a PROX reactor and several mixers and heat exchangers. The model can be used to determine the life cycle cost of the system.

Mohamed and Koivo [73] have modelled a micro-grid comprised of a PEFC stack, a wind turbine, a micro-turbine, a diesel generator, PV array and battery storage. The economic model, which describes the costs associated with emissions, startup, operation, maintenance, daily income and outgo from sold or purchased electricity supports proper power management of the micro-grid.

Wallmark and Alvfors [68] have applied pinch analysis to model a PEFC/CHP system

consisting of a fuel cell stack, steam reformer, water gas shift, preferential oxidation reactor, air compressor, water deioniser and filter, air fan and water pump, rectifier and inverter. Pinch analysis involves evaluation and design of a heat exchanger network to obtain a solution with high heat utilisation. In the considered system, the heat exchanger network connects the reformer, burner, gas cleaning, hot water storage and the PEFC stack. By deploying heat exchangers efficiently, reductions in capital and energy cost can be achieved.

3.5.3.4 PEFC-gas turbine hybrid cogeneration plant

Marechal et al. [25] have presented a thermo-economic model of a PEFC-gas turbine hybrid plant. The plant is composed of the following subsystems: fuel processing, PEFC stack and post combustion. The MINLP model allows investigation of different technologies or combination of technologies for converting fuel into electricity. For example, the fuel processing step can proceed either by steam reforming or by partial oxidation and reforming. The alternatives for fuel post processing step include a low temperature water gas shift reaction or medium temperature shift reaction or two-step reactor systems with high temperature and low temperature reactors. For the post combustion step, the options are using either a conventional post combustion system or an air compressor, or a gas turbine. The model selects a particular configuration depending on the values of the system efficiency and the specific cost of electricity produced by the system.

3.5.3.5 Other hybrid cogeneration plant based on PEFC

Petruscu et al. [64] have simulated the performance of a solar Stirling power plant using hydrogen/oxygen fuel cells. The system is composed of a solar module (which includes a solar energy concentrator, receiver, solar Stirling engine and electric generator), electrolyser to produce electrical energy using previously stored hydrogen and a PEFC stack. Kaviani et al. [27] have demonstrated the potential of coupling a PEFC

stack with renewable power sources. The modelled wind-PV-PEFC hybrid system has six major components: wind turbine generators, PV arrays, electrolyser, hydrogen storage tank, PEFC stack and DC/AC converter and inverter. The model can be used to estimate the total annual cost and the reliability of the modelled power generator. Subramanyan et al. [26] have presented a model for a SOFC-PEFC hybrid system. The plant is made up of a fuel pre-reformer, a SOFC stack, a low temperature shifter, a selective catalytic oxidiser, a PEFC and a heat recovery steam generator. The model can be used to investigate the capital cost, cost of electricity, CO₂ emissions and overall efficiency of the plant.

3.5.3.6 Cogeneration plant based on other types of fuel cell

Au et al. [55] have investigated the influence of operating temperature on the efficiency of CHP plant composed of five subsystems: MCFC stack, anode gas recirculation and moisture separation, heat exchange reformer and fuel preheat, cathode gas recirculation, expander and waste heat reboiler. Verda and Nicolini [67] have performed thermo-economic modelling of a MCFC/micro gas turbine hybrid for the combined production of electricity and hydrogen. The system includes a MCFC stack, a reformer, a catalytic burner, heat exchangers and a pressure swing adsorber. The model can be used to analyse the plant efficiency and the average cost of electricity. Gamou et al. [56] have presented a model for a PAFC cogeneration system. The system comprises a PAFC stack, a single-stage absorption refrigerator, a boiler and a radiator. The model can be used to investigate the influence of uncertainties in energy demands on a system economics and equipment capacity.

3.6 System optimisation

Optimisation is the determination of the values of design variables or decision variables, which correspond to and provide the maximum or minimum of one or more desired

objectives [106]. As shown in Figure 3.1, optimisation and modelling are strongly intertwined. The nature of the model determines the optimisation algorithm to be used. A good model can make an optimisation almost trivial, whereas a bad one can make optimisation difficult or impossible [107]. Modelling is often more challenging than optimisation because of the availability and advancement in numerical algorithms and software. Furthermore, optimisation often involves the evaluation of a large number of design alternatives, which translates into high computational requirements. Thus, a fuel cell system model for optimisation should be simple enough to allow for repeated calculations during optimisation, whilst complex enough to differentiate accurately between alternative designs. Moreover, the design solutions obtained from optimisation are only useful within the limitations of the model assumptions. The quality of the solution mainly depends on how well the model has been formulated. Many details are neglected because of modelling difficulties. The assumptions need to be well understood to understand the model's limitation and accurately interpret the results. Siegel [44] presents an exhaustive list of assumptions commonly used in fuel cell modelling.

There are several approaches used for model-based design and optimisation. For fuel cell systems, the most commonly used methods are parametric analysis, single-objective optimisation and multi-objective optimisation. Table 3.2 provides an overview of the optimisation studies performed on fuel cell systems.

Table 3.2: Summary of optimisation studies performed on fuel cell systems.

Ref.	System application	System	Model application*	Objectives	Design variables
Alotto et al. [74]	Portable	DMFC system	MOO	Cell duration between two consecutive fuel charges and methanol crossover	Current density, methanol concentration and catalyst loadings
Au et al. [55]	Stationary	MCFC CHP plant	PS	System efficiency	Temperature
Baratto and Diwekar [70]	Transportation	SOFC-based APU	MOO	System efficiency, total cost, and environmental and health impact	Diesel intake, system pressure, cathode stoichiometric ratio, air preheating temperature, reformer temperature, fuel utilisation in the fuel cell, steam/diesel ratio, SOFC temperature and steam temperature
Burer et al. [19]	Stationary	SOFC/gas turbine hybrid plant	MOO	Annual total cost and annual CO ₂ emission rate	SOFC fuel flow, pinch heat recovery, SOFC temperature and SOFC pressure
Calise et al. [20, 21]	Stationary	SOFC/gas turbine hybrid plant	SOO	Annual total cost	Geometric and thermodynamic decision variables
Chachuat et al. [71]	Portable	SOFC system	SOO	Specific energy density of the fuels	System temperature and nominal power demand
Frangopoulos and Nakos [48]	Transportation	PEFC-based APU	MOO	System efficiency, power density and present worth cost	Current density and temperature
Gamou et al. [56]	Stationary	PAFC CHP plant	SOO	Annual total cost	Equipment capacities and utility demands
Godat and Marechal [51]	Stationary	PEFC CHP plant	PS	System efficiency	Steam to carbon ratio, steam reformer temperature, PEFC temperature and fuel utilisation
Hawkes and Leach [57]	Stationary	SOFC CHP plant	SOO	Lifetime cost	power output, natural gas consumption, and imported power from the grid

Ref.	System application	System	Model application*	Objectives	Design variables
Hawkes et al. [58]	Stationary	SOFC micro-CHP plant	SOO	Annual total cost	Capacities of the components of the plant
Jemei et al. [76]	Transportation	PEFC electric vehicle propulsion system	PS	Stack voltage	Gas flow rates, air humidity level, stack temperature and current density
Kaviani et al. [27]	Stationary	PEFC/wind/PV hybrid plant	SOO	Annual total cost	Number of wind turbine generators, number of installation angle of PV arrays, and capacities of electrolyser, hydrogen tank, fuel cell, and DC/AC converter
Kim et al. [17]	Transportation	PEFC/battery hybrid vehicle propulsion system	SOO	System efficiency	Capacity of the fuel cell stack and number of sub-batteries
Kim and Peng [16]	Transportation	PEFC/battery hybrid vehicle propulsion system	SOO	Fuel economy	Number of fuel cells and compressor diameter
Koyama and Kraines [22]	Stationary	SOFC/gas turbine hybrid plant	MOO	Cost of electricity and CO ₂ emissions	SOFC pressure, SOFC air utilisation ratio, rated output-to-maximum output ratio for SOFC, air inlet temperature to SOFC, fuel inlet temperature to SOFC and SOFC system generation capacity
Lagorse et al. [15]	Portable	PEFC/PV/battery hybrid system	SOO	Total cost	PV power, battery capacity, fuel cell power, PV tilt angle, and fuel cell starting and stopping battery state of charge
Marechal et al. [25]	Stationary	PEFC/gas turbine hybrid plant	MOO	System efficiency and specific cost of electricity	Temperature, pressure, component ratio in the streams, and integer variables denoting different technologies and interconnection between them

Ref.	System application	System	Model application*	Objectives	Design variables
Mazumder et al. [75]	Transportation	SOFC-based APU	PS	Temperature distribution, fuel utilisation and stack voltage	Flow rates, compositions and temperatures of reactant streams, cell geometric parameters, and cell current
Mohamed and Koivo [73]	Stationary	Micro-grid (PEFC, wind turbine, micro turbine, diesel generator, PV array, and battery storage)	SOO	Aggregate of emissions cost, startup cost, operation and maintenance cost, daily income and outgo from sold or purchased power	power output of the generation units making up the micro-grid
Oyarzabal et al. [60, 61]	Stationary	PEFC CHP plant	SOO	Lifetime cost	Temperature of the streams, fraction of methane combusted to heat by the steam reformer, change in temperature of the reformat in the steam reformer, rate of hydrogen production, power required for fuel processing, stack operating pressure and active area of the membrane
Palazzi et al. [62]	Stationary	SOFC CHP plant	MOO	System efficiency and investment cost	Temperature, flows, pressure and conversion in the streams, and integer variables representing the use of a technology or an interconnection between them
Schell et al. [18]	Transportation	PEFC/battery hybrid vehicle propulsion system	SOO	Fuel economy	Vehicle speed, wheel speed, battery state of charge, fuel cell voltage and battery power limit
Subramanyan et al. [26]	Stationary	SOFC/PEFC hybrid plant	MOO	Capital cost, system efficiency and SOFC current density	Fuel utilisation, equivalence ratio, pressure of the PEM, fuel flow and air flow

Ref.	System application	System	Model application*	Objectives	Design variables
Tsourapas et al. [52]	Transportation	PEFC-based APU	SOO	System efficiency	Fuel and air flow rates
Vasallo et al. [14]	Portable	PEFC/battery hybrid system	SOO	Life cycle cost	Size of stack and battery
Verda and Nicolin [67]	Stationary	MCFC/micro gas turbine hybrid plant	MOO	System efficiency and average cost of electricity	Pressure ratio, inlet turbine temperature, reforming temperature, MCFC reaction temperature, biogas mass flow rate, ratio between inlet compressor air and air extraction to cathode, ratio between air to cathode and biogas mass flow rate to MCFC
Weber et al. [77]	Stationary	SOFC polygeneration plant (provides electricity, heating and cooling)	MOO	Total cost and CO ₂ emissions from operation and manufacturing	Size of devices
Wu and Gao [10]	Transportation	PEFC/supercapacitor hybrid vehicle propulsion system	SOO	Total cost	Number of fuel cell units and supercapacitor units
Xue and Dong [49]	Transportation	PEFC electric vehicle propulsion system	MOO	power output and average efficiency	Active membrane area and air stoichiometric ratio
Yeh and Chen [12]	Portable	Passive DMFC system	PS	Power density	Catalyst loading, catalyst layer thickness, PEM thickness and methanol concentration
Yi et al. [23]	Stationary	SOFC/gas turbine hybrid plant	PS	System efficiency	Moisture content of the gas out of humidifier, excess air, overall compression ratio and intercooler location

Ref.	System application	System	Model application*	Objectives	Design variables
Zhao et al. [24]	Stationary	SOFC/gas turbine hybrid plant	PS	System efficiency and power output	SOFC operating temperature, temperature ratio and heat transfer coefficients ratio of the gas turbine cycle, and parameters related to the heat transfer between subsystems and the heat leak to the surroundings

* PS: Parametric study; SOO: Single-objective optimisation; MOO: Multi-objective optimisation

3.7 Parametric study

In a parametric study, the design solutions are obtained by changing one or more parameters whilst fixing the value of the remaining ones. By doing so, the impact of a parameter or a combination of parameters on the design objectives can be assessed. A parametric study is usually performed prior to formal optimisation (i.e., using a numerical method) to explore the nature of the problem, narrow down the number of design variables and identify their appropriate ranges, and specify the design constraints. However, because some of the parameters are held constant, there is no guarantee that the maximum or the minimum solution is achieved. In other words, the optimal solutions from parametric studies are specific to the parameter combination used in the analysis. Several parametric studies have considered system efficiency as the design objective [23,24,51,55]. In Ref. [55], the influence of the operating temperature on the efficiency of a portable DMFC system was investigated. The temperature is varied over the range between 600–700°C whilst keeping the rest of the system the same as far as possible. It was reported that the effect of temperature on system electrical efficiency is small in the considered range because in the formulation of the model the production of electricity was given more importance than the production of heat. In Ref. [51], the efficiency of a PEFC cogeneration plant was investigated with respect to steam-to carbon ratio, temperature of the reformer and stack, and fuel utilisation. The parametric studies performed by Yi et al. [23] and Zhao et al. [24] have both analysed the system efficiency of a SOFC/gas turbine hybrid cogeneration plant. The former have considered the moisture content of gas leaving the humidifier, excess air, overall compression ratio and intercooler location as the design variables; whilst the latter have regarded the SOFC operating temperature, temperature ratio and heat transfer coefficient ratio of the gas turbine cycle, and parameters related to heat transfer between subsystems and heat loss to the surroundings.

In other parametric analyses, such as those performed by Yeh and Chen [12] and Zhao et

al. [24], the design objective is the power density. In Ref. [12], the influence of catalyst loading, catalyst layer thickness, PEM thickness and methanol concentration on power density of a portable DMFC system was analysed, with the cathode catalyst loading and cathode catalyst layer thickness having the most effect. The study conducted by Maxoulis et al. [50] investigated the effects of stack size, reaction rate constant and water concentration in the channels, on stack temperature rise, cell voltage and fuel consumption of a vehicle propulsion system based on PEFC. Furthermore, Mazumder et al. [75] have varied the flow rates, compositions and temperatures of reactant streams to determine their effects on spatial distribution of temperature, fuel utilisation and stack voltage of a SOFC-based APU.

3.8 Single-objective optimisation

Single-objective optimisation identifies a single alternative, which corresponds to the minimum or maximum value of a single objective. This type of optimisation can provide useful insights into the nature of the problem. However, it cannot provide a set of alternative solutions that trade off different objectives against each other.

A single-objective optimisation problem is typically expressed as:

$$\begin{aligned}
 \min_{\mathbf{x}} \quad & f(\mathbf{x}) & (3.1) \\
 \text{subject to} \quad & h_j(\mathbf{x}) = 0, \quad j = 1, 2, \dots, p \\
 & g_k(\mathbf{x}) \leq 0, \quad k = 1, 2, \dots, r \\
 & \mathbf{x}^L \leq \mathbf{x} \leq \mathbf{x}^U
 \end{aligned}$$

In this formulation, \mathbf{x} is an n -dimensional vector of design variables (also referred to as decision variables), $\mathbf{x} = (x_1, x_2, \dots, x_n)$, f is the objective function, $h_j, j = 1, 2, \dots, p$, is the set of equality constraints, and $g_k, k = 1, 2, \dots, r$, is the set of inequality constraints. Some applications may involve maximisation of an objective, which can be reformulated

by multiplying by -1 or taking the reciprocal (whilst ensuring that the denominator does not become zero) as the objective to be minimised. The design variables can either be all continuous within the respective lower and upper bounds (\mathbf{x}^L and \mathbf{x}^U) or a mixture of continuous, binary (i.e., 0 or 1) and integer variables.

For fuel cell systems, the equality constraints, h_j , arise from mass and energy balances, electrochemical equations, equilibrium or thermodynamic relations, mass and heat transport expressions, amongst others, which can be algebraic and/or differential equations. The inequality constraints, g_k , are due to application-specific requirements and equipment, material, safety and other considerations. Examples of inequality constraints include the requirement that the temperature difference across the membrane should be lower than a specified value to avoid membrane degradation, and the membrane water content should be above a certain value to prevent membrane dehydration.

There is a wide variety of methods for solving single-objective optimisation problems. The choice of the solution method mainly depends on the nature of the model. Biegler and Grossman have provided an overview of the optimisation methods used in process systems engineering [108], and have discussed some of the issues and challenges in optimisation [109].

3.8.1 Cost optimisation

The majority of optimisation studies have considered cost as a design objective.

Hawkes and Leach [57] have minimised the net present value of the cost of meeting the electrical and heat demand over the lifetime of a SOFC-based cogeneration system. The lifetime cost takes into account the operating and maintenance costs and the capital cost of the CHP generator and boiler. The design variables are power output, natural gas consumption, and power imported from the grid. In a related study, Hawkes et al. [58] have minimised the equivalent annual cost of meeting a given electricity and heat demand considering the capacities of the components of a SOFC micro-cogeneration

system as the design variables. In this work, the total cost is made up of capital cost, maintenance cost, fuel cost for the stack and supplementary boiler, electricity import cost minus the revenue from electricity export.

Other studies that have minimised the total cost include Refs. [15,20,27,56]. Calise et al. [20] have minimised the total annual cost of a SOFC/gas turbine hybrid cogeneration plant with respect to the geometric and thermodynamic design variables using a genetic algorithm [110]. The total cost was formulated as the sum of the amortised capital cost and fuel cost, minus the thermal energy savings. Gamou et al. [56] have determined the equipment capacities and utility demands that minimise the annual total cost, which was taken as the sum of the annualised capital and operating costs, subject to meeting the energy demands on a PAFC cogeneration system.

Using a Particle Swarm Optimisation approach [110], Kaviani et al. [27] have minimised the annual total cost (investment, replacement, operation, maintenance and loss of load) of a PEFC/wind/PV hybrid cogeneration system, with respect to the number of wind turbine generators, number and installation angle of PV arrays, and capacities of electrolyser, hydrogen tank, fuel cell, and DC/AC converter. The problem is subject to the maximum allowable Equivalent Loss Factor, which is a reliability index that gives the ratio of the effective forced outage hours to the total number of hours.

Lagorse et al. [15] have optimised the size of the different components of a portable PEFC-PV-battery hybrid system. The total cost, which is the objective to be minimised, is made up of the PV cost, the battery cost, the fuel cell cost and the penalty cost. The penalty cost depends on two cases. First, if the battery capacity is large enough the penalty cost is associated with the surplus of energy. Excess energy implies that the system is oversized and the PV power could be reduced to obtain a cheaper system. Otherwise, if the capacity of the battery is insufficient, the penalty cost depends on the minimum state of charge of the battery. The optimisation problem is solved using two algorithms: a genetic algorithm to approximate the global optimum and then a simplex algorithm to improve on the previous results.

The objective that Mohamed and Koivo [73] considered was an aggregate of costs of emissions, startup, operation and maintenance, daily income and outgo from sold or purchased electricity associated with a micro-grid consisting of a PEFC stack, wind turbine, micro-turbine, diesel generator, PV array and battery storage. The Mesh Adaptive Direct Search algorithm was used to minimise the cost objective with respect to the power output of the components making up the power grid whilst constraining the system to meet the customer demand and safety of the system.

The life cycle cost has also been considered as a design objective [14, 61]. Oyarzabal et al. [61] have minimised the life cycle cost of a PEFC-based cogeneration plant using a decomposition method with a gradient-based optimisation algorithm. The design variables include the temperature of the streams, the fraction of methane combusted to heat the steam reformer, the change in temperature of the reformat, the rate of hydrogen production, the power required for fuel processing, the stack operating pressure and active area of the membrane. Vasallo et al. [14], on the other hand, have determined the optimal size of a portable PEFC-supercapacitor hybrid system based on a minimum life-cycle cost criterion. An existing sizing tool for hybrid systems, called HOMER [111], was used to determine a minimum-cost backup power system given a load profile and backup time.

3.8.2 System efficiency optimisation

Several optimisation studies have considered the system efficiency as a design objective [17, 52]. Kim et al. [17] have proposed a methodology to optimise the size of a PEFC/battery hybrid system for minibus propulsion. The objective is to maximise the efficiency of a minibus during one cycle of a given driving schedule. The decision variables are the capacity of the stack and the number of sub-batteries. Also, Tsourapas et al. [52] have maximised the system efficiency of a PEFC-based APU using a modified-gradient method considering the fuel and air flow rates as the design variables. The optimal steady-state operating point with respect to the overall system efficiency was

subsequently used as a set point for a controller that was designed to regulate the reactor temperature and minimise the hydrogen starvation.

Instead of the system efficiency, the fuel economy or the fuel consumption is typically considered as an objective for the design of a transportation fuel cell system. Using stochastic dynamic programming [110], Kim and Peng [16] have identified an optimal power management strategy and optimal sizes of the components in a PEFC-battery hybrid propulsion system so that the hydrogen consumption is minimised whilst satisfying the constraints on vehicle drivability. Similarly, Schell et al. [18] have applied stochastic dynamic programming to the energy management of a PEFC-battery hybrid propulsion to optimise the fuel economy whilst ensuring good drivability. The problem was formulated as a constrained dynamic optimisation problem with the fuel economy as the design objective subject to the higher-priority goals of drivability and charge sustaining, and local considerations such as fuel cell reliability and battery life. The design variables are wheel speed, battery state of charge, fuel cell voltage and battery power limit.

3.9 Multi-objective optimisation

The main focus of optimisation of fuel cell systems so far has been optimisation for one objective at a time. However, practical applications of fuel cell systems involve several objectives to be considered simultaneously. The appropriate objectives for a particular application are often conflicting, which means achieving the optimum for one objective requires compromise on one or more other objectives. Multi-objective optimisation is the determination of the values of decision variables which correspond to and provide the optimum of more than one objective [106, 112, 113]. Unlike single-objective optimisation, which gives a unique solution (or multiple optima such as local and global optima in the case of non-convex problems), there will be many optimal solutions for a multi-objective optimisation problem; the exception is when the objectives are not

conflicting, in which case only one unique solution may be expected.³

The formulation of a multi-objective optimisation is similar to Eq. 3.1 except that it involves two or more objective functions

$$\begin{aligned} \min_{\mathbf{x}} \quad & f_i(\mathbf{x}), \quad i = 1, 2, \dots, m \\ \text{subject to} \quad & h_j(\mathbf{x}) = 0, \quad j = 1, 2, \dots, n \\ & g_k(\mathbf{x}) \leq 0, \quad k = 1, 2, \dots, p \\ & \mathbf{x}^L \leq \mathbf{x} \leq \mathbf{x}^U \end{aligned} \tag{3.2}$$

The solutions of a multi-objective optimisation problem are known as the Pareto-optimal solutions or, less commonly, Edgeworth-Pareto, after the two economists, Edgeworth and Pareto, who developed the theory in the late 19th century [106, 112, 113]. These solutions are also referred to as non-dominated, non-inferior, efficient or simply Pareto solutions. The extrema of the Pareto front consist of solutions which are equally good in a sense that each one of them is better than the rest in at least one objective. This implies that one objective improves whilst at least one other objective worsens when one moves from one optimal solution to another. Designers and engineers will then be able to choose one of the optimal solutions with the full knowledge of the variation of conflicting objectives besides their own experience and other considerations which could not be included in the optimisation problem.

3.9.1 Methods

Many methods are available for solving multi-objective optimisation problems. Many of them involve converting the multi-objective optimisation into one or a series of single-objective optimisation problems. Each of these problems involves the optimisation of a *scalarising* function, which is a function of the original objectives, by a suitable method

³In some cases, there may be multiple solutions even if the objectives are not conflicting. There may be a continuum of points in the decision space for which all the points have the same objective function values. This also applies to single-objective optimisation.

for single-objective optimisation. There are many ways of defining a scalarising function, and therefore many multi-objective optimisation approaches exist. Although the scalarisation approach is conceptually simple, the resulting single-objective optimisation problems may not be easy to solve.

Available methods for multi-objective optimisation can be classified in different ways. One of them is based on the role of the decision maker in solving the multi-objective optimisation problem. This particular classification, adopted by Miettinen [113] and Diwekar [112], is shown in Figure 3.3. The decision maker can be one or more individuals who will select one of the Pareto-optimal solutions for implementation based on their experience and other consideration not included in the multi-objective optimisation problem.

As shown in Figure 3.3, multi-objective optimisation methods are classified into two main groups: generating methods and preference-based methods. The generating methods do not require any inputs from the decision maker. The solutions obtained are then presented to the decision maker for selection. On the other hand, preference-based methods use the preferences specified by the decision maker at some stage/s in solving the multi-objective optimisation problem.

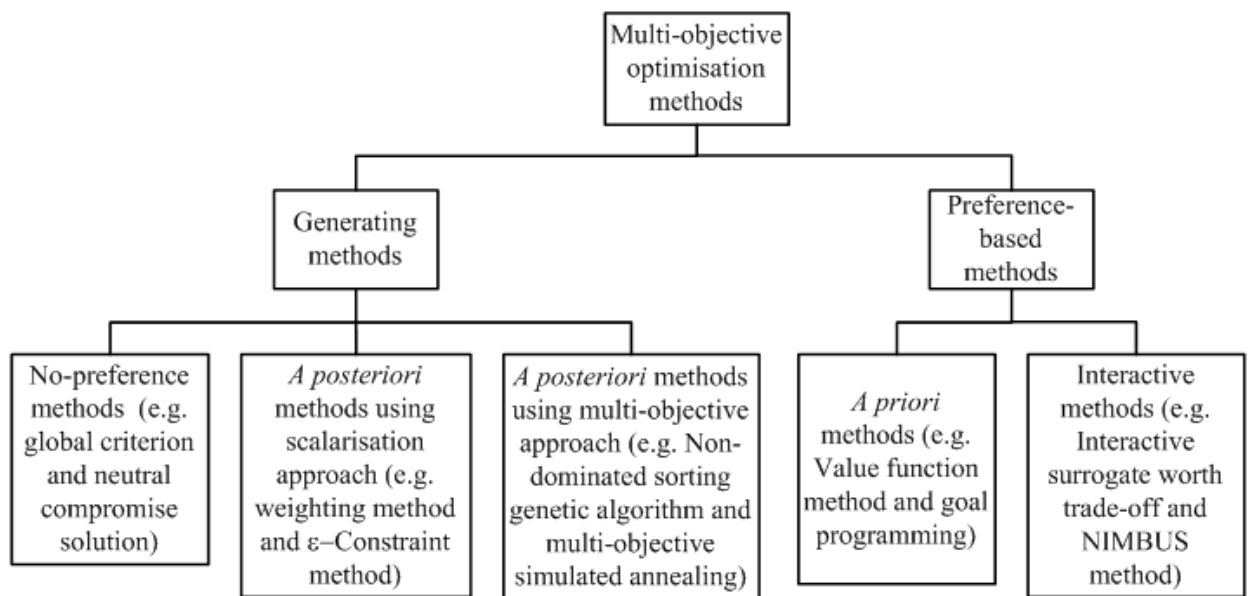


Figure 3.3: Classification of multi-objective optimisation methods.

3.9.1.1 Generating methods

The generating methods are further divided into three sub-groups, namely, no-preference methods, *a posteriori* methods using the scalarisation approach and *a posteriori* methods using the multi-objective approach.

No-preference methods

These methods do not require the relative priority of objectives. Although a particular method gives only one Pareto-optimal solution, a few Pareto-optimal solutions can be obtained by using different no-preference methods. Methods in this sub-group include global criterion [114] and neutral compromise solution [115].

A posteriori methods using the scalarisation approach

These methods convert a multi-objective optimisation problem into a single-objective optimisation problem, which can then be solved by a suitable method to find one Pareto-optimal solution. A series of such single-objective optimisation problems will have to be solved to find the other Pareto-optimal solutions. The ε -constraint [106, 116] and weighting methods [106, 116] belong to this sub-group.

A posteriori methods using the multi-objective approach

These methods rank multiple trial solutions simultaneously based on objective values and finally find many Pareto-optimal solutions. They include population-based methods such as non-dominated sorting genetic algorithm [117] and multi-objective simulated annealing [118].

3.9.1.2 Preference-based methods

The preference-based methods, on the other hand, are further divided into two sub-groups, namely, *a priori* methods and interactive methods.

***A priori* methods**

These methods seek for the preferences of the decision maker and include them in the initial formulation of a suitable single-objective optimisation problem. Examples of *a priori methods* value functions [113] and goal programming [119].

Interactive methods

These methods require interaction with the decision maker during the solution of the multi-objective optimisation problem. After an iteration, the decision maker reviews the Pareto-optimal solution(s) obtained and articulates, for example, further change (either improvement, compromise or none) desired in each of the objectives. These preferences of the decision maker are then incorporated in formulating and solving the optimisation problem in the next iteration. At the end of the iterations, the interactive methods provide one or several Pareto-optimal solutions. Examples of these methods are interactive surrogate worth trade-off method [120] and the NIMBUS method [121].

The relative merits and limitations of group of methods are summarised in Table 3.3.

Table 3.3: Main features, merits and limitations of multi-objective optimisation methods.

Methods	Features, merits and limitations
No preference methods (<i>e.g.</i> , global criterion and neutral compromise solution)	These methods, as the name indicates, do not require any inputs from the decision maker either before, during or after solving the problem.
<i>A posteriori</i> methods using scalarisation approach (<i>e.g.</i> , weighting and ε -constraint methods)	These classical methods require solution of single-objective optimisation problems many times to find several Pareto-optimal solutions. ε -constraint method is simple and effective for problems with a few objectives. Weighting method fails to find Pareto optimal solutions in the non-convex region although modified weighting methods can do so. It is difficult to select suitable values of weights and ε . Solution of the resulting single-objective optimisation problem may be difficult or non-existent.
<i>A posteriori</i> methods using multi-objective approach (many based on evolutionary algorithms, simulated annealing, ant colony techniques, <i>etc.</i>)	These relatively recent methods provide many Pareto-optimal solutions and thus more information is useful for decision making is available. Role of the decision maker is after finding optimal solutions, to review and select one of them. Many optimal solutions found will not be used for implementation, and so some may consider it as a waste of computational time.
<i>A priori</i> methods (<i>e.g.</i> , value function, lexicographic and goal programming methods)	These have been studied and applied for a few decades. Their recent applications in engineering are limited. These methods require preferences in advance from the decision maker, who may find it difficult to specify preferences with no/limited knowledge on the optimal objective values. These methods may provide one Pareto-optimal solution consistent with the given preferences, and so may be considered as efficient.
Interactive methods (<i>e.g.</i> , interactive surrogate worth trade-off and NIMBUS methods)	The decision maker plays an active role during the solution by interactive methods, which are promising for problems with many objectives. Since these methods may find one or a few optimal solutions meeting the preferences of the decision maker and not many other solutions, one may consider them as computationally efficient. Time and effort from the decision maker are continually required, which may not always be practical. The full range of Pareto optimal solutions may not be available.

3.9.2 Multi-objective optimisation in fuel cell systems design

3.9.2.1 Bi-objective optimal design

The majority of the multi-objective optimisation studies in the literature involve two objectives. The study performed by Burer et al. [19] have simultaneously minimised the total cost and the CO₂ emissions rate of a SOFC/gas turbine hybrid plant with respect to SOFC fuel flow, pinch heat recovery, SOFC temperature and SOFC pressure using a multi-objective evolutionary algorithm [122]. Koyama and Kraines [22] have investigated the tradeoff between the cost of electricity generation and CO₂ emissions of a SOFC/gas turbine hybrid plant to meet a given electricity demand using a queueing multi-objective optimisation [123]. The design variables are the SOFC pressure, air utilisation ratio, ratio of rated output-to-maximum output, air and fuel inlet temperatures, and generation capacity.

Marechal et al. [25] have considered the system efficiency and the specific cost of electricity of a PEFC/gas turbine hybrid plant as the design objectives. The design variables are the temperature, pressure, stream component ratios and integer variables denoting different technologies and the interconnections between them. The problem was solved using a multi-objective evolutionary algorithm. Using the same numerical method, Palazzi et al. [62] have maximised the system efficiency and minimised the specific investment cost of a SOFC-based cogeneration plant with respect to temperature, flow rate, pressure and conversion in the streams, and integer variables representing the use of a technology or an interconnection between them. Weber et al. [77] have also optimised a linear programming model of a SOFC-based polygeneration plant using a multi-objective evolutionary algorithm. The design objectives are the total cost and CO₂ emissions whilst the design variables are the size of the devices.

Verda and Nicolin [67] have performed multi-objective optimisation of a MCFC/micro gas turbine hybrid plant considering the system efficiency and the average cost of electricity as the design objectives. The design variables include the pressure ratio, inlet

turbine temperature, reforming temperature, MCFC reaction temperature, biogas mass flow rate, ratio between inlet compressor air and air extraction to cathode, ratio between air to cathode and biogas mass flow rate to the MCFC. The optimisation was conducted by separating the plants into two parts: the power components and the heat transfer network; the former was optimised by selecting some design parameters, whilst the latter was calculated using pinch analysis.

Alotto et al. [74] have coupled the model for a portable passive DMFC system with a particle swarm optimiser based on the Tribes algorithm [124] to perform a multi-objective optimisation. The objective is to maximise the duration between two consecutive fuel charges and minimise the methanol crossover. Methanol crossover is a waste of fuel, and the fuel cell lifetime is shortened by catalyst poisoning due to carbon monoxide from crossover methanol oxidation. The current density, methanol concentration and catalyst loading were considered as the design variables.

Xue and Dong [49] have considered the power output and the average efficiency as the design objectives for the joint optimisation of a PEFC-based vehicle propulsion system with the active membrane area and air stoichiometric ratio as the design variables.

3.9.2.2 Tri-objective optimal design

In the work conducted by Frangopoulos and Nakos [48], the system efficiency, power density and present worth cost were considered as the design objectives, whilst the current density and temperature were treated as the design variables. In their study, the interaction between the objectives was not considered; they optimised each objective individually. Also, for each objective, one of the two design variables was treated as a parameter. This resulted in a one-variable, single-objective optimisation problem, which was then solved at different values of the parameter.

Considering the system efficiency, total cost and environmental and health impact, Baratto and Diwekar [70] have conducted a multi-objective optimisation for a SOFC-based APU. The design variables are the diesel intake, system pressure, cathode stoi-

chiometric ratio, air preheating temperature, reformer temperature, fuel utilisation in the fuel cell, steam-diesel ratio, SOFC temperature and steam temperature.

Subramanian et al. [26] have optimised the capital cost, overall efficiency and SOFC current density of a SOFC/PEFC hybrid cogeneration plant considering the fuel utilisation, equivalence ratio, pressure of the PEFC, fuel flow and air flow as the design variables. The multi-objective optimisation was performed using Minimisation of Single-Objective Optimisation problems (MINSOOP), which picks up one of the objectives to minimise whilst the remaining ones are turned into inequality constraints.

3.10 Conclusions

The design of a fuel cell system is a decision-making process, which involves the identification of possible design alternatives and the selection of the most suitable one. A good design is one that meets the design requirements and represents a trade-off amongst the different design objectives. This chapter presented the current state of modelling and computer-based optimisation with regard to fuel cell systems design.

The existing fuel cell models in the literature can be characterised by approach, state, system boundary, spatial dimension and complexity or detail. System-level models are necessary for the investigation of specific applications of fuel cells such as portable, stationary and transportation. A system-level model predicts the behaviour of a fuel cell system, which is composed of different subsystems such as fuel cell stack, fuel supply, oxidant supply, water management, heat management, power conditioning, instrumentation and controls and, in some cases, hybrid components. System-level models are also preferred for use in optimisation because individual components perform differently when operated as part of a system. To date, the majority of the available system-level fuel cell models are lumped, semi-empirical, steady-state and based on either PEFC or SOFC.

Three model-based design approaches commonly used in fuel cell systems design were

also presented: parametric study, single-objective optimisation and multi-objective optimisation. In parametric study, the design solutions are specific to the parameter combination used during the analysis, thus there is no guarantee that an optimal solution is obtained. Single-objective optimisation can identify an optimum value of a single objective but it cannot provide a set of alternative solutions that trade different objectives with each other. Multi-objective optimisation determines a set of trade-off optimal solutions that simultaneously considers conflicting design objectives, also known as a Pareto set.

The remaining chapters in this thesis present in detail the development of models for a single fuel cell, a fuel cell stack, and a fuel cell-based micro-cogeneration system. These models can be used to obtain important information and make informed predictions which can be useful in improving the design of the system. The succeeding chapters also highlight the use of modelling and optimisation in informing system design by generating different design alternatives, thus allowing design engineers to make decisions in a quantitative and rational way.

Chapter 4

Modelling of a PEFC

This chapter presents a two-dimensional, non-isothermal, multi-phase mass and heat transfer model of a PEFC. The model was adopted from the work of Nguyen and White (1993) [125] and forms the framework of the multi-objective optimisation models developed in the subsequent chapters. The model accounts for mass transport of water and gaseous reactants across the membrane and along the flow channels and heat transport from the solid phases to the gases and vice versa along the flow channels. The model describes the water transport across the membrane by electro-osmosis and diffusion, heat transfer from the solid phase to the gas phase and latent heat associated with water evaporation and condensation in the flow channels. For a PEFC, proper water and heat management are crucial for achieving a high power density and high energy efficiency performance. Essential information about appropriate water and heat management can be obtained from the model. In this chapter, the model is used to evaluate the effectiveness of a conventional humidification design.

4.1 Model Description

The model was derived by the application of the mass and energy conservation equations together with the Tafel and Nernst equations. The two flow channels on both sides

of the membrane, one for each electrode, were considered as the model regions. Figure 2.1 shows the schematic diagram of a single PEFC. The modelled region is presented in Figure 4.1. Note that the x-axis represents the direction along the fuel channel, whilst the y-axis denotes the direction across the membrane. The model describes the mass transport of water and gaseous reactants along the flow channels and across the membrane and heat transfer between the solid phases and gases along the flow channels. It also takes into consideration the reactants consumption, water (both liquid and vapour) content, water condensation and evaporation, water transport across the membrane by electro-osmosis (drag) and diffusion, generation of water at the cathode, latent heat involved with the evaporation and condensation of water in the flow channels, and the electrochemical reaction.

4.2 Assumptions

The assumptions in the model are as follows [125]:

1. The temperature of the solid, which includes the electrodes, plates and membrane, is constant and uniform.
2. Plug flow condition exists within the channel.
3. The total pressure is constant, or equivalently, there is no pressure drop along the channels.
4. Heat transfer by conduction in the gas phase is negligible.
5. Only water in the form of vapour can penetrate the electrode/membrane.
6. The electrode layer is “ultrathin”, thus, the gas diffusion through the electrode porous layer can be neglected.
7. The gas mixture behaves ideally.

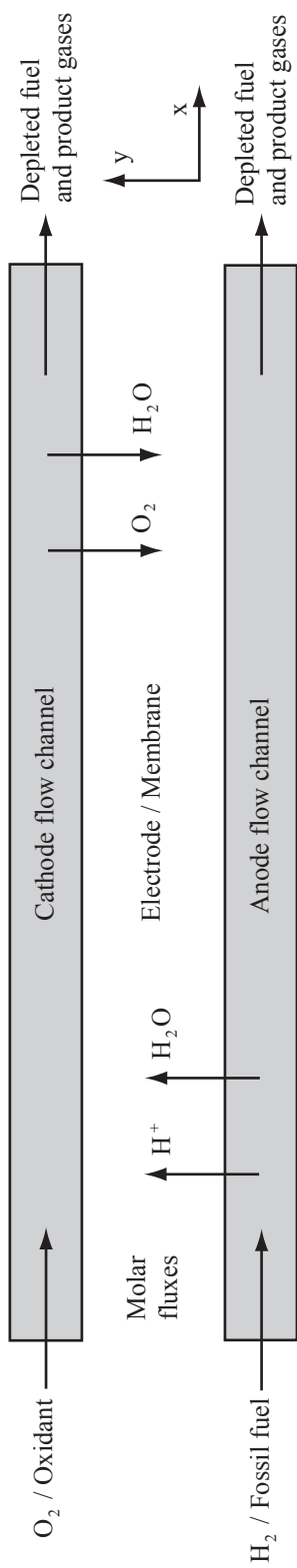


Figure 4.1: Schematic of the region considered in modelling [125].

8. Liquid water is present in the form of small droplets, thus, the volume can be neglected.
9. The electro-osmotic coefficient and the diffusion coefficient of water in the membrane are primarily determined by the activity of the water in the anode flow channel. This is particularly valid at high current densities since at this state the anode side of the membrane is most likely to be drier than the cathode side.
10. The current collectors are highly conductive; therefore there is no voltage drop along the flow channel.

4.3 Governing equations

4.3.1 Mass Balance

The normal flux in the y -direction (across the fuel cell) into or out of the membrane, given by the following equations, brings about change in the number of moles of each component.

$$N_{\text{H}_2, y, a}(x) = \frac{I(x)}{2F} \quad (4.1)$$

$$N_{\text{O}_2, y, c}(x) = \frac{I(x)}{4F} \quad (4.2)$$

$$N_{\text{N}_2, y, c}(x) = 0 \quad (4.3)$$

$$N_{w, y, a}^v(x) = \frac{\alpha I(x)}{F} \quad (4.4)$$

$$N_{w, y, c}^v(x) = \frac{(1 + 2\alpha) I(x)}{2F} \quad (4.5)$$

where F is the Faraday constant and $I(x)$ is the local current density of the fuel cell. The local current density changes along the length of the channel as the membrane conductivity and electrodes overvoltage vary. The parameter α denotes the net water

molecule per proton flux ratio [126]. It can be calculated as follows:

$$\text{Net water flux} = N_{\text{w,y,a}}^{\text{v}}(x) = \alpha \frac{I(x)}{F} = n_{\text{d}} \frac{I(x)}{F} - D_{\text{w}} \frac{dc_{\text{w}}}{dy} \quad (4.6)$$

The first term on the right hand side denotes the effect of migration, whilst the second one represents diffusion. Manipulation of the equation yields the expression for α :

$$\alpha = n_{\text{d}} - \frac{F}{I(x)} D_{\text{w}} \frac{dc_{\text{w}}}{dy} \quad (4.7)$$

This can be further simplified by assuming that the difference in concentration of water between the cathode and anode can be approximated by a single-step linear difference.

$$\alpha = n_{\text{d}} - \frac{F}{I(x)} D_{\text{w}} \frac{(c_{\text{w,c}} - c_{\text{w,a}})}{t_{\text{m}}} \quad (4.8)$$

where t_{m} is the membrane thickness. The parameter n_{d} is the electro-osmotic (drag) coefficient, which is equal to the number of water molecules carried by a proton. This quantity is dependent on the water content in the membrane, which is also a function of the activity of water in the gas phase next to the membrane. Partial dehydration along the anode and saturation along the cathode is most likely to happen especially at high current densities. This is because of the higher water transport rate by electro-osmosis (drag) from the anode to the cathode compared to the rate of back diffusion of water from the cathode to the anode. Physically, this implies that water content at the anode side is lower, thus justifying the 9th assumption stated in the previous section. For this reason, the activity of the water on the anode side can be used to calculate the electro-osmotic coefficient across the membrane. The electro-osmotic coefficient as a function of the activity of water in the anode flow channel [126] can be expressed as:

$$n_{\text{d}} = \begin{cases} 0.0049 + 2.02a_{\text{a}} - 4.53a_{\text{a}}^2 + 4.09a_{\text{a}}^3, & a_{\text{a}} \leq 1 \\ 1.59 + 0.159(a_{\text{a}} - 1), & a_{\text{a}} > 1 \end{cases} \quad (4.9)$$

The parameter D_w [126] is also needed to be able to compute α from Eq. 4.8. This quantity gives the diffusion coefficient of water in the membrane. It is supposed that the diffusion coefficient of water in the membrane is dependent on the water content in the membrane in the same way as the electro-osmotic coefficient.

$$D_w = n_d D^\circ \exp \left[2416 \left(\frac{1}{303} - \frac{1}{T_s} \right) \right] \quad (4.10)$$

The concentration of water as a function of the respective water activity in the electrodes [127] is given by:

$$c_{w,k} = \begin{cases} \frac{\rho_{m,dry}}{M_{m,dry}} (0.043 + 17.8a_k - 39.8a_k^2 + 36.0a_k^3), & a_k \leq 1 \\ \frac{\rho_{m,dry}}{M_{m,dry}} [14 + 1.4(a_k - 1)], & a_k > 1 \end{cases} \quad (4.11)$$

Either the anode or cathode can be substituted for the subscript k . $\rho_{m,dry}$ and $M_{m,dry}$ are the density and equivalent weight of a dry proton exchange, respectively. The water activity in the anode and cathode are as follows:

$$a_a = \frac{x_{w,a} P}{P_{w,a}^{sat}} = \left(\frac{M_{w,a}^v}{M_{w,a}^v + M_{H_2}} \right) \frac{P}{P_{w,a}^{sat}} \quad (4.12)$$

$$a_c = \frac{x_{w,c} P}{P_{w,c}^{sat}} = \left(\frac{M_{w,c}^v}{M_{w,c}^v + M_{O_2} + M_{N_2}} \right) \frac{P}{P_{w,a}^{sat}} \quad (4.13)$$

Eq. 4.14 expresses the water vapour as a function of temperature:

$$\log_{10} P_{w,k}^{sat} = 2.95 \times 10^{-2} (T_k - 273) - 9.18 \times 10^{-5} (T_k - 273)^2 + 1.44 \times 10^{-7} (T_k - 273)^3 - 2.18 \quad (4.14)$$

The change in the number of moles of each reactant can be determined by substituting Eqs. 4.1 - 4.3 to Eq. 4.15. Eq. 4.15 describes the manner in which the reactants are consumed:

$$\frac{dM_i}{dx} = -h N_{i,y,k}(x), \quad i = H_2, O_2, N_2 \quad (4.15)$$

The change in the number moles of liquid water in each flow channel is determined mainly by the evaporation and condensation rates [125]:

$$\frac{dM_{w,k}^l}{dx} = \left(\frac{k_c h d}{RT_k} \right) \left(\frac{M_{w,k}^v}{M_{w,k}^v + M_{H_2/O_2}} P - P_{w,k}^{\text{sat}} \right) \quad (4.16)$$

where k_c is homogeneous rate constant for the condensation and evaporation of water, whilst h and d are the width and height of the channel, respectively. The amount of liquid water in the flow channels is proportional to the difference between the partial pressure and vapour pressure of water. Physically, this means that liquid water will condense if the water vapour partial pressure is higher than its vapour pressure. Similarly, if liquid water is present, and the partial pressure of the water vapour is lower than its vapour pressure, the liquid water will vaporise.

The change in the number of moles of water vapour along the flow channels is described by the following equation:

$$\frac{dM_{w,k}^v}{dx} = -\frac{dM_{w,k}^l}{dx} - hN_{w,y,k}^v(x) \quad (4.17)$$

The following factors affect the amount of water vapour in the flow channels: (1) the reaction of oxygen with proton and electron at the cathode produces water; (2) the water generated at the cathode may diffuse through the membrane to the anode due to concentration difference; (3) the protons migrating from the anode to the cathode bring along with them water vapour (via drag or electro-osmosis); and (4) condensation of water vapour and evaporation of liquid water depending on the difference in partial pressure and vapour pressure. The first term on the right of Eq. 4.17 is the condensation and evaporation of water, while the second term is the net transport of water vapour across the membrane. The transport of water is the net result of the difference or gradient in the concentration and pressure, as well as water molecules being carried by migrating protons.

4.3.2 Energy balance

The local temperature at the anode and cathode can be obtained by:

$$\frac{dT_k}{dx} = \frac{(H_{w,k}^v - H_{w,k}^l) \frac{dM_{w,k}^l}{dx} + Ua(T_s - T_k)}{\sum_i (M_i C_{p,i})} \quad (4.18)$$

where k is either the anode or cathode and U is the overall heat-transfer coefficient. The parameter a in Eq. 4.18 represents the heat-transfer area per unit length of the flow channel and can be computed as follows [125]:

$$a = 2(h + d) \quad (4.19)$$

In Eq. 4.18, the first term in the numerator is the enthalpy change due to condensation of water vapour and evaporation of liquid water, whereas the second term denotes the heat transfer between the mass surface and the fluid. The latent heat, $(H_{w,k}^v - H_{w,k}^l)$ as a function of temperature is given by Eq. 4.20 [125].

$$\begin{aligned} (H_{w,k}^v - H_{w,k}^l) &= 45070 - 41.9(T_k - 273) + 3.44 \times 10^{-3}(T_k - 273)^2 \\ &\quad + 2.54 \times 10^{-5}(T_k - 273)^3 - 8.98 \times 10^{-10}(T_k - 273)^4 \end{aligned} \quad (4.20)$$

4.3.3 Electrochemistry

Using the Nernst and Tafel equations, the effective cell voltage can be expressed as the difference between the thermodynamically reversible cell voltage and the losses due to overpotential.

$$V_{\text{cell}} = V_{\text{oc}} - \frac{RT_s}{0.5F} \ln \left[\frac{I(x)}{I^0 P_{\text{O}_2}(x)} \right] - \frac{I(x) t_m}{\sigma_m(x)} \quad (4.21)$$

where V_{oc} is the open-circuit potential of the fuel cell, I^0 is the exchange current density at one atmosphere of oxygen and $P_{\text{O}_2}(x)$ is the partial pressure of oxygen in the cathode stream. The second term in Eq. 4.21 is the activation overpotential, whilst the third

term is the ohmic overpotential. As can be observed from Eq. 4.21 the cell voltage is inversely proportional to the current density. Since the solid-phase temperature, which is also the fuel cell temperature, is assumed to be constant with time and distance the dependence of exchange current density and the open-circuit potential on temperature was ignored.

The parameter, σ_m , in Eq. 4.21 is the membrane conductivity, which is a function of the water content in the membrane at the anode interface.

$$\sigma_m(x) = \left(0.00514 \frac{M_{m,dry}}{\rho_{m,dry}} c_m(x) - 0.00326 \right) \exp \left[1268 \left(\frac{1}{303} - \frac{1}{T_s} \right) \right] \quad (4.22)$$

Table 4.1: Summary of the governing equations for the PEFC model.

Description	Equation
<i>Anode</i>	
Hydrogen flow rate	$\frac{dM_{H_2}(x)}{dx} = -\frac{h}{2F} I(x)$
Liquid water flow rate	$\frac{dM_{w,a}^l}{dx} = \left(\frac{hd}{RT_a} \right) \left(\frac{M_{w,a}^v}{M_{w,a}^v + M_{H_2}} P - P_{w,a}^{sat} \right)$
Water vapour flow rate	$\frac{dM_{w,a}^v}{dx} = -\frac{dM_{w,a}^l}{dx} - \frac{\alpha I(x)h}{F}$
Temperature	$\sum_i (M_i C_{p,i}) \frac{dT_a}{dx} = (H_{w,a}^v - H_{w,a}^l) \frac{dM_{w,a}^l}{dx} + Ua(T_s - T_a)$
<i>Cathode</i>	
Oxygen flow rate	$\frac{dM_{O_2}(x)}{dx} = -\frac{h}{4F} I(x)$
Nitrogen flow rate	$M_{N_2} = M_{N_2}^0 = 0$
Liquid water flow rate	$\frac{dM_{w,c}^l}{dx} = \left(\frac{hd}{RT_c} \right) \left(\frac{M_{w,c}^v}{M_{w,c}^v + M_{O_2} + M_{N_2}} P - P_{w,c}^{sat} \right)$
Water vapour flow rate	$\frac{dM_{w,c}^v}{dx} = -\frac{dM_{w,c}^l}{dx} + \frac{(1+2\alpha)I(x)h}{2F}$
Temperature	$\sum_i M_i C_{p,i} \frac{dT_c}{dx} = (H_{w,c}^v - H_{w,c}^l) \frac{dM_{w,c}^l}{dx} + Ua(T_s - T_c)$
Cell potential	$V_{cell} = V_{oc} - \frac{RT_s}{0.5F} \ln \left[\frac{I(x)}{I^0 P_{O_2}(x)} \right] - \frac{I(x)t_m}{\sigma_m(x)}$
Net water flux per proton flux ratio	$\alpha = n_d - \frac{F}{I(x)} D_w \frac{(c_{w,c} - c_{w,a})}{t_m}$

Electro-osmotic coefficient	$n_d = \begin{cases} 0.0049 + 2.02a_a - 4.53a_a^2 + 4.09a_a^3, & a_a \leq 1 \\ 1.59 + 0.159(a_a - 1), & a_a > 1 \end{cases}$
Diffusion coefficient of water	$D_w = n_d \bar{D}^\circ \exp \left[2416 \left(\frac{1}{303} - \frac{1}{T_s} \right) \right]$
Concentration of water at k interface of the membrane	$c_{w,k} = \begin{cases} \frac{\rho_{m,dry}}{M_{m,dry}} (0.043 + 17.8a_k - 39.8a_k^2 + 36.0a_k^3), & a_k \leq 1 \\ \frac{\rho_{m,dry}}{M_{m,dry}} [14 + 1.4(a_k - 1)], & a_k > 1 \end{cases}$
Activity of water in anode stream	$a_a = \frac{x_{w,a}P}{P_{w,a}^{sat}} = \left(\frac{M_{w,a}^V}{M_{w,a}^V + M_{H_2}} \right) \frac{P}{P_{w,a}^{sat}}$
Activity of water in cathode stream	$a_c = \frac{x_{w,c}P}{P_{w,c}^{sat}} = \left(\frac{M_{w,c}^V}{M_{w,c}^V + M_{O_2} + M_{N_2}} \right) \frac{P}{P_{w,c}^{sat}}$
Activity of water in the membrane	$a_m = \frac{a_a + a_c}{2}$
Concentration of water in the membrane	$c_m = \begin{cases} \frac{\rho_{m,dry}}{M_{m,dry}} (0.043 + 17.8a_m - 39.8a_m^2 + 36.0a_m^3), & a_m \leq 1 \\ \frac{\rho_{m,dry}}{M_{m,dry}} [14 + 1.4(a_m - 1)], & a_m > 1 \end{cases}$
Vapour pressure of water	$\log_{10} P_{w,k}^{sat} = 2.95 \times 10^{-2} (T_k - 273) - 9.18 \times 10^{-5} (T_k - 273)^2 + 1.44 \times 10^{-7} (T_k - 273)^3 - 2.18$
Heat of condensation and evaporation	$(H_{w,k}^V - H_{w,k}^L) = 45070 - 41.9 (T_k - 273) + 3.44 \times 10^{-3} (T_k - 273)^2 + 2.54 \times 10^{-5} (T_k - 273)^3 - 8.98 \times 10^{-10} (T_k - 273)^4$
Heat capacity of liquid water	$C_{p,w}^L = 75.38 \text{ J (mol } ^\circ\text{C)}^{-1}$
Heat capacity of water vapour	$C_{p,w}^V = 33.46 + 6.88 \times 10^{-3} (T_k - 273) + 7.60 \times 10^{-6} (T_k - 273)^2 - 3.59 \times 10^{-9} (T_k - 273)^3$

Heat capacity of hydrogen gas	$C_{p,H_2} = 28.84 + 7.65 \times 10^{-5} (T_k - 273) + 3.29 \times 10^{-6} (T_k - 273)^2 - 8.70 \times 10^{-10} (T_k - 273)^3$
Heat capacity of oxygen gas	$C_{p,O_2} = 29.10 + 1.16 \times 10^{-3} (T_k - 273) - 6.08 \times 10^{-6} (T_k - 273)^2 + 1.31 \times 10^{-9} (T_k - 273)^3$
Heat capacity of nitrogen gas	$C_{p,N_2} = 29.00 + 2.20 \times 10^{-3} (T_k - 273) + 5.72 \times 10^{-6} (T_k - 273)^2 - 2.87 \times 10^{-9} (T_k - 273)^3$
Activation overpotential	$\eta(x) = \frac{RT_s}{0.5F} \ln \left[\frac{I(x)}{I^0 P_{O_2}(x)} \right]$
Ohmic overpotential	$\Omega(x) = \frac{I(x)l_m}{\sigma_m(x)}$
Membrane conductivity	$\sigma_m(x) = \left(0.00514 \frac{M_{m,dry}}{\rho_{n,dry}} c_m(x) - 0.00326 \right) \exp \left[1268 \left(\frac{1}{303} - \frac{1}{T_s} \right) \right]$

4.4 Numerical method

The algorithm used to obtain the model solution is given in Figure 4.2. An average current density, I_{avg} , is first set to a specific value. A value for the cell voltage, V_{cell} , is then guessed. Based on these quantities, initial values of flow rates of hydrogen, oxygen, nitrogen (if air is used), water vapour and liquid are calculated. The model, which is composed of ordinary differential equations and algebraic equations, can be written as:

$$u' = f(x, u, v) \quad (4.23)$$

$$0 = g(x, u, v) \quad (4.24)$$

In this notation, x (channel length) is the independent variable which is implicit in the model; u represents the differential variables, whilst v stands for the algebraic variables. One solution approach is to solve Eq. 4.23 as ODEs. Solving the derivative for a given values of u will require evaluating the algebraic equations (Eq. 4.24) for

the corresponding values of v . This can be done in MATLAB using the Runge-Kutta method and the Newton-Raphson method, as was performed by Nguyen and White [125]. However, this approach proves to be computationally expensive.

A more effective solution approach is to treat the system as differential algebraic equations [128, 129]. Combining the differential and the algebraic parts, Eqs. 4.23-4.24 can be written as:

$$M \times y' = F(x, y) \quad (4.25)$$

where $M = \begin{bmatrix} I & 0 \\ 0 & 0 \end{bmatrix}$ and $y = \begin{bmatrix} u \\ v \end{bmatrix}$. For the problem at hand, the identity matrix, I , in the mass matrix, M , has a 9 by 9 dimension. In addition, the mass matrix, M , is singular, but this setback was effectively overcome by using MATLAB's ODE15s.

The calculation of water content in the anode and cathode is quite troublesome. Eq. 4.16, as formulated, is only applicable if liquid water is present in the channel, which occurs when the partial pressure is greater than the saturation pressure. Apparently, if liquid water is not present there can be no evaporation no matter what the vapour pressure is. Thus, for each step in the DAE calculation, the amount of liquid water in the anode and cathode is checked for zero or positive values. If the value of the liquid water flow rate happens to be negative for each integration step, it is set to zero.

After integration, the average current density is calculated using the expression:

$$I_{\text{avg}} = \frac{1}{L} \int_0^L I(x) dx \quad (4.26)$$

where L is the channel length and $I(x)$ is the local current density at every point along the channel length. The calculated I_{avg} is compared to the guessed I_{avg} . If they turn out to be equal, a solution is found and the calculation is terminated. Otherwise, another guess is specified for V_{cell} and the calculation is repeated until convergence. In this study, the computation was made relatively faster by avoiding manual iteration. The correct cell voltage was obtained by employing negative and positive perturbations, and

then interpolating the correct value of V_{cell} .

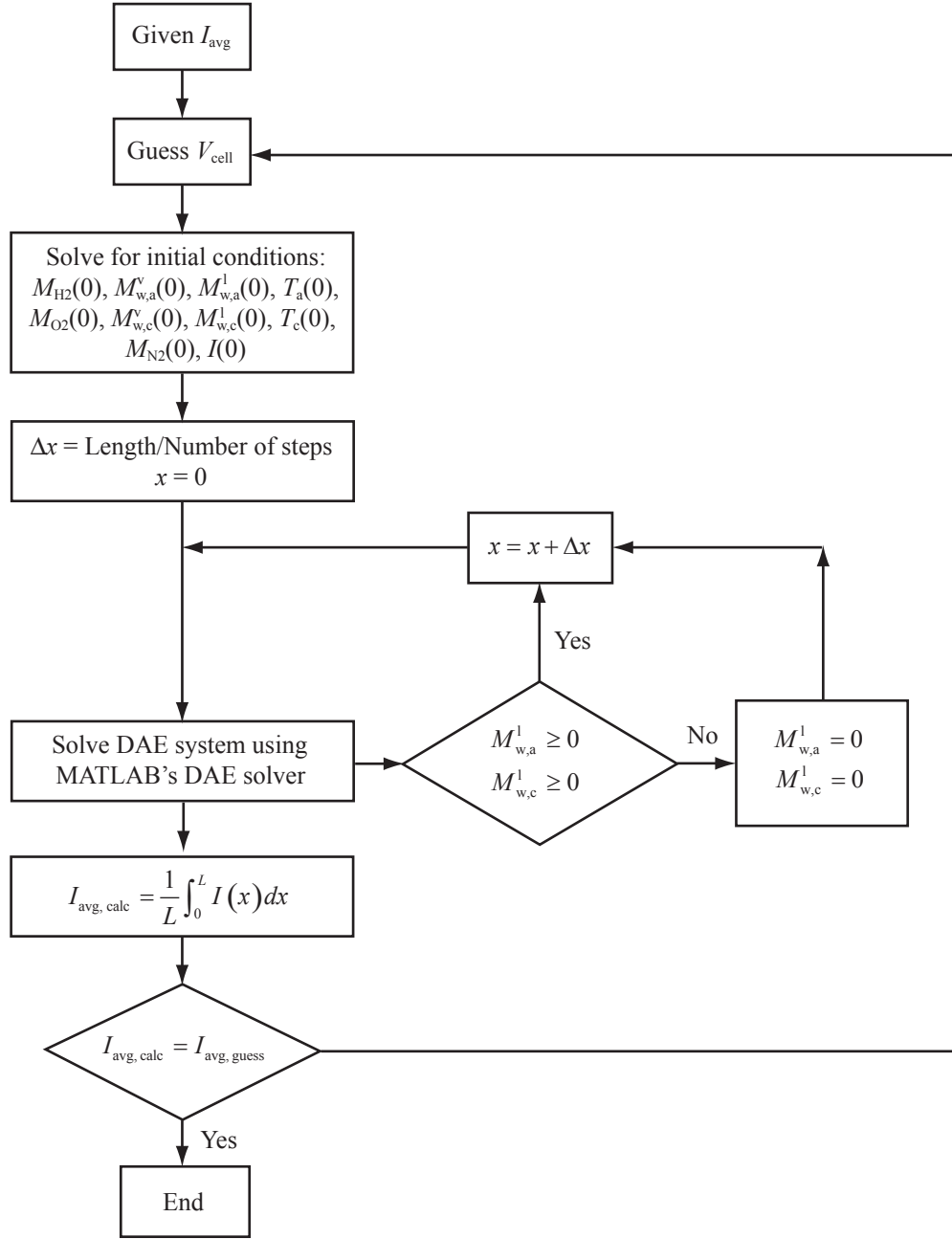


Figure 4.2: Flowchart for the determination of the model solution.

4.5 Model simulation

In this section, the single-cell model presented above is used to evaluate the effectiveness of a conventional humidification design. The operating conditions are similar to the base

case conditions presented in Ref. [125], *i.e.*, the PEFC is operating on pure hydrogen and oxygen at 2 atm absolute, 90 °C and a current density of 1 A cm⁻². The anode gas stream enters the fuel cell saturated with water vapour. The humidification temperature is the same as the cell temperature. The values for the other parameters used in the simulation are presented in Table 4.2.

Table 4.2: Parametric constants used in the model taken from Nguyen and White (1993) [125].

Parameter	Value
<i>Physical data</i>	
Channel width (h)	0.2 cm
Channel height (d)	0.2 cm
Channel length (L)	10 cm
Total pressure (P)	2 atm, absolute
Heat transfer coefficient (U)	0.0025 J (s cm ² K) ⁻¹
Condensation rate constant (k_c)	1.0 s ⁻¹
Temperature of solid phase (T_s)	363 K
Density of dry membrane ($\rho_{m,dry}$)	2.0 g cm ⁻³
Equivalent weight of dry membrane ($M_{m,dry}$)	1100
Membrane thickness (t_m)	0.01275 cm
Fuel cell open-circuit voltage (V_{oc})	1.1 V
Oxygen exchange current density (I^0)	0.01 A cm ⁻²
Diffusion parameter (D^0)	5.5×10^{-7} cm ² s ⁻¹
<i>Anode</i>	
Inlet temperature (T_a)	90°C
Inlet hydrogen flow rate ($M_{H_2}(0)$)	$1.5 \frac{I_{avg}}{2F} Lh$ mol s ⁻¹
Inlet water vapour flow rate ($M_{w,a}^v(0)$)	Saturated
Inlet liquid water flow rate ($M_{w,a}^l(0)$)	0
<i>Cathode</i>	
Inlet temperature (T_c)	363 K
Inlet oxygen flow rate ($M_{O_2}(0)$)	$2 \frac{I_{avg}}{4F} Lh$ mol s ⁻¹
Inlet nitrogen flow rate ($M_{N_2}(0)$)	0
Inlet water vapour flow rate ($M_{w,c}^v(0)$)	Dry
Inlet liquid water flow rate ($M_{w,c}^l(0)$)	0

Figure 4.3 shows the water and temperature profile along the channel length. Apart from the partial pressure of water vapour, all variables are plotted in dimensionless form. The temperatures are divided by the solid-phase temperature, whilst the moles of liquid water are divided by the total initial moles of gases. Figure 4.4 gives the partial

pressures of hydrogen and oxygen along the flow channels. The corresponding current distribution along the channel length is presented in Figure 4.5. The results conform very closely to the results obtained by Nguyen and White (1993) [125].

Similar to what had been observed by Nguyen and White, the amount of water vapour in the anode stream decreases along the channel and settles down to a low value (Figure 4.3). This is because near the fuel cell inlet, the membrane is highly conductive because of high water concentration. Consequently, the electro-osmotic drag coefficient is high and the membrane can conduct higher current (see current distribution curve in Figure 4.5). Moreover, because dry cathode gas stream enters the fuel cell, the amount of water in the cathode stream is low, thus water back diffusion is low. This implies that the net flux of water across the membrane is high, resulting in high current density and high consumption rates of hydrogen and oxygen (Figure 4.4).

Farther down the channel, the water content in the anode gas stream decreases which results in a decrease in the water content in the membrane, electro-osmotic drag coefficient, and membrane conductivity. Furthermore, the water transport from the cathode back to the anode by diffusion is greater due to the higher water content in the cathode side. As a result, the local current density decreases and the net water flux across the membrane also decreases, resulting in a lower depletion rate of water from the anode gas stream, a lower production rate of water in the cathode and a lower depletion rate of hydrogen and oxygen.

Figure 4.3 also presents the condensation of water in the cathode when the cathode partial pressure becomes higher than the water vapour pressure. The production of water due to the oxygen reaction and diffusion of water from anode to cathode both lead to increase of liquid water in the cathode. Liquid water is not present in the anode. Furthermore, an increase in cathode temperature is observed because of the heat given off (latent heat) during water condensation. There is no observed changes on the anode temperature, however, because the gas stream enters the anode at the cell temperature, and no phase changes took place. Conversely, farther down the channel,

the water content in the anode gas stream decreases which implies a decrease in the amount of water in the membrane, electro-osmotic drag coefficient, and membrane conductivity. Furthermore, back diffusion of water from the cathode to the anode is higher because of the higher water content at the cathode side. This results to lower local current density and smaller net flux of water across the membrane, leading to a lower depletion rate of water in the anode, lower accumulation rate of water in the cathode, thus lower depletion rate of hydrogen and oxygen. This can be verified from Figures 4.3 - 4.5.

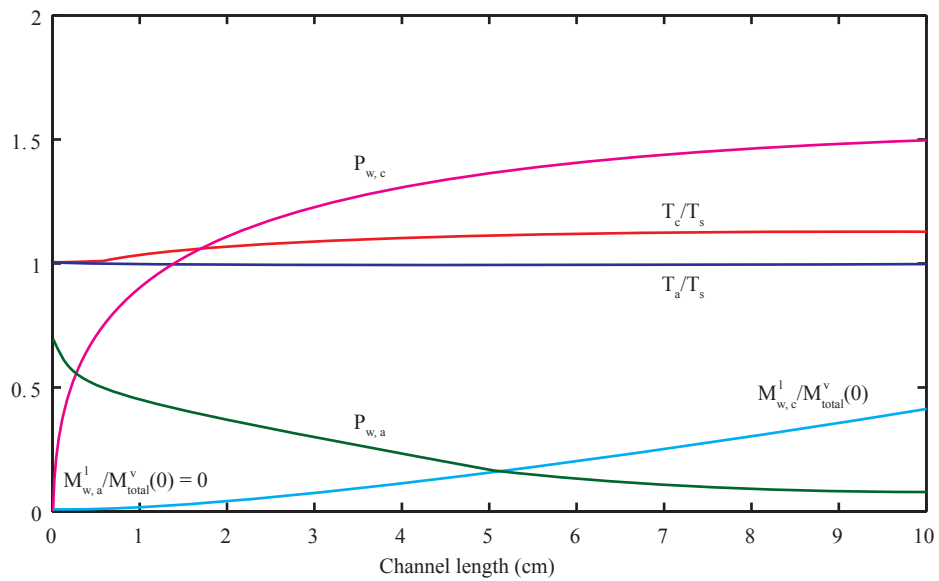


Figure 4.3: Water and temperature profiles along the flow channels.

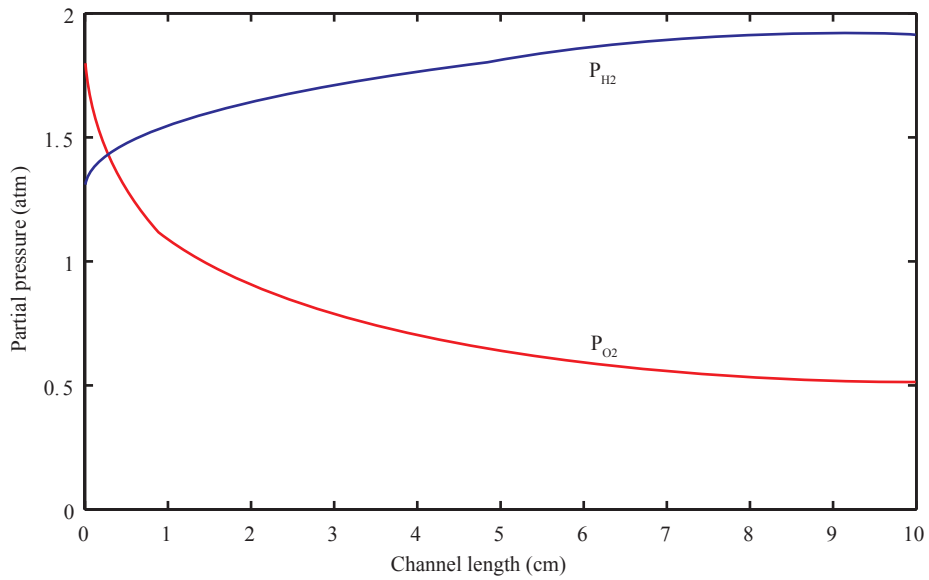


Figure 4.4: Partial pressures of oxygen and hydrogen along the flow channels.

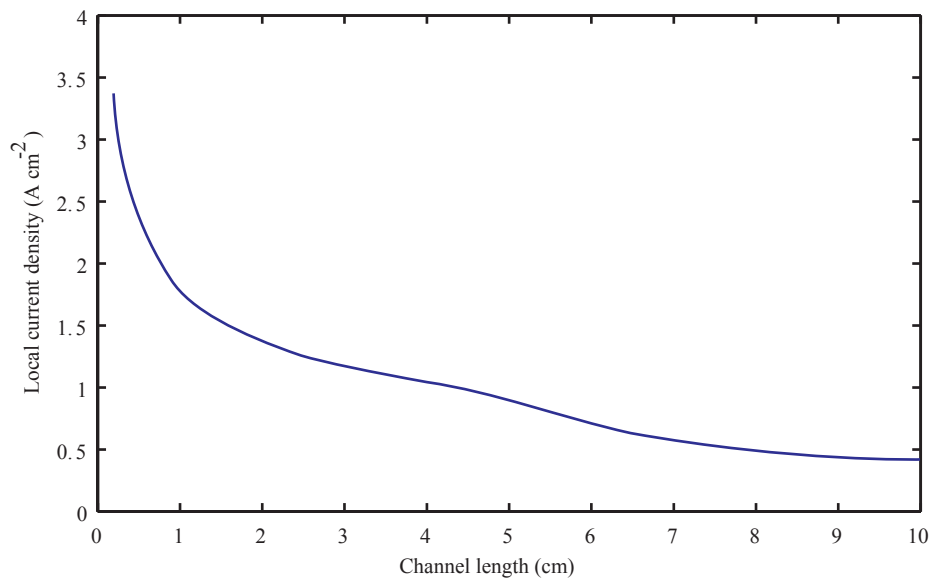


Figure 4.5: Current distribution along the flow channels.

4.6 Conclusions

This chapter presents the basis model for the multi-objective optimisation models developed in the following chapters. The model is a two-dimensional, non-isothermal, mass and heat transfer model for a PEFC suitable for water and heat management investigation. The model can be used as a design tool to evaluate the effectiveness of

various heat removal and humidification designs and the effects of various design and operating parameters on the performance of a PEFC. In this chapter, the effectiveness of a conventional humidification design previously presented in Ref. [125] was revisited. The results can be useful in determining an optimal fuel cell design for a specific application. The subsequent chapters present the development of a stack-level and a system-level mathematical models based on the single-cell fuel cell model presented in this chapter.

Chapter 5

Optimal design of a fuel cell stack

The design of fuel cell systems inherently involves simultaneous optimisation of two or more conflicting objectives. Achieving an optimum for one objective often requires a compromise on two or more other objectives. This chapter presents an optimisation model for a PEFC stack suitable for efficiency and size trade-offs investigation. Simulation of the model for a base case shows that for a given power output, a more efficient system is bigger and *vice versa*. Using the weighting method to perform a multi-objective optimisation, the Pareto sets were generated for different stack power outputs. A Pareto set, presented as a plot of the optimal efficiency and area of the membrane electrode assembly (MEA), gives a quantitative description of the compromise between efficiency and size.

5.1 Introduction

The trade-off between efficiency and size is inherent in the design of a PEFC stack. These two objectives are both related to economics. Fuel consumption, hence operating cost, is directly determined by the efficiency. On the other hand, the bulk of the capital cost is contributed by the size of the MEA. The costs of the other components, such as the bipolar plates and auxiliaries (humidifiers, air compressor, and water coolant)

which add up to the capital cost are strongly correlated with the variation in the area of the MEA [130]. However, the compromise between the capital investment and operating cost is not the only motivation for the trade-off investigation between size and efficiency. In the current consumer demographic, size and portability, for instance, may be the deciding factors for mobile users. On the other hand, other users may value operating costs more than portability.

Significant effort has been exerted in recent years to achieve optimal PEFC system design. Even though most of these studies make significant contributions to the expanding PEFC literature (e.g. formulation of PEFC models with different levels of complexity and development of various optimisation techniques), most of them are limited to a single design objective. Many studies optimised the performance [51, 131–138], whilst some considered the cost [139], the durability [54], and the emission [140] as objectives for the design. Moreover, some of the papers performed single-objective optimisation for a specific part of the PEFC system such as the membrane electrode assembly (MEA) [141], the electrode [142], the bipolar plate and diffusion layer [143], the cathode and air distributor [144], and the catalyst layer [105, 145]. However, the results of these studies might be misleading because the interaction or coupling between the multiple objectives has not been considered [146]. In addition, the potentially conflicting nature of the objectives makes the determination of the optimal solution more challenging.

There are a few papers in the literature that have dealt with multi-objective optimisation. Barbir and Gomez [147] analysed the cost and performance of PEFCs at different load profiles and design and cost scenarios. Their efficiency model was based on a linear polarisation curve. Similar objectives were considered by Xue and Dong [49] in their multi-objective optimisation of the 120 kW Ballard Mark V Transit Bus fuel cell system with the stack active intersection area and the air stoichiometric ratio as the design variables. Frangopoulos and Nakos [48] investigated the Ballard Mark V PEFC stack consisting of 35 5 kW cells for a merchant ship application. The system efficiency, power density and present worth cost were the design objectives, whilst the current

density and temperature were the design variables. In their study, the interaction between the objectives was not considered; they optimised each objective individually. Also, for each objective, one of the two design variables was treated as a parameter. This resulted in a one-variable, single-objective optimisation problem, which was then solved at different values of the parameter. Na and Gou [146] optimised the efficiency and cost of a 50 kW PEFC system for transportation, using the system pressure, the hydrogen and air stoichiometric ratios, and the current density as the design variables. The Pareto set that they obtained using MATLAB's `fminimax` function, however, was influenced by the choice of the initial values of the design variables used in the solver, indicating the non-globality of the solution.

This chapter presents a model suitable for multi-objective optimisation which allows the investigation of the efficiency and size trade-offs involved in the design of a PEFC stack. The objective is to determine a set of trade-off optimal solutions, called the non-dominated or Pareto set, that maximises the efficiency and minimises the size of the system with respect to the current density, the cell voltage, the system pressure, the hydrogen and air stoichiometric ratios, and the relative humidities of fuel and air. To date, papers on multi-objective optimisation of PEFCs have considered models that are specific to the application described in the paper [26, 48, 49, 146]. The model presented in this chapter is more general and, thus, will be suitable for a wide range of applications. Furthermore, the model considers the multi-phase existence of water in the channels, thus capturing the fuel cell phenomena more thoroughly. This chapter is arranged as follows: Section 5.2 presents a generic PEFC stack and the model. Section 5.3 describes the multi-objective optimisation problem formulation based on this model and the solution approach taken. Section 5.3 also presents results for a case study involving different power outputs and highlights the important results from the analyses of the generated Pareto sets for the efficiency and size trade-offs.

5.2 Model formulation

The major components of a general hydrogen-air PEFC system are shown in Figure 5.1. The system includes a stack and the auxiliaries needed to operate the fuel cell. The model in this chapter does not consider components such as a reformer or fuel processor, the power electronics, controllers, and any auxiliary power sources. At the anode side, pure pressurised hydrogen is fed; at the cathode side, there is an air supply system which includes a compressor. A humidifier is located on both sides for stack water management. A coolant regulates the operating temperature of the cell. This study assumes uniform temperature and pressure throughout the stack. The amount of power produced depends on several factors including the cell size, operating temperature and pressure, and flow rates and humidity of the gases supplied to the cell.

Multi-objective optimisation requires the evaluation of a large number of design alternatives with correspondingly high computational requirements. At present the use of a complex model is not practical for this purpose. This chapter presents a simple and fast model for multi-objective optimisation. The model has an acceptable accuracy and is complex enough to differentiate between alternative designs, whilst being simple enough to allow for repeated calculations during optimisation.

The model is based on established, and well validated, principles proposed by Nguyen and White [125], which was discussed in Chapter 4. In addition to the assumptions in Ref. [125], the model in this chapter does not account for the spatial variations of the variables in the flow channels. Furthermore, the water balance of Nguyen and White [125] was modified to address its non-validity in the event of no liquid water in the channels [148], and its inconsistency when both liquid and vapour phases of water are present, *i.e.*, their model does not guarantee the equality between the partial pressure and vapour pressure of water at equilibrium. Also, the expression for the concentration of water in the membrane was taken from Hinatsu *et al.* [127], as appropriate for the operating temperature range considered in this study.

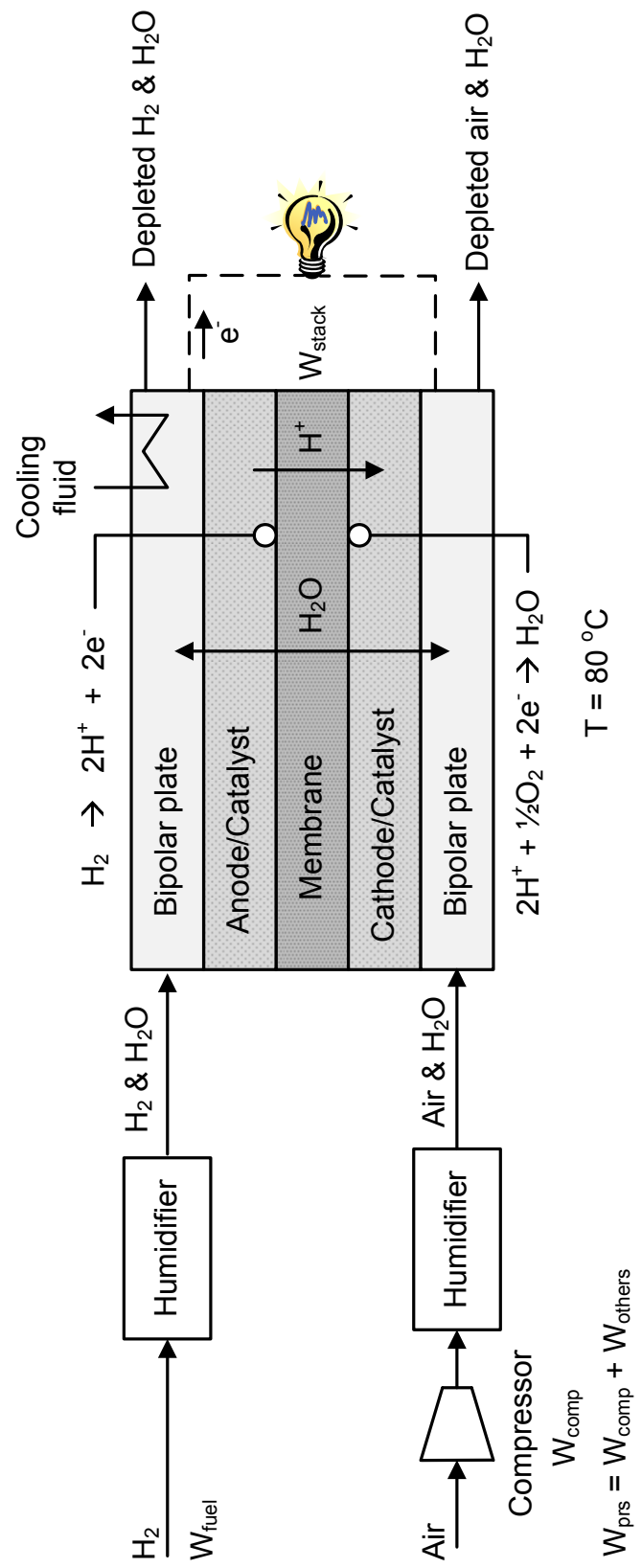


Figure 5.1: A general hydrogen-air PEMFC system with a single-cell stack.

5.2.1 Mass balances

For a given current density, the respective hydrogen and oxygen mass balances are

$$M_{\text{H}_2,\text{in}} = M_{\text{H}_2} + \frac{AI}{2F} \quad (5.1)$$

$$M_{\text{O}_2,\text{in}} = M_{\text{O}_2} + \frac{AI}{4F} \quad (5.2)$$

The second term on the right of equations 5.1 and 5.2 are the consumption of hydrogen and oxygen, respectively.

Nitrogen does not participate in the reaction, thus, the incoming flow rate is equal to the outgoing flow rate.

$$M_{\text{N}_2,\text{in}} = M_{\text{N}_2} \quad (5.3)$$

The flow rates of water in the channels and the presence of liquid and vapour phases are affected by the production of water at the cathode by the electrochemical reaction, the transport of water from the anode to the cathode via electro-osmosis or drag, the back diffusion of water from the cathode to the anode due to a hydraulic pressure gradient, and the condensation and evaporation of water depending on the difference between the partial pressure and vapour pressure [125, 148–150] .

The water balance in the anode channel is

$$M_{\text{w},\text{a},\text{in}}^{\text{v}} = M_{\text{w},\text{a}}^{\text{v}} + M_{\text{w},\text{a}}^{\text{l}} + \frac{A\alpha I}{F} \quad (5.4)$$

where α is the net water molecules per proton flux ratio. The water vapour going into the anode channel either leaves as vapour or liquid or migrates across the membrane to the cathode channel. The fraction of liquid water, f_{a} , and the water vapour-liquid

equilibrium in the anode channel are described by the following equations:

$$f_a = \frac{M_{w,a}^l}{M_{w,a}^v + M_{w,a}^l} \quad (5.5)$$

$$0 = f_a \left[\frac{M_{w,a}^v}{M_{w,a}^v + M_{H_2}} P - P_w^{\text{sat}} \right] \quad (5.6)$$

where $f_a \in [0, 1]$. If both liquid and vapour phases of water are present in the anode channel, i.e. $f_a \neq 0$, the expression inside the bracket of equation 5.6, representing the vapour-liquid equilibrium condition, must be zero. In this case, Raoult's Law describes the flow rate of water vapour going out of the anode channel, $M_{w,a}^v$. The flow rate of liquid water going out of the anode channel, $M_{w,a}^l$, can be computed from equation 5.4. Conversely, if liquid water is not present in the anode channel, i.e. $f_a = 0$, equilibrium between liquid and vapour phases of water does not exist. In this case, $M_{w,a}^l = 0$ and $M_{w,a}^v$ can be calculated from equation 5.4.

Similarly, the water balance in the cathode channel can be expressed as

$$M_{w,c,\text{in}}^v = M_{w,c}^v + M_{w,c}^l - \frac{A\alpha I}{F} - \frac{AI}{2F} \quad (5.7)$$

The terms on the right of equation 5.7 are the flow rates of water vapour and liquid going out of the cathode channel, the water vapour that migrated from the anode to the cathode channel, and the water generated at the cathode by the electrochemical reaction, respectively. The fraction of liquid water, f_c , and the water vapour-liquid equilibrium in the cathode channel are given by

$$f_c = \frac{M_{w,c}^l}{M_{w,c}^v + M_{w,c}^l} \quad (5.8)$$

$$0 = f_c \left[\frac{M_{w,c}^v}{M_{w,c}^v + M_{N_2} + M_{O_2}} P - P_w^{\text{sat}} \right] \quad (5.9)$$

where $f_c \in [0, 1]$. The same reasoning given for equations 5.4 - 5.6 applies to equations 5.7 - 5.9.

The hydrogen and air flow rates going into the channels are determined by their respective stoichiometric ratios, λ_{H_2} and λ_{air} .

$$M_{\text{H}_2,\text{in}} = \lambda_{\text{H}_2} \frac{IA}{2F} \quad (5.10)$$

$$M_{\text{O}_2,\text{in}} = \lambda_{\text{air}} \frac{IA}{4F} \quad (5.11)$$

The water vapour flow rate going into the anode channel can be computed from the relative humidity of the hydrogen fuel,

$$M_{\text{w},\text{a},\text{in}}^{\text{v}} = \frac{y_{\text{w},\text{a},\text{in}}}{1 - y_{\text{w},\text{a},\text{in}}} M_{\text{H}_2,\text{in}} \quad (5.12)$$

$$y_{\text{w},\text{a},\text{in}} = RH_{\text{fuel}} \frac{P_{\text{w}}^{\text{sat}}}{P} \quad (5.13)$$

where $y_{\text{w},\text{a},\text{in}}$ is the mole fraction of water vapour going into the anode and $P_{\text{w}}^{\text{sat}}$ is the saturation pressure.

Similarly, the water vapour flow rate going into the cathode channel can be described as follows:

$$M_{\text{w},\text{c},\text{in}}^{\text{v}} = \frac{y_{\text{w},\text{c},\text{in}}}{1 - y_{\text{w},\text{c},\text{in}}} (M_{\text{O}_2,\text{in}} + M_{\text{N}_2,\text{in}}) \quad (5.14)$$

$$y_{\text{w},\text{c},\text{in}} = RH_{\text{air}} \frac{P_{\text{w}}^{\text{sat}}}{P} \quad (5.15)$$

5.2.2 Electrochemistry

The effective cell voltage can be expressed as the difference between the thermodynamically reversible cell voltage and the losses due to overpotential,

$$V_{\text{cell}} = V_{\text{oc}} + \frac{RT}{2F} \ln \left(\frac{P_{\text{H}_2} P_{\text{O}_2}^{0.5}}{P_{\text{H}_2\text{O}}} \right) - \frac{RT}{0.5F} \ln \left(\frac{I}{I^{\circ} P_{\text{O}_2}} \right) - \frac{It_{\text{m}}}{\sigma_{\text{m}}} - \beta I^{\text{k}} \ln \left(\frac{I_{\text{L}}}{I_{\text{L}} - I} \right) \quad (5.16)$$

where V_{oc} is the open-circuit potential, I_0 is the exchange current density, βI^k is the amplification term associated with the total mass transport overpotential, expressed in potential units [151], and I_L is the limiting current density. The first two terms on the right of equation 5.16 represent the thermodynamic reversible voltage based on the Nernst equation [148]. The third term is the activation overpotential [125], which is the voltage loss due to the rate of reactions on the surface of the electrodes. This assumes that the activation overpotential is mainly located at the cathode. The fourth term is the ohmic overpotential [125], which is the voltage drop due to the resistance to the flow of protons in the electrolyte. The last term is the overall concentration overpotential [151], which is the voltage loss due to the mass transport limitation.

5.2.3 System efficiency

Efficiency is a key property of a fuel cell and can be used to evaluate its performance. The efficiency of the system is defined by

$$\eta = \frac{W_{\text{stack}} - W_{\text{prs}}}{W_{\text{fuel}}} \quad (5.17)$$

where W_{stack} is the power output of the stack, W_{prs} is the parasitic power and W_{fuel} is the power inherent in the fuel used:

$$W_{\text{stack}} = n_{\text{cell}} A I V_{\text{cell}} \quad (5.18)$$

$$W_{\text{prs}} = W_{\text{comp}} + W_{\text{others}} \quad (5.19)$$

$$W_{\text{fuel}} = \lambda_{\text{H}_2} n_{\text{cell}} \frac{IA}{2F} \text{LHV} \quad (5.20)$$

$$W_{\text{comp}} = \frac{c_p T_e}{\eta_c \eta_{\text{mt}}} \left[\left(\frac{P}{P_{\text{in}}} \right)^{0.286} - 1 \right] m_{\text{air}} \quad (5.21)$$

$$m_{\text{air}} = 3.57 \times 10^{-7} \lambda_{\text{air}} n_{\text{cell}} I A \quad (5.22)$$

$$W_{\text{others}} = 0.05 W_{\text{stack}} \quad (5.23)$$

In this chapter, $n_{\text{cell}} = 1$, thus A represents the total active MEA area. Equations 5.18, 5.19, 5.21 and 5.22 were taken from Pei *et al.* [152]. The parasitic power is composed of the power consumption of the compressor, W_{comp} , and the other power losses, W_{others} . Pei *et al.* [152] assumed W_{others} to be equal to 2 kW based on a stack power output of 62.5 kW. Instead, in this work W_{others} was set to 5% of the nominal stack power output for the equations above to be applicable at different stack power outputs. Also, the compressor and motor efficiencies are functions of size of the compressor and fraction of full load. However, it is assumed that the compressor and motor efficiencies are constant, similar to what was done in Refs. [146, 152].

Table 5.2 presents the expressions for the physical parameters used in the model, whilst Table 5.1 gives the values of the constant parameters.

Table 5.1: Parametric constants in the model

Parameter	Value	Ref.
Amplification constant (β)	$0.085 \text{ V}(\text{cm}^2\text{A}^{-1})^k$	[28, 151]
Dimensionless power in the amplification term (k)	1.1	[28, 151]
Limiting current density (I_L)	1.4 A cm^{-2}	[28]
Lower heating value of hydrogen (LHV)	$2.4 \times 10^5 \text{ J mol}^{-1}$	[48]
Oxygen exchange current density (I_0)	0.01 A cm^{-2}	[149]
Reversible open-circuit potential (V_{oc})	1.1 V	[149]
<i>Membrane</i>		
Diffusion coefficient of water in membrane (D_0)	$5.5 \times 10^{-7} \text{ cm}^2 \text{ s}^{-1}$	[125]
Dry density ($\rho_{\text{m,dry}}$)	2.0 g cm^{-3}	[125]
Dry equivalent weight ($M_{\text{m,dry}}$)	1100 g mol^{-1}	[125]
Thickness (t_m)	$5 \times 10^{-3} \text{ cm}$ (50 μm)	
<i>Compressor</i>		
Connecting efficiency (η_c)	0.85	[152]
Entry air temperature (T_e)	288 K	
Inlet pressure (P_{in})	1 atm	
Motor efficiency (η_{mt})	0.85	
Specific heat constant of air (c_p)	$1004 \text{ J K}^{-1}\text{kg}^{-1}$	

5.2.4 Model validation

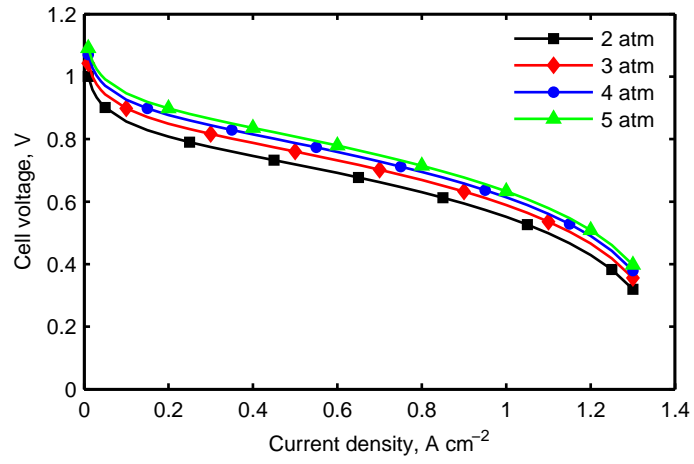
The model was solved for a base case corresponding to a stack having a MEA total active area of $25 \times 10^4 \text{cm}^2$ and an operating temperature of 80°C . Pure hydrogen at 100% relative humidity and air at 50% relative humidity are supplied to the anode and cathode channels, respectively. The hydrogen stoichiometric ratio is 1.25 (i.e. hydrogen utilisation rate of 80%), whilst the air stoichiometric ratio is 2.

Figures 5.2(a)-(c) show the effects of operating pressure and current density on polarisation, system efficiency, and power density curves, respectively. With respect to the current density, the polarisation curve, which is commonly used as a measure of the performance of fuel cell systems, is in direct correlation with the system efficiency. The voltage, and hence the efficiency, decreases with increasing current density due to the combined irreversibility contributions of activation, ohmic and concentration overpotentials. The power density, on the other hand, increases with increasing current density and displays a maximum at a particular value of the current density. The polarisation curves also show that gains in voltage result when pressure is increased. However, the pressure has no significant effect on the system efficiency because the increase in cell potential is offset by the increase in parasitic power with increasing pressure. Furthermore, at high current densities, the power density increases with increasing pressure. These results are in agreement with the literature [2, 153–158].

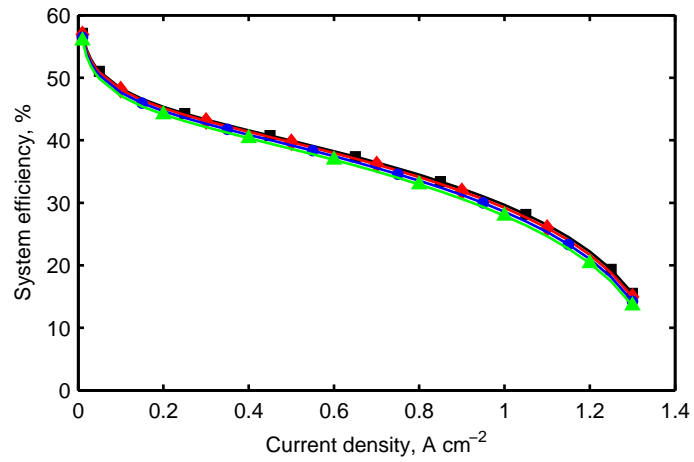
The solution of the base case suggests that the efficiency and size are conflicting objectives. To achieve high efficiency, the system must be operated at low current density. At low current density the power density is also low, which means a larger system per unit of power. Conversely, for the same power output, a small system requires high power density, which demands high current density, resulting in a lower efficiency. The systematic and detailed investigation of the trade-offs between the efficiency and size is the focus of the succeeding sections.

Table 5.2: Expressions for the physical parameters in the model

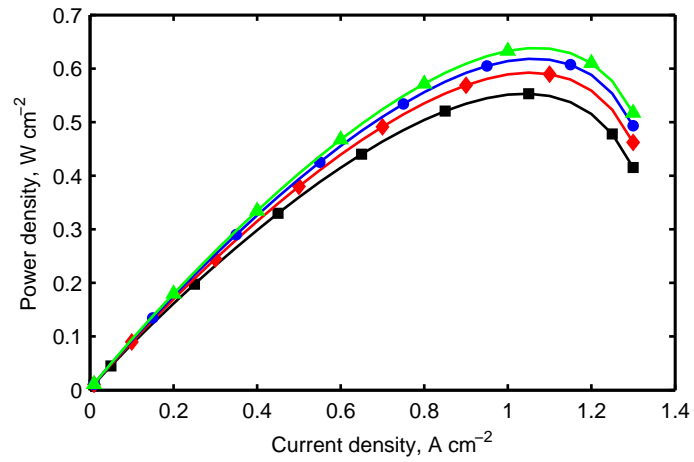
Description	Equation	Ref.
Activity of water in the anode channel	$a_a = \frac{y_{w,a}P}{P_{\text{sat}}^w} = \left(\frac{M_{w,a}^V}{M_{w,a}^V + M_{\text{H}_2}} \right) \frac{P}{P_{\text{sat}}^w}, a_a \in [0, 1]$	
Activity of water in the cathode channel	$a_c = \frac{y_{w,c}P}{P_{\text{sat}}^w} = \left(\frac{M_{w,c}^V}{M_{w,c}^V + M_{\text{O}_2} + M_{\text{N}_2}} \right) \frac{P}{P_{\text{sat}}^w}, a_c \in [0, 1]$	
Concentration of water at the k interface of the membrane	$c_{w,k} = \frac{\rho_{m,\text{dry}}}{M_{m,\text{dry}}} (0.300 + 10.8a_k - 16.0a_k^2 + 14.1a_k^3), k = a, c, a_k \in [0, 1]$	[127]
Diffusion coefficient of water in the membrane	$D_w = n_d D^\circ \exp \left[2416 \left(\frac{1}{303} - \frac{1}{T} \right) \right]$	[126]
Electro-osmotic coefficient	$n_d = 0.0049 + 2.024a_a - 4.53a_a^2 + 4.09a_a^3, a_a \in [0, 1]$	[126]
Membrane conductivity	$\sigma_m = \left(0.00514 \frac{M_{m,\text{dry}}}{\rho_{m,\text{dry}}} c_m - 0.00326 \right) \cdot \exp \left[1268 \left(\frac{1}{303} - \frac{1}{T} \right) \right]$	[126]
Net water molecules per proton flux ratio	$\alpha = n_d - \frac{F}{I} D_w \frac{(c_{w,c} - c_{w,a})}{t_m}$	[126]
Partial pressure of component i	$P_i = \frac{M_i}{\sum M_i} P$, anode: $i = \text{H}_2$ and H_2O , cathode: $i = \text{O}_2, \text{N}_2$, and H_2O	
Saturation pressure	$\log_{10} P_{\text{sat}}^w = -2.18 + 2.95 \times 10^{-2} (T - 273) - 9.18 \times 10^{-5} (T - 273)^2 + 1.44 \times 10^{-7} (T - 273)^3$	[126]



(a)



(b)



(c)

Figure 5.2: Simulation of the system for a base case: (a) polarisation curve, (b) power density, and (c) system efficiency, all with respect to the current density at various operating pressures.

5.3 Case study: Trade-off between efficiency and size of stack

The model for the base case reveals that for a given power output, a more efficient fuel cell is bigger and *vice versa*. We now wish to use this model within an optimisation-based design framework. The aim is to identify the efficiency and size trade-offs involved in the design of PEFC system for any given power output. The determination of a set of optimal solutions that represent the compromise between the objectives, called the non-dominated or Pareto set, requires a multi-objective optimisation technique.

5.3.1 Multi-objective optimisation

The weighting method is used to approximate the Pareto set. This method transforms the multi-objective optimisation problem into a single-objective optimisation problem by associating each objective function with a weighting coefficient and then minimising the weighted sum of the objectives:

$$\min z = \sum_{i=1}^N \omega_i z_i \quad (5.24)$$

where $\omega_i \in [0, 1]$ with $\sum_{i=1}^N \omega_i = 1$, z is the weighted sum of the objectives, z_i is a single-objective and ω_i is a weighting factor. The solution of equation 5.24 produces a single result that is as good as the selection of the weights [159]. A Pareto set can be generated by evaluating a series of single-objective optimisation problems at different values of the weighting factor to avoid having to, *a priori*, select a particular weighting between objectives.

The PEFC system efficiency-size multi-objective optimisation problem is

$$\min_{I, P, \lambda_{H_2}, \lambda_{air}, RH_{fuel}, RH_{air}} z = -\omega \eta + (1 - \omega) A \quad (5.25)$$

subject to:

$$0.11 \text{ A cm}^{-2} \leq I \leq 1.3 \text{ A cm}^{-2}$$

$$1.2 \text{ atm} \leq P \leq 5 \text{ atm}$$

$$1.1 \leq \lambda_{\text{fuel}} \leq 10$$

$$1.1 \leq \lambda_{\text{air}} \leq 10$$

$$0.5 \leq RH_{\text{fuel}} \leq 1$$

$$0.5 \leq RH_{\text{air}} \leq 1$$

The system efficiency, η , is given by equation 5.17, whereas the system size is represented by the total active area of the MEA, A . The size of the other components such as the bipolar plates and auxiliaries (humidifiers, air compressor, and water coolant) are directly correlated with the variation in the area of the MEA. A single-cell fuel cell stack has been considered. Once the total active area is known, the number of cells can be determined given the active area of a single cell. Although a fuel cell's performance will be affected by the temperature, in this study the temperature is fixed at 80°C. It is difficult to derive a reliable analytical expression for the exchange current density, I_0 , as a function of the temperature, since it depends on the specifics of the catalyst used. The lower bound on the pressure is 1.2 atm because the compressor cannot provide a pressure below atmospheric (i.e. the system pressure is always higher than the atmospheric pressure) [146]. The lower bound on the hydrogen and air stoichiometric ratios should be higher than the minimum limit to prevent depletion [146]. When using air as the oxidant, it is a common practice to use at least 50% relative humidity. Using the same set of objective function and constraints, the Pareto set is obtained at different stack power outputs, namely 1, 25, 50, 75 and 100 kW.

In equation 5.25, $\omega \in [0, 1]$ represents the weighting factor. The negative sign in front of the efficiency objective indicates a maximisation problem. The extreme points $\omega = 0$

and $\omega = 1$ represent the single-objective optimisation problems where the size and the efficiency are minimised and maximised, respectively. Solving the optimisation problem for any $\omega \in (0, 1)$ will generate solutions between these two extremes where the two objectives will be considered simultaneously. The value of ω will determine the relative importance of each objective. For example, at $\omega = 0.25$, the size is of higher importance than the efficiency. The reverse is true at $\omega = 0.75$, in which more weight is given to the efficiency than size. However, assigning equal weights to the objectives does not necessarily mean giving equal importance to the objectives. Furthermore, as the relative weights matter in this technique, the objectives were scaled to have comparable values. In addition, since the problem involves both maximisation and minimisation, the solver may be ineffective in searching the region at which the value of the weighted sum of the objectives is zero. This can be overcome by translating the problem (i.e. adding an appropriate constant to equation 5.25) such that the values of the weighted sum of the objectives are either positive or negative for all ω s.

The optimisation model was written in the GAMS [160] modelling language and was solved using LINDOGlobal. LINDOGlobal employs branch-and-cut method to break a nonlinear programming (NLP) model down into a list of subproblems [161]. A discussion of the branch-and-cut method is given in [162]. For a given weighting factor, ω , an optimisation run usually converges to a solution with a relative tolerance of 0.01% after approximately 120 seconds on a desktop computer with a 2.66 GHz Intel Core Duo CPU and with 2GB RAM.

5.3.2 Results and discussion

Figure 5.3 gives the trade-off solutions for a stack power output of 50 kW. The efficiency and the MEA area are plotted on the two axes and the curve consists of a set of designs that are all optimal in a Pareto sense. For comparison, the base case solution at stack power output of 50 kW and pressure of 2 atm (referred later as base case) is given in the first row of Table 5.3. The highest point (top right) in Figure 5.3 represents

the optimal solution at $\omega = 1$, which corresponds to the single objective optimisation problem of maximising the efficiency of the system without taking the size into account. This solution is 20% more efficient but 112% bigger in size relative to the base case. This solution requires operation at a lower current density (thus, a higher voltage), at a higher pressure, and with lower hydrogen and air stoichiometric ratios with respect to the base case. As a consequence of the higher efficiency, this solution has a lower fuel consumption. However, the parasitic loss is higher due to the increase in the pressure. Conversely, the lowest point (bottom left) in the curve corresponds to the optimal solution at $\omega = 0$, which is the minimisation of the size regardless of the efficiency. This solution represents a design that is 42% smaller in size but 44% less efficient than the base case. In comparison with the base case, this design has a higher operating current density (thus, a lower voltage), operates at a higher pressure, and with lower hydrogen and air stoichiometric ratios. This design has higher power consumption and parasitic loss. From the results, it can be concluded that the efficiency and size of the system must be optimised simultaneously. If only the efficiency is maximised, the outcome is a possibly impractically large system. On the other hand, optimising for size results in a system almost four times smaller in size but efficiency that is less than desirable.

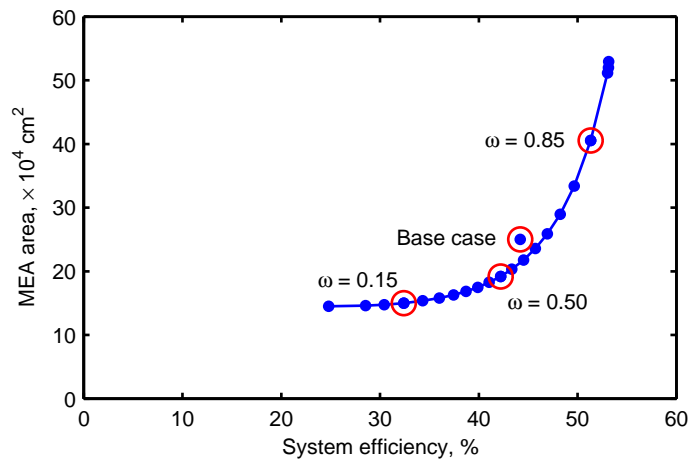


Figure 5.3: Pareto set at stack power output of 50 kW.

As shown in Figure 5.3, the base case is a dominated solution because it lies “inside” of

Table 5.3: Comparison of the representative solutions in the Pareto set (Figure 5.3) with the base case at stack power output of 50 kW.

	η (%)	A ($\times 10^4 \text{cm}^2$)	I (A cm^{-2})	V (V)	P (atm)	λ_{H_2}	λ_{air}	RH_{fuel}	RH_{air}	W_{fuel} (kW)	W_{prs} (kW)
Base case	44.18	25	0.25	0.79	2	1.25	2	1	0.5	98.52	6.47
$\omega = 1$	53.15	52.93	0.11	0.86	3.03	1.10	1.66	1	0.5	79.66	7.66
$\omega = 0.85$	51.33	40.56	0.14	0.87	4.91	1.10	1.53	1	0.5	78.44	9.74
$\omega = 0.5$	42.20	19.19	0.35	0.75	5.00	1.10	1.58	1	0.5	91.65	11.32
$\omega = 0.15$	32.41	15.00	0.56	0.60	5.00	1.10	1.46	1	0.5	114.96	12.74
$\omega = 0$	24.80	14.51	0.67	0.51	5.00	1.20	1.39	1	0.5	145.60	13.89

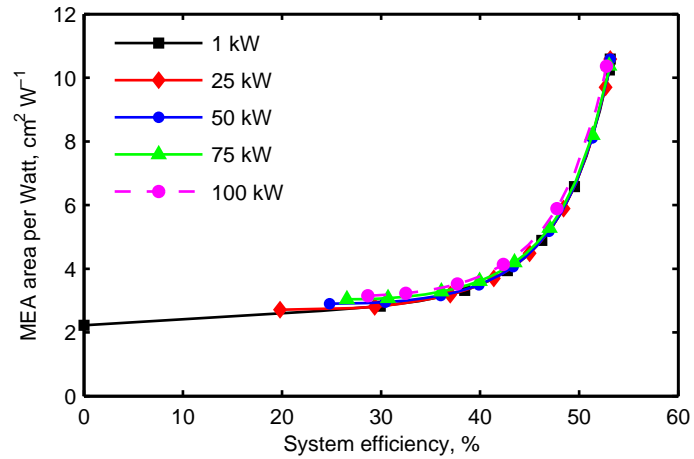
the Pareto set. In Figure 5.3, the points that correspond to $\omega = 0.60$ up to $\omega = 0.65$ have both a higher efficiency and a smaller size compared to the base case so they improve on both objectives.

The points at the far right of Figure 5.3 represent solutions in which the size of the system is compromised in favour of the efficiency. Moving down the curve, to the left, the size of the system is improved but the efficiency reduces. None of the points is essentially superior and the final design choice will depend on the factors specific to the application. For stationary applications, the size of the system can be traded for the efficiency. This is not the case, however, for mobile and transportation applications which require highly efficient and small systems. Furthermore, at the efficiency of approximately 47% and above, the slope of the curve is very steep. In this region large increases in the size of the system result in small gains in efficiency. For instance, 51% efficiency is better than 52% from an economic point of view. This is because approximately 6 m² (15%) additional MEA area is likely to be too much to justify the 1% increase in the efficiency. Conversely, at the efficiency of about 40% and below, the curve appears to be flat. This suggests that in this region, a small change in the size of the system leads to a large impact on the efficiency. An example from Figure 5.3 is a 5% efficiency jump from 25% to 30% will only require 0.20 m² (1.5%) increased in the MEA area. In this region, the average increase in the MEA area is roughly 0.20 m² for every 1% increase in the efficiency. Overall, to make the most of the trade-off behaviour in Figure 5.3, the PEFC system must be operated at an efficiency of at least 40%.

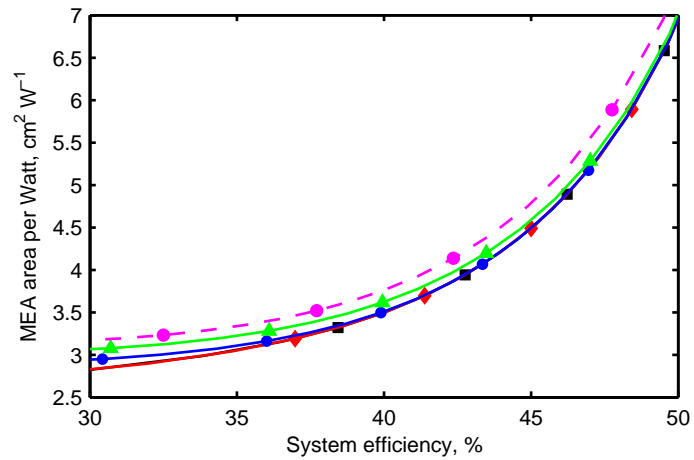
Table 5.3 gives the optimal values of the design variables for the representative solutions highlighted in Figure 5.3. The extreme points, $\omega = 1$ and $\omega = 0$ represent the single-objective optimisation solutions and, thus are not expected to follow the trend of how each variable behaves. In general, moving from a high efficiency, large size solution to a non-dominated, low efficiency, small size solution in the Pareto set involves increases in the operating current density (thus, decreased cell voltage) and pressure.

The optimal values of the hydrogen fuel and air relative humidity turn out to be 1 and 0.5, respectively, for all ω 's. The optimal hydrogen stoichiometric ratio is 1.1 (i.e. hydrogen utilisation rate of 91%) for all ω 's except at an extreme point. Finally, in moving along the Pareto set in the mentioned manner, the fuel consumption and parasitic loss increase.

Similar analyses were performed for different stack power outputs, namely, 1, 25, 50, 75 and 100 kW. Figure 5.4(a) shows the comparison of the generated Pareto sets. In this figure, the MEA area per Watt is plotted against the efficiency for each stack power output. The Pareto sets are qualitatively similar in shape but differ in span. Also, the solutions of the single-objective efficiency maximisation at different stack power outputs nearly completely converge with an efficiency of 53% and a MEA area of 10.5 cm² per Watt. On the other hand, the solutions of the single-objective size minimisation settled at an average MEA area of 2.8 cm² per Watt with increasing efficiency as stack power output increases. A region of interest is enlarged in Figure 5.4(b) to emphasise the difference in the solutions at different stack power output. It can be observed that for a particular value of the efficiency, increasing the stack power output eventually results to an increase in the MEA area required per Watt of power produced. For example, at an efficiency of 45%, the MEA area per Watt at stack power output of 75 kW and 100 kW are 3% and 7%, respectively, bigger relative to the MEA area per Watt at stack power output of 1, 25, and 50 kW.



(a)



(b)

Figure 5.4: Comparison of the Pareto sets at different stack power outputs, showing (a) the entire range and (b) an enlarged region to emphasise the difference in the solutions.

Figures 5.5 and 5.6 show the optimal values of the design objectives and some of the design variables, respectively, plotted against the current density for different stack power outputs. The solutions that are large in size and high in efficiency, forming the right branches of the Pareto sets in Figure 5.4(a), occur at low current density. Conversely, the left branches of the Pareto sets in Figure 5.4(a), containing the solutions that are small in size and low in efficiency, occur at high current density. Overall, with respect to the current density, the MEA area, efficiency and voltage are decreasing, whilst the input power and parasitic power are increasing. Furthermore, the input power and parasitic power are increasing, whilst the voltage and air stoichiometric ratio are decreasing with increasing stack power output. Moreover, the single-objective

size minimisation at the stack power output of 1 kW resulted to a solution with zero efficiency. In this particular solution, the power produced by the stack is all consumed by the system as the parasitic loss resulting in a zero net power output.

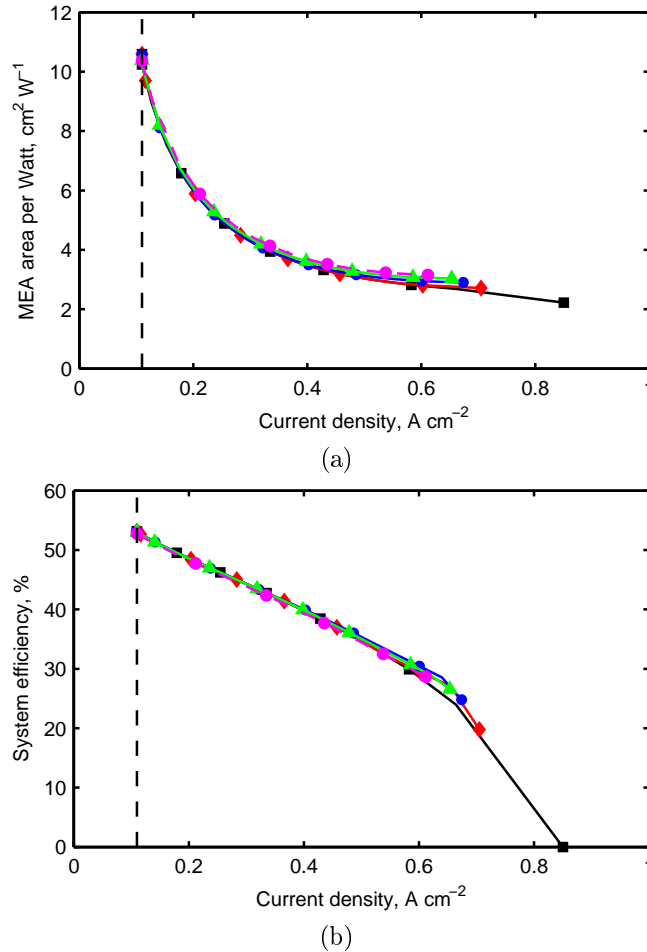


Figure 5.5: Optimal values of the design objectives plotted against the current density: (a) MEA area per Watt and (b) system efficiency.

It can also be observed from Figure 5.6 that some of the bounds on the design variables were hit during optimisation, specifically the lower bound on the current density, the upper bound on the pressure, and the bounds on the hydrogen stoichiometric ratio. Lowering the bounds on the current density and hydrogen stoichiometric ratio are not useful because in an actual operation current density below 0.11 A/cm² and hydrogen stoichiometric ratio less than 1.1 are not practical. Comparison of Figure 5.6(b) with Figure 5.4(a) shows that the solutions that hit the upper bound on the pressure correspond to the region in Figure 5.4(a) where the branches of the Pareto sets appear to

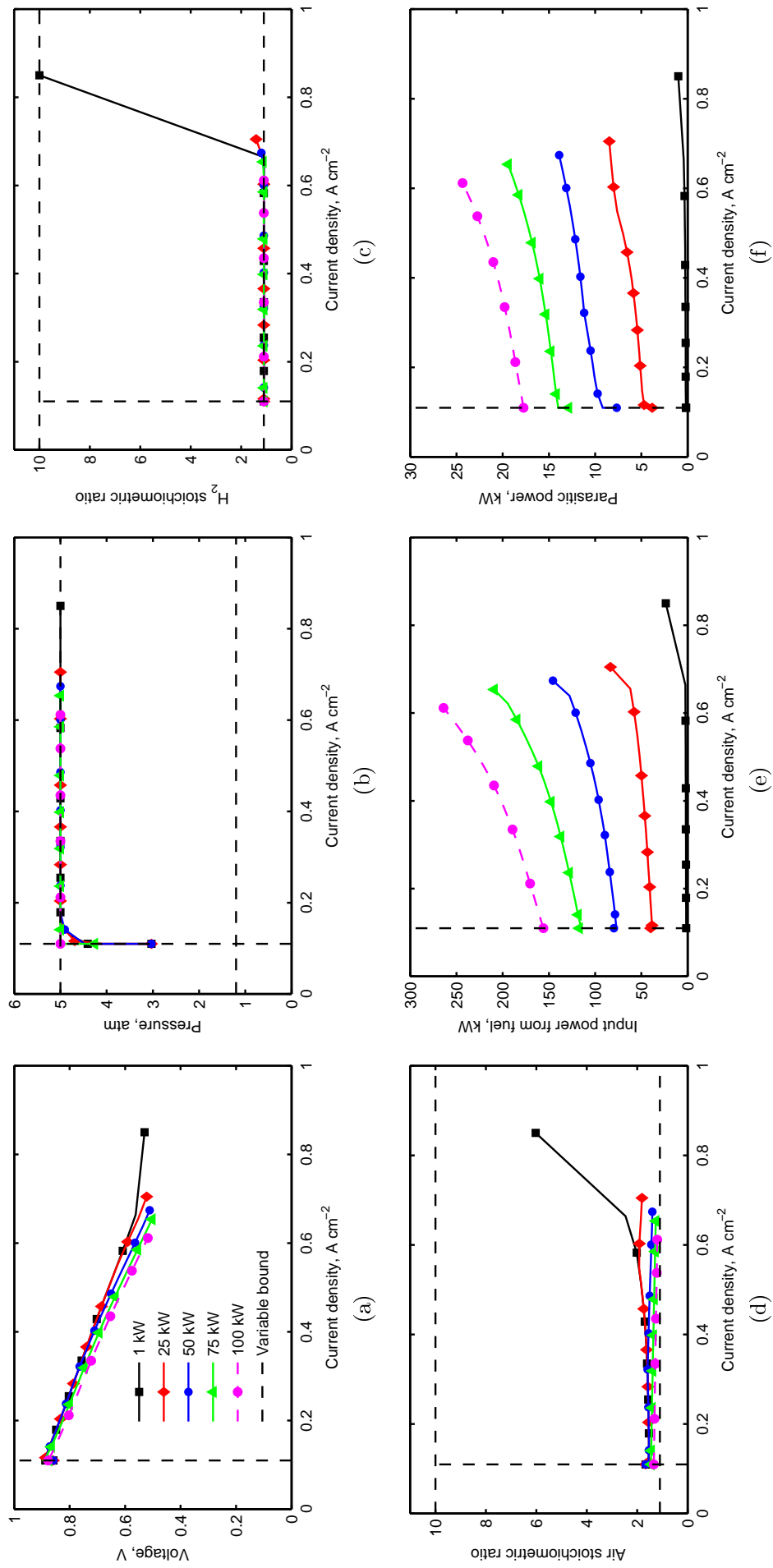


Figure 5.6: Optimal values of some of the design variables plotted against the current density: (a) voltage, (b) pressure, (c) hydrogen stoichiometric ratio, (d) air stoichiometric ratio, (e) input power and (f) parasitic power.

be separated. These solutions could have achieved smaller sizes and higher efficiency values if the bound on the pressure had allowed them to.

Consequently, the effect of increasing the upper bound on the pressure to 10 atm was investigated. Pressures higher than 5 atm are not usually used in actual operation. This upper bound was only considered for diagnostic purposes. In Figure 5.7, the solutions that previously hit the 5 atm upper bound on the pressure assumed higher values of pressure when the bound is relaxed. The resulting Pareto sets for different stack power outputs are shown in Figure 5.8. As an illustration, for the stack power output of 100 kW at an efficiency of 45%, the size is reduced by 6.25% by using an upper bound on the pressure of 10 atm (MEA area of 45 m²) instead of 5 atm (MEA area of 48 m²). Moreover, the Pareto sets for different stack power outputs appear to be closer to each other when compared with Figure 5.4. The slight separation is due to the solutions still reaching the 10 atm upper bound on the pressure at high current density.

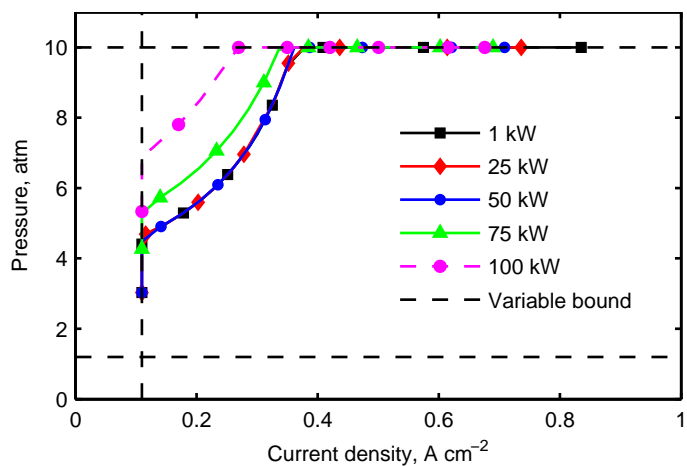
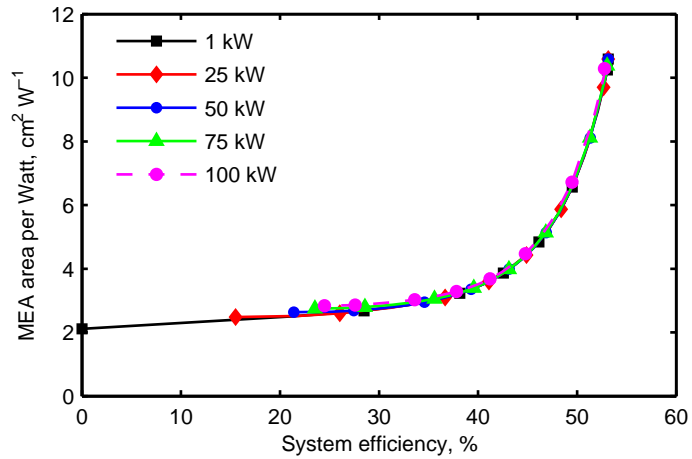
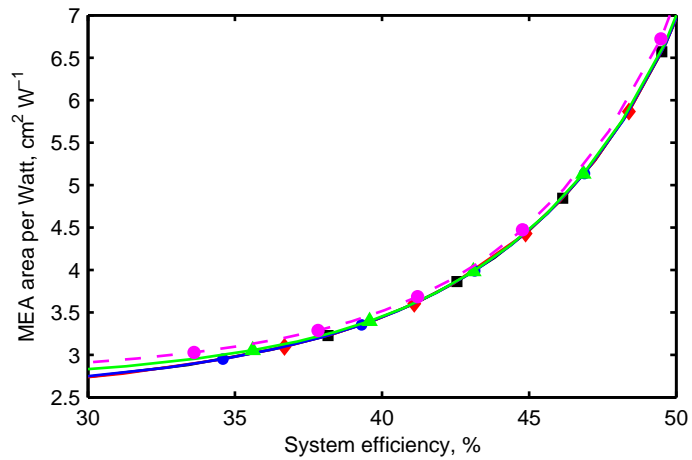


Figure 5.7: Optimal values of the operating pressure with the upper bound increased to 10 atm.



(a)



(b)

Figure 5.8: Comparison of the Pareto sets at different stack power output with the upper bound on the pressure increased to 10 atm, showing (a) the entire range and (b) an enlarged region to emphasise the difference in the solutions

5.4 Conclusions

An optimisation model for a PEFC stack, suitable for use within a multi-objective framework, has been proposed. This model allows us to investigate the trade-offs between the efficiency and the size. The simulation of the model for a base case shows that for a given power output, a more efficient system is bigger and *vice versa*. The Pareto sets, generated for different power outputs, represent a quantitative description of the trade-offs between efficiency and size. The results of this study illustrate the importance of formulating the problem as a multi-objective optimisation. Maximisation of

the efficiency without taking the size into account will result to a possibly impractically large system. Conversely, a significantly small system but with very low efficiency will result if the only objective is size. Overall, the system must be operated at an efficiency of at least 40% but not more than 47% to make the most of the size-efficiency trade-off behaviour. Furthermore, the MEA area should be at least 3 cm² per Watt for the efficiency to be practically useful. Moreover, given the constraints of the model, which are based on technical practicalities, a PEFC stack such as the one presented cannot reach an efficiency of more than 54%. This chapter presents a method of determining the PEFC stack optimal design such that for a particular application, a balance between efficiency and size is achieved.

Chapter 6

Introduction to the design of a fuel cell micro-cogeneration plant

Micro-cogeneration is a promising technology that has the potential to replace grid electricity and conventional home space heating and hot water systems. They offer the promising benefits of lower energy costs and CO₂ emissions in the residential housing sector. Amongst the different micro-cogeneration technologies, fuel cells have the highest electrical efficiency, lowest emissions and a low heat-to-power ratio that is well suited for residential applications. This chapter discusses the important issues relevant to the design of a fuel cell micro-cogeneration plant.

6.1 Introduction

The conventional method of power generation and delivery is a relatively inefficient process. Figure 6.1 illustrates the efficiency losses associated with a conventional centralised power plant. Even the most modern combined cycle power plants can only achieve efficiencies of 50 - 60% [98]. The majority of the energy content of the fuel is lost at the power plant through the discharge of waste heat. Further losses take place in the transmission and distribution of electric power to the end user. The inefficien-

cies and the pollution associated with centralised power generation motivate the new developments in distributed or decentralised or on-site power generation.

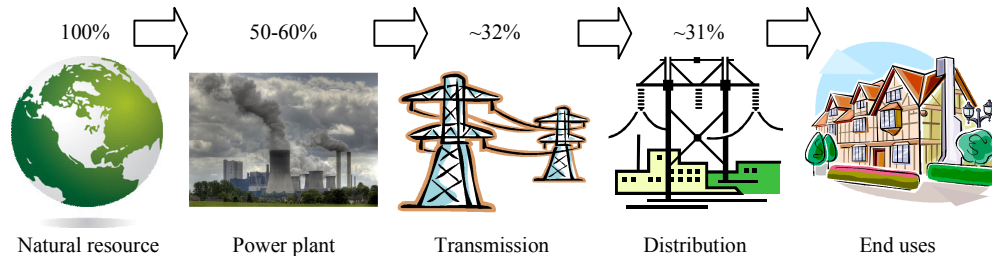


Figure 6.1: Efficiency of a centralised power generation and delivery.

Distributed power generation allows consumers to generate power on-site, using any appropriate generation method. Consumers can adapt their generation directly to their load, making them independent from grid power failures. It also offers opportunity for consumers to export electricity to the grid. Distributed power generation could be an effective solution to efficiency, pollution and deregulation issues that the electric utility industry currently experiences.

Distributed energy systems include combined heat and power, micro-combined heat and power, micro-turbines, photovoltaic systems, reciprocating engines, small wind power systems, amongst others [163]. This chapter introduces the optimal design of micro-combined heat and power systems based on fuel cell.

6.2 Micro-cogeneration

Micro-cogeneration is the decentralised and simultaneous generation of heat and power for residential and small commercial applications. It is sometimes referred to as micro-combined heat and power (micro-CHP) or residential cogeneration [163, 164]. The EU Cogeneration directive defines an upper limit on capacity of 50 kW_e [165], whereas others define “domestic” micro-cogeneration as being under 3 kW_e [102].

A micro-cogeneration system can be thought of as a small-scale power station generating energy in the home. The by-product heat that would otherwise be wasted

is instead captured and utilised for space and water heating. It is anticipated that micro-cogeneration may provide an installed generation capacity of a similar order of magnitude to the nuclear industry [166]. A micro-cogeneration system can also be looked at as an effective replacement for the gas central heating boiler. It can supply heat and hot water as usual but additionally provides the majority of the home's electricity needs. The potential success of micro-cogeneration lies in the large number of systems that may ultimately be installed in the millions of homes in the UK and other European countries where natural gas is currently the dominant heating fuel.

Figure 6.2 illustrates the micro-cogeneration concept applied to a home. Natural gas enters the building from the gas distribution network; the fuel cell (or other cogeneration technology) generates heat to service the space and water heating loads and electrical power for lights and other appliances. Electricity can be exported to the grid at times of excess production, and imported at times of high electrical load. Net or “smart metering” allows the balance of export and import to be logged. Similarly, excess production or demand for heat can be accommodated by a hot water storage tank.

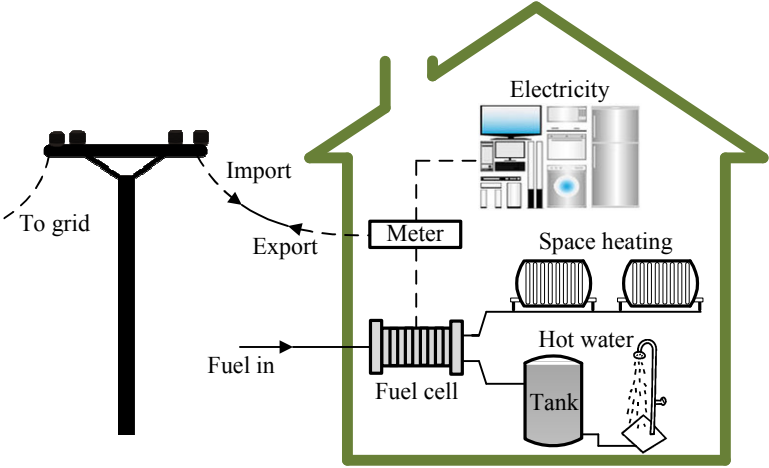


Figure 6.2: The micro-cogeneration concept showing the import/export of electricity.

Applying micro-cogeneration technology in residential and small commercial buildings is an attractive option because of the large potential market, as shown in Figure 6.3. The domestic and small commercial sectors account for 34% of the total electricity and gas consumption in the UK [167]. Also, about 91% of urban dwellings and 63% of

rural dwellings in England and Wales are connected to the mains natural gas supply and nearly all are connected to the mains electricity supply [168]. The widespread availability of natural gas and electricity, the predicted growth in the number of homes (e.g., from 20.3 million in England and Wales in 1996 to an estimated 24 million by 2021) and the relatively large differential between unit gas and electricity prices in the domestic sector are important facilitators for micro-cogeneration.

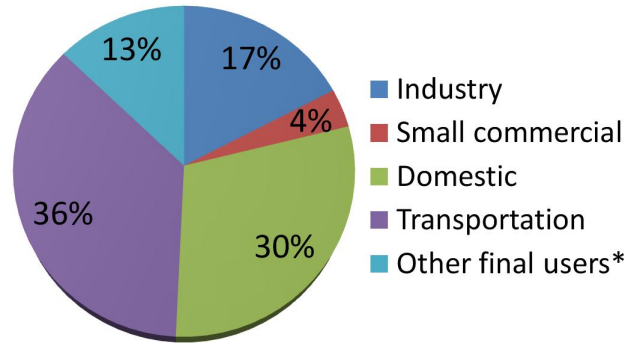


Figure 6.3: Energy consumption in the UK by end user 2000 to 2008 [167].

6.3 Classification

Generally, a micro-cogeneration system will be installed within, or close to, the dwelling and the recovered heat will be delivered to a thermal store (e.g., the common domestic hot water tank) and/or to the central heating circuit). Depending on the system’s design and operating regime, the electrical output may be connected to the electricity distribution network (e.g., for frequency synchronisation and exporting surplus generation) and/or to local energy stores. This leads to the following broad classification of micro-cogeneration units.

1. ‘Network-connected’ systems, which provide significant proportions of the household’s heat and power demands, but rely on network electricity whenever the electrical output of the micro-cogeneration system is less than the instantaneous demand of the household. Most micro-cogeneration system developers are focusing on units that will be connected to the electricity network.

2. ‘Autonomous’ systems, which provide all (or very high proportions) of the household’s heat and power demands and are designed to meet the transient fluctuations in demand. These systems will have little or no interaction with the electricity network.

Both types require a prime mover (e.g., an engine or fuel cell), a heat-recovery system and a control system, but autonomous micro-cogeneration systems additionally require energy stores and conversion/reconversion hardware [169].

6.4 Technologies

At present, several different types of micro-cogeneration technologies are under development including the internal combustion engine, the Stirling engine and the fuel cells [102, 163, 164, 170]. Examples are given in Figure 6.4. All of them consume fuel to produce heat and electricity simultaneously. In the case of internal combustion and Stirling engines, an engine drives a generator to produce electricity. A fuel cell, on the other hand, generates direct current (DC) electric power by consuming fuel within electrochemical cells. Amongst the candidates for micro-cogeneration applications, fuel cells have the highest electrical efficiency and lowest emissions [2, 28, 171]. Currently, the low-temperature PEFC and the high temperature solid oxide fuel cell (SOFC) are the ones mostly deployed for micro-cogeneration. PEFCs are recently attracting interest for micro-cogeneration applications due to their stable and non-corrosive electrolyte, and many advances leading to lower cost and improved anode poisoning tolerance [1].



(a) An internal combustion micro-cogeneration system.



(b) A Stirling engine micro-cogeneration system.



(c) A fuel cell micro-cogeneration system.

Figure 6.4: Different micro-cogeneration technologies [102].

6.5 Literature survey on micro-cogeneration

The increasing interest in micro-cogeneration is evident in the growing number of publications in the open literature. This is partly due to the escalating attention given to climate change and the increasing awareness of the urgent need for reductions in CO₂ emissions, and rising concerns regarding the security of energy supply and the unpredictability of energy market.

There are a number of microgeneration-related published reviews. Bergman et al. [172] explored the publications regarding the government policy and behavioural aspects

associated with the adoption of micro-cogeneration in the UK. Mago and Chamra [173] reviewed the energy, economical, and environmental benefits of the use of micro-cogeneration systems for small commercial buildings. Gibbs and Steel [174] looked at the changes in the European electricity market and described the market sector currently being targeted by micro-cogeneration manufacturers. Biezma et al. [175] provided a review of the investment criteria for the selection of cogeneration plants. Wu et al. [10] examined the status of the development of micro-cogeneration in the US, Europe, Asia and the Pacific.

Several works assessed the benefits of micro-cogeneration. For instance Refs. [169, 176–180] evaluated micro-cogeneration in terms of economic and environmental performance. Hawkes and Leach [181] introduced a new concept to appraise the benefits of the technology. They defined *capacity credit* as a measure of the amount of conventional generation that would be displaced by an alternative technology.

Some papers are concerned with the operational aspect of the system. For example, Colella et al. [182] considered different methods of rapidly varying the heat-to-power ratio necessary for instantaneously meeting the demands for heat and electricity. Giddey et al. [183] investigated the effect of methane and carbon dioxide composition in the fuel on the power output. Gigliucci et al. [184] evaluated performance, flexibility and operational requirements at different possible operating conditions of an installed residential micro-cogeneration system based on PEFC. Au et al. [55] investigated the influence of operating temperature on the efficiency of a fuel cell micro-cogeneration plant fuelled by natural gas.

The majority of the models for micro-cogeneration systems in the literature either considered thermo-economics or engineering design. Thermo-economic modelling combines thermodynamics and cost analyses to assess and improve the performance of energy systems [185]. Some of the studies that performed thermo-economic modelling include Refs. [100, 101, 179, 185]. Also, there are models that considered engineering design from a technical point of view. However, most of these are limited to a specific

subsystem or component of the system. For example, Campanari et al. [186] presented a lumped-volume approach for a membrane reformer for hydrogen production applied to a PEFC micro-cogeneration system. Their model calculates the energy balance and the flow composition based on utilisation factors and reactant compositions. Jahn and Schroer [187] presented a lumped model of a natural gas steam reformer being part of a residential fuel cell power plant. Pukrushpan et al. [188] developed a model for a catalytic partial oxidation reactor that reforms natural gas to hydrogen-rich mixture to feed the anode field of fuel cell stack. Ersoz et al. [189] simulated the fuel processing subsystem using Aspen-Hysys process simulation software. Colella et al. [190] provided a model for the afterburner implemented in Aspen Plus chemical engineering software. Studies that present a complete model for the whole system are scarce. The work presented in this thesis tries to fill this gap by presenting a comprehensive model that describes the behaviour and the operation of both the main and the auxiliary components of the entire system.

Several studies dealt with achieving an optimal micro-cogeneration system design. The majority of these works optimised the cost [58, 66, 191–195]. Hawkes et al. [58, 193] minimised the equivalent annual cost consisting of capital cost, maintenance cost, fuel cost, electricity import cost and annual revenue from electricity export. The decision variables are stack electrical output capacity, supplementary boiler capacity, stack electrical output, natural gas consumption by the supplementary boiler, electricity import, and electricity export. Al-Azri and Al-Thubaiti [191] developed an optimisation model for a process cogeneration system with a particular focus on the power cycle and how it integrates with the overall process. Their model can be used to identify the optimum equipment size and the operating parameters such as boiler pressure, superheat temperature and steam load. They illustrated the application of their model in minimising the cost, satisfying the heat requirement of the process, and producing the maximum power. El-Sharkh et al. [192] presented a hybrid evolutionary programming and Hill-Climbing based approach to evaluate the impact of change of cost parameters (tariff

rates for purchasing or selling electricity, fuel cost, and hydrogen selling price) on the optimal operational strategy (hourly generated power, amount of thermal power recovered, power trade with the local grid, and quantity of hydrogen that can be produced) of a fuel cell power plant. Lozano et al. [195] proposed an integrated energy-planning framework based on mixed integer linear programming to determine the optimal configuration of energy supply systems for tertiary sector buildings. The objective function is the annual total cost and considers the legal constraints imposed in selling the surplus electricity to the grid. Although these studies made significant contribution to micro-cogeneration system design, their results might be misleading because the coupling or interaction between the multiple objectives has not been considered [146].

6.6 Criteria for the design of a micro-cogeneration plant

As was discussed in Chapter 2, a good fuel cell system design satisfies the design requirements and represents a trade-off amongst the different design objectives [31]. Thus, it is imperative to identify the critical criteria and those that can be sacrificed without jeopardising the design. In addition to the general fuel cell system design criteria discussed in Section 3.2, this section considers the key issues for some of the most important criteria specific for the design of a fuel cell micro-cogeneration plant.

6.6.1 Size

The optimal sizing of a micro-cogeneration unit is a continuing point of discussion amongst engineers. A large unit can potentially provide higher electrical outputs, thus higher cost and carbon savings. However, oversizing the unit increases the capital cost, and can lead to excessive heat dumping which erodes the economic and environmental benefits of the system if the power cannot be sufficiently turned down. Also, oversizing

often results in cycling operation (repeated short operating cycles), which reduces the efficiency due to the losses incurred during startup and shutdown [196]. Undersizing a micro-cogeneration system, however, will lead to greater reliance on backup heating systems and grid electricity. If such backups are not available, the property will heat up less quickly and may not reach comfortable internal temperatures [102].

Another key issue in sizing is the electrical output of the system relative to the site's base load electricity demand. If export tariffs are not available, it is beneficial to ensure that all the electricity generated is used on-site. If they are, it may be economically viable to generate large amounts of electricity provided that the property can utilise the additional heat produced. In some cases there may be a benefit from using a heat storage which can act as an effective buffer to support the production of hot water at times of peak demand. However, any potential benefits may be undermined by the heat losses associated with currently available heat storage.

The field trials undertaken by the Carbon Trust suggest that matching the capacity of the micro-cogeneration to the heat demand of the property is often advantageous [102]. In this case, the rated heat output of the micro-cogeneration system is sized to adequately meet the comfort requirements of the end user on the coldest winter days. Anything larger than this involves some modulating capability, heat dumping and/or heat storage [197].

How a fuel cell micro-cogeneration unit is sized and operated is a trade-off between system efficiency (fuel cost), unit size (capital cost) and heat-to-power ratio. Ang *et al.* [3] have quantified the trade-offs between the efficiency and the size of a PEFC stack. In practice, accurate and detailed demand data for heat and electricity are fundamental to accurately sizing a micro-cogeneration unit. Figure 6.5 shows a representative heat and power load variation over the course of 24 h for a typical family home.

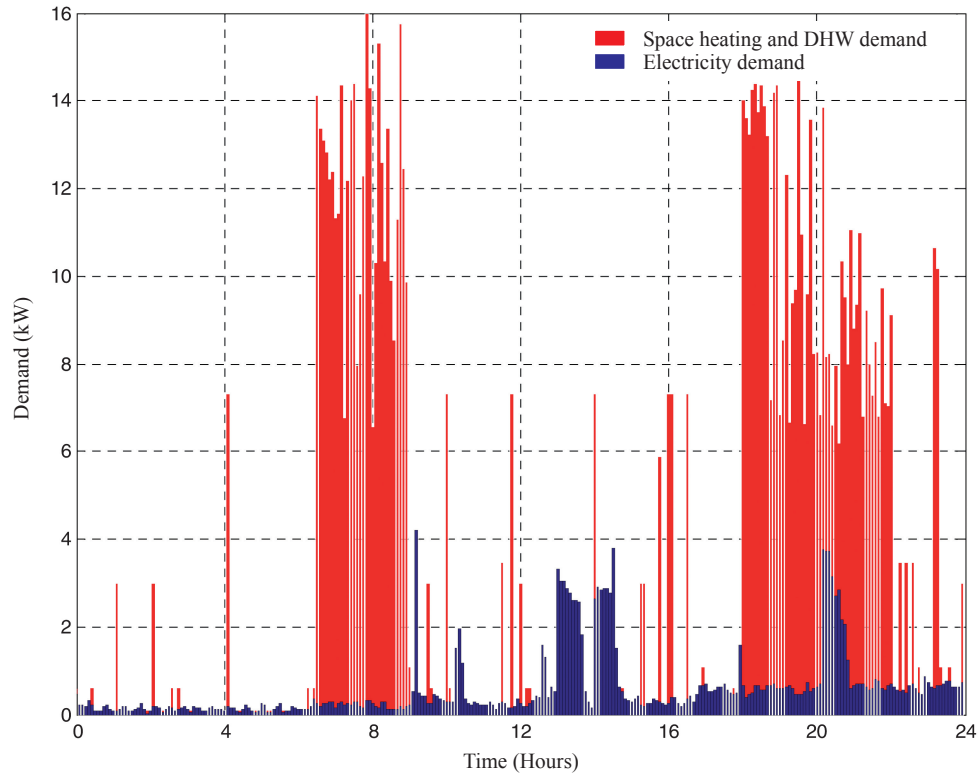


Figure 6.5: Illustration of a typical electrical and heat load for a UK dwelling. Values are in (average) kW, for each 5 min period of a typical winter day. Based on data from IEA Annex 42 [198].

6.6.2 Conversion efficiency

The efficiency of a micro-cogeneration system is the fraction of the chemical energy in the input fuel that can be recovered as electrical power and heat. There are three primary efficiencies associated with micro-cogeneration: the electrical efficiency, the thermal efficiency and the overall efficiency. In general, maximising the overall efficiency often results in a high performance operation [102]. For micro-cogeneration, the electrical efficiency is more important than the thermal efficiency due to the higher value of electricity relative to heat, in terms of both cost and carbon intensity. Fuel cells offer significantly higher electrical efficiency than engine-based technologies and can rival modern combined cycle gas turbine (CCGTs). However, their overall efficiency is currently lower than engines, which is largely due to their relative immaturity and difficulties in capturing low-grade waste heat [103].

6.6.3 Heat-to-power ratio

The heat-to-power ratio affects the overall energy, cost and carbon savings benefits of micro-cogeneration. Although the overall efficiency is important, the relative level of electrical output has the biggest impact on carbon saving performance. Relatively small increases in electrical efficiency (*i.e.* decreases in heat-to-power ratio) can result in significant increases in potential carbon savings [102]. The heat-to-power ratio of a micro-cogeneration system can be varied by operating at different electrical loads and invoking the use of an auxiliary burner [103].

Fuel cells have relatively low heat-to-power ratio ($\sim 0.6\text{-}2:1$) compared with other micro-cogeneration technologies. They are therefore able to operate well in properties with limited demand for heat.

6.6.4 Transient response

Low temperature fuel cells are expected to operate intermittently in people's homes, starting up and shutting down on most days [196,199,200]. The energy required to start and stop the fuel cell system over the course of a year can be significant, as electronic systems must run before and after operation to provide adequate stack conditions, and a long period of pre-heating is required to raise the generator's mass up to the operating temperature. Although the fuel cell stack may be able to operate from ambient temperature (in the case of PEFC), the fuel processor must be heated to several hundred degrees before hydrogen can be produced. The annual seasonal efficiency of a fuel cell micro-cogeneration system will be lower than when measured at steady-state, as the additional gas and electricity consumed during startup and shutdown need to be accounted for [196].

6.6.5 Reliability / availability / lifetime

Fuel cell micro-cogeneration systems are expected to operate for 40,000 to 80,000 hours, equivalent to 10-20 years of intermittent usage. The effect of real-life conditions such as impurities in fuel and oxidant can make the system's operating life shorter.

The latest PEFC systems are expected to exceed the 40,000 target [201]; however, as none of these units have been operating for more than a year in the field this is impossible to verify at present. The longest reported lifetimes so far from the Japanese field trials have been around 20,000 hours [196]. Due to challenging materials requirements, SOFC lifetimes are currently around half those for PEFC, with up to 15,000 hours reported in field trials, and 20,000 hours expected to be attainable by micro-cogeneration systems by 2015 [196].

Currently, both PEFC and SOFC stacks lose power at a rate between 0 and 5% per thousand hours, depending on the design and materials used. Reduced catalytic activity in the cells and reformer, combined with increasing cell resistance causes a gradual drop in output voltage, and thus power output. This can shorten stack lifetime, but mechanical deterioration of the cells is usually the limiting factor.

6.7 Conclusions

Fuel cells offer many benefits for residential micro-cogeneration because of their high electrical efficiency, low emissions and low heat-to-power ratio, though it has yet to reach full commercialisation. There are several key technical challenges, such as improving the efficiency and durability of operating systems and lowering the capital cost, that need to be overcome for this technology to be successful. This chapter provides the context for interest in fuel cell micro-cogeneration systems, the classification and the technologies. The current state of the art of technology was surveyed and the criteria relevant to the design of a fuel cell micro-cogeneration was discussed.

The design of fuel cell micro-cogeneration systems involves decision-making in which trade-offs are made between conflicting objectives. The next chapters illustrate the use of modelling and optimisation in informing system design by generating different design alternatives that contain these trade-offs, thus allowing the design engineers to make decisions in a quantitative and rational way.

Chapter 7

Optimal design of a fuel cell micro-cogeneration plant

A system-level mathematical model for a PEFC micro-cogeneration system is developed by integrating the PEFC stack model presented in Chapter 5 with the necessary subsystems, namely the fuel processing subsystem, the thermal management subsystem and the power management subsystem, for it to operate as a residential heat and power generator. The design of such system naturally involves simultaneous optimisation of two or more conflicting objectives including many decision variables and constraints. A case study is presented to illustrate the use of the model in investigating the trade-off between conflicting objectives. For example, at a given thermal power rating there is a trade-off between the net power output and the fuel consumption. These two design criteria are vital in assessing the economic benefits of the technology. Pareto sets, which give the quantitative description of the trade-offs between the net power output and the fuel consumption, can be generated at different thermal power ratings. Several results on the design of a PEFC micro-cogeneration system for a single family dwelling are presented.

7.1 System description

Figure 7.1 shows a schematic of a typical PEFC based fuel cell system for residential micro-cogeneration running on reformed hydrogen from natural gas (the description of the subsystems are given in Ref. [202]). This system has been used as the basis for modelling and optimisation studies performed on a fuel cell micro-cogeneration.

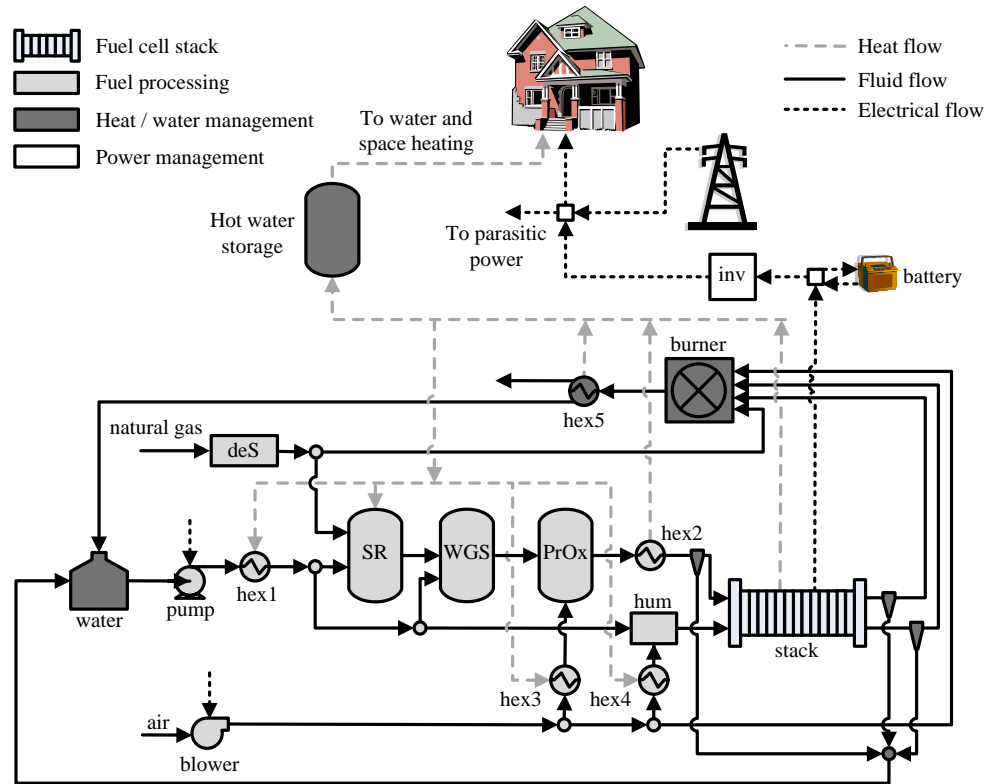


Figure 7.1: Schematic of a fuel cell micro-cogeneration system. The symbols in the diagram refer to: deS: desulphuriser; hex: heat exchanger; hum: humidifier; inv: DC/AC converter; PrOx: preferential oxidation reactor; SR: steam reformer; WGS: water gas shift reactor.

A PEFC micro-cogeneration system converts natural gas, liquid petroleum gas (LPG), or other readily accessible fuels into electrical or thermal energy via four subsystems. In this study, natural gas is considered as the fuel. Thus, the system takes advantage of the already established infrastructure and system for natural gas distribution in the UK. First, the fuel processing subsystem, shown in light grey in Figure 7.1, generates a hydrogen-rich gas mixture from the natural gas via steam reforming. Second, the fuel

cell stack subsystem transforms the chemical potential in the hydrogen gas mixture into DC electricity. Third, the thermal management subsystem, shown in dark grey in Figure 7.1, manages the heat recovered from the fuel processing subsystem and fuel cell subsystem for water and space heating. Fourth, the power management subsystem, shown in white in Figure 7.1, converts the electric power into alternating current (AC) and coordinates the electric power produced by the fuel cell with that drawn from grid. Through these four subsystems, a PEFC micro-cogeneration system provides power and heat for a home, office or other building.

The subsequent sections discuss the mathematical model of the main components of each subsystem.

7.2 Fuel processing subsystem

The equipment for fuel, air and water supplies are incorporated with the fuel processing subsystem.

This subsystem is mainly composed of three reactors in series - steam reformer, water gas shift reactor and preferential oxidation reactor. Hydrogen is generated from natural gas via steam reforming. To produce hydrogen pure enough to be used in PEFCs, additional processes such as water gas shift reaction and preferential oxidation are employed. The shift and preferential oxidation reactors reduce the content of CO in the reformat gases to the level acceptable for the PEFC. In this study, sulfur compounds present in the fuel are assumed to be negligible, thus a desulfurisation step is not necessary.

The reformat gases are further processed in a heat exchanger to bring down its temperature to that of the fuel cell stack. Also, the air supplied to the cathode of the stack is humidified to prevent the membrane of the fuel cell from dehydrating.

7.2.1 Fuel, air and water supplies

Natural gas from the gas distribution network is supplied to the fuel processor. At times of high thermal and low electricity demands, the fuel processor, hence the fuel cell stack, may be bypassed and the fuel may be fed directly into the afterburner. The flow rate of natural gas supplied to the system is:

$$M_{\text{CH}_4,\text{in}} = M_{\text{CH}_4,\text{sr},\text{in}} + M_{\text{CH}_4,\text{burn},\text{in}} \quad (7.1)$$

A compressor is used to provide air to the system. The fuel processing subsystem and the fuel cell subsystem may share the same air supply as they typically operate at the same pressure. The air drawn by the compressor is distributed to the preferential oxidation reactor, the fuel cell stack and the afterburner. The flow rate of air supplied to the system is:

$$M_{\text{air},\text{in}} = M_{\text{air},\text{hex3},\text{in}} + M_{\text{air},\text{hex4},\text{in}} + M_{\text{air},\text{burn},\text{in}} \quad (7.2)$$

In Figure 7.1, heat exchangers, hex3 and hex4, are used to heat up the air to the temperature of the preferential oxidation reactor and the fuel cell stack, respectively. The heat required by the heat exchangers are:

$$\begin{aligned} Q_{\text{hex3}} = & (M_{\text{O}_2,\text{hex3},\text{out}}C_{p,\text{O}_2} + M_{\text{N}_2,\text{hex3},\text{out}}C_{p,\text{N}_2}) (T_{\text{hex3}} - T_{\text{ref}}) \\ & - (M_{\text{O}_2,\text{hex3},\text{in}}C_{p,\text{O}_2} + M_{\text{N}_2,\text{hex3},\text{in}}C_{p,\text{N}_2}) (T_{\text{air},\text{in}} - T_{\text{ref}}) \end{aligned} \quad (7.3)$$

$$\begin{aligned} Q_{\text{hex4}} = & (M_{\text{O}_2,\text{hex4},\text{out}}C_{p,\text{O}_2} + M_{\text{N}_2,\text{hex4},\text{out}}C_{p,\text{N}_2}) (T_{\text{hex4}} - T_{\text{ref}}) \\ & - (M_{\text{O}_2,\text{hex4},\text{in}}C_{p,\text{O}_2} + M_{\text{N}_2,\text{hex4},\text{in}}C_{p,\text{N}_2}) (T_{\text{hex4},\text{in}} - T_{\text{ref}}) \end{aligned} \quad (7.4)$$

Similarly, the water supplied by the pump is converted to steam and is allocated to the

steam reformer, the shift reactor and the humidifier.

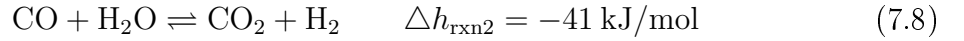
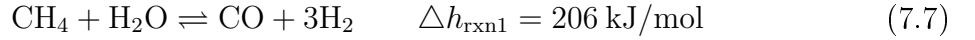
$$M_{w,hex1,out}^v = M_{w,sr,in}^v + M_{w,wgs,in}^v + M_{w,hum,in}^v \quad (7.5)$$

The heat needed for steam generation, Q_{hex1} , is:

$$Q_{hex1} = M_{w,hex1,out}^v C_{w,hex1}^v (T_{hex1} - T_{ref}) + M_{w,hex1,out}^v \Delta H_{vap} - M_{w,pump,out}^l C_{p,w}^l (T_{pump} - T_{ref}) \quad (7.6)$$

7.2.2 Steam reforming

The two main reactions taking place in the steam reformer are steam reforming and slight water gas shift reaction



The model for the steam reformer is based on the model presented by Jahn and Schroer [187], in which the steam reformer is considered as an equilibrium reactor. Reactions 7.7 and 7.8 are independent [187], hence, the component balances can be expressed in terms of the extent of reactions. Equation 7.9 represents the CH_4 , H_2O (vapour), H_2 , CO_2 and CO component balances.

$$\begin{pmatrix} M_{CH_4,sr,out} \\ M_{w,sr,out}^v \\ M_{H_2,sr,out} \\ M_{CO_2,sr,out} \\ M_{CO,sr,out} \end{pmatrix} = \begin{pmatrix} M_{CH_4,sr,in} \\ M_{w,sr,in}^v \\ 0 \\ 0 \\ 0 \end{pmatrix} + \xi_1 \begin{pmatrix} -1 \\ -1 \\ 3 \\ 0 \\ 1 \end{pmatrix} + \xi_2 \begin{pmatrix} 0 \\ -1 \\ 1 \\ 1 \\ -1 \end{pmatrix} \quad (7.9)$$

where ξ_1 and ξ_2 are the extent of reactions 7.7 and 7.8, respectively:

$$\xi_1 = p_1 q M_{w, sr, in}^V \quad (7.10)$$

$$\xi_2 = p_2 q M_{w, sr, in}^V \quad (7.11)$$

Polynomial approximations, based on two-dimensional Taylor series, are used to describe the equilibrium. The correlations are valid only at a constant pressure of 3 bar and within a certain range of reactor temperature, T_{sr} , and steam-to-carbon ratio, $\lambda_{S/C}$, specifically 773 K–1073 K and 2–5, respectively.

$$q = \left(1 \quad w \quad w^2 \quad w^3 \quad x \quad x^2 \quad x^3 \quad wx \quad w^2x \quad wx^2 \right)^T \quad (7.12)$$

$$w = \frac{T_{sr}}{100} - 9 \quad (7.13)$$

$$x = \frac{M_{w, sr, in}^V}{M_{CH_4, sr, in}} - 3.5 = \lambda_{S/C} - 3.5 \quad (7.14)$$

$$p_1 = 10^{-3} \times \begin{pmatrix} 195.0 & 88.22 & -5.504 & -9.538 & -30.41 & 7.821 \\ -2.223 & -27.61 & -4.443 & 7.684 \end{pmatrix} \quad (7.15)$$

$$p_2 = 10^{-3} \times \begin{pmatrix} 134.5 & 14.02 & -19.62 & 2.491 & -11.94 & 0.09909 \\ 0.3631 & 0.7817 & 2.711 & -2.110 \end{pmatrix} \quad (7.16)$$

The overall reaction is endothermic. The heat needed for the reaction, Q_{sr} , comes from the overall heat recovered by the system and is given by equation 7.17.

$$\begin{aligned} Q_{sr} = & (M_{CH_4, sr, out} C_{p, CH_4} + M_{w, sr, out}^V C_{p, w}^V + M_{H_2, sr, out} C_{p, H_2} + M_{CO_2, sr, out} C_{p, CO_2} \\ & + M_{CO, sr, out} C_{p, CO}) (T_{sr} - T_{ref}) - M_{w, sr, in}^V C_{p, w}^V (T_{hex1} - T_{ref}) \\ & - M_{CH_4, sr, in} C_{p, CH_4} (T_{CH_4, in} - T_{ref}) + \xi_1 \Delta h_{rxn1} - \xi_2 \Delta h_{rxn2} \end{aligned} \quad (7.17)$$

7.2.3 Water gas shift

The reformat gases leaving the steam reformer is a mixture of mainly hydrogen, carbon dioxide, water vapour, some methane and carbon monoxide. As the platinum catalyst in the fuel cell is extremely prone to CO poisoning, the reformat gases are taken to the water shift gas reactor where CO reacts with additional steam producing more H₂ and CO₂.

The shift reactor is also modelled as an equilibrium reactor. The equilibrium composition and temperature of the gases leaving the shift reactor are calculated from mass and energy balances and temperature-dependent correlation for the equilibrium constant for the shift reaction. Since the equilibrium data is the equilibrium constant instead of the extent of reaction, it is more straightforward to use elemental balances in place of component balances. Equation 7.18 gives the overall mass balance and the C, H and O elemental balances.

$$\begin{pmatrix} 1 & 1 & 1 & 1 & 1 & 1 \\ 1 & 0 & 0 & 1 & 1 & 0 \\ 2 & 1 & 1 & 0 & 0 & 1 \\ 0 & 1 & 0 & 2 & 1 & 1 \end{pmatrix} \begin{pmatrix} M_{\text{CH}_4,\text{sr},\text{out}} \\ M_{\text{w},\text{sr},\text{out}}^{\text{v}} \\ M_{\text{H}_2,\text{sr},\text{out}} \\ M_{\text{CO}_2,\text{sr},\text{out}} \\ M_{\text{CO},\text{sr},\text{out}} \\ M_{\text{w},\text{wgs},\text{in}}^{\text{v}} \end{pmatrix} = \begin{pmatrix} 1 & 1 & 1 & 1 & 1 \\ 1 & 0 & 0 & 1 & 1 \\ 2 & 1 & 1 & 0 & 0 \\ 0 & 1 & 0 & 2 & 1 \end{pmatrix} \begin{pmatrix} M_{\text{CH}_4,\text{wgs},\text{out}} \\ M_{\text{w},\text{wgs},\text{out}}^{\text{v}} \\ M_{\text{H}_2,\text{wgs},\text{out}} \\ M_{\text{CO}_2,\text{wgs},\text{out}} \\ M_{\text{CO},\text{wgs},\text{out}} \end{pmatrix} \quad (7.18)$$

The equilibrium constant, K_p , expressed in terms of the partial pressures of the gases leaving the shift reactor can be expressed as:

$$K_p = \frac{P_{\text{CO}_2,\text{wgs}} P_{\text{H}_2,\text{wgs}}}{P_{\text{CO},\text{wgs}} P_{\text{w},\text{wgs}}} \quad (7.19)$$

where P_i is the partial pressure of each gaseous component:

$$P_i = P_{\text{wgs}} \frac{M_i}{\sum M_i}, \quad i = \text{CO}_2, \text{H}_2, \text{CO}, \text{H}_2\text{O} \quad (7.20)$$

For reaction 7.8, the dependence of K_p on the temperature of the shift reactor is given by equation 7.21 [203].

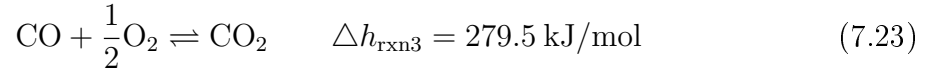
$$K_p = \exp \left[\frac{4577.8}{T_{\text{wgs}}} - 4.33 \right] \quad (7.21)$$

The temperature of the gases leaving the shift reactor, T_{wgs} , can be determined from the energy balance:

$$\begin{aligned} & (M_{\text{CH}_4, \text{sr}, \text{out}} C_{\text{p}, \text{CH}_4} + M_{\text{w}, \text{sr}, \text{out}}^{\text{v}} C_{\text{p}, \text{w}}^{\text{v}} + M_{\text{H}_2, \text{sr}, \text{out}} C_{\text{p}, \text{H}_2} + M_{\text{CO}_2, \text{out}, \text{sr}} C_{\text{p}, \text{CO}_2} \\ & + M_{\text{CO}, \text{sr}, \text{out}} C_{\text{p}, \text{CO}}) (T_{\text{sr}} - T_{\text{ref}}) + M_{\text{w}, \text{wgs}, \text{in}}^{\text{v}} C_{\text{p}, \text{w}}^{\text{v}} (T_{\text{wgs}, \text{in}} - T_{\text{ref}}) \\ & = (M_{\text{CH}_4, \text{wgs}, \text{out}} C_{\text{p}, \text{CH}_4} + M_{\text{w}, \text{wgs}, \text{out}}^{\text{v}} C_{\text{p}, \text{wgs}} + M_{\text{H}_2, \text{wgs}, \text{out}} C_{\text{p}, \text{H}_2} + M_{\text{CO}_2, \text{wgs}, \text{out}} C_{\text{p}, \text{CO}_2} \\ & + M_{\text{CO}, \text{wgs}, \text{out}} C_{\text{p}, \text{CO}}) (T_{\text{wgs}} - T_{\text{ref}}) - (M_{\text{CO}, \text{sr}, \text{out}} - M_{\text{CO}, \text{wgs}, \text{out}}) \Delta h_{\text{rxn}2} \end{aligned} \quad (7.22)$$

7.2.4 Preferential oxidation

To ensure that the CO concentration in the resulting gas is at an acceptable level that is not detrimental to PEFC (typically below 100 ppm), the CO content is further reduced in the preferential oxidation reactor where CO is catalytically oxidised with oxygen from air.



The molar flow rates of the gases leaving the preferential oxidation reactor can be

determined from the mass balances around the preferential oxidation reactor:

$$\begin{pmatrix} M_{\text{CH}_4,\text{prox},\text{out}} \\ M_{\text{w},\text{prox},\text{out}}^{\text{v}} \\ M_{\text{H}_2,\text{prox},\text{out}} \\ M_{\text{CO},\text{prox},\text{out}} \\ M_{\text{CO}_2,\text{prox},\text{out}} \\ M_{\text{O}_2,\text{prox},\text{out}} \\ M_{\text{N}_2,\text{prox},\text{out}} \end{pmatrix} = \begin{pmatrix} M_{\text{CH}_4,\text{wgs},\text{out}} \\ M_{\text{w},\text{wgs},\text{out}}^{\text{v}} \\ M_{\text{H}_2,\text{wgs},\text{out}} \\ M_{\text{CO}_2,\text{wgs},\text{out}} \\ M_{\text{CO},\text{wgs},\text{out}} \\ M_{\text{O}_2,\text{hex3},\text{out}} \\ M_{\text{N}_2,\text{hex3},\text{out}} \end{pmatrix} + \xi_3 \begin{pmatrix} 0 \\ 0 \\ 0 \\ -1 \\ 1 \\ -0.5 \\ 0 \end{pmatrix} \quad (7.24)$$

The temperature of the gases leaving the preferential oxidation reactor can be obtained from the energy balance:

$$\begin{aligned} & (M_{\text{CH}_4,\text{wgs},\text{out}} C_{\text{p},\text{CH}_4} + M_{\text{w},\text{wgs},\text{out}}^{\text{v}} C_{\text{p},\text{w}}^{\text{v}} + M_{\text{H}_2,\text{wgs},\text{out}} C_{\text{p},\text{H}_2} + M_{\text{CO}_2,\text{wgs},\text{out}} C_{\text{p},\text{CO}_2} \\ & + M_{\text{CO},\text{wgs},\text{out}} C_{\text{p},\text{CO}}) (T_{\text{wgs}} - T_{\text{ref}}) + (M_{\text{O}_2,\text{hex3},\text{out}} C_{\text{p},\text{O}_2} + M_{\text{N}_2,\text{hex3},\text{out}} C_{\text{p},\text{N}_2}) (T_{\text{hex3}} - T_{\text{ref}}) \\ = & (M_{\text{CH}_4,\text{prox},\text{out}} C_{\text{p},\text{CH}_4} + M_{\text{w},\text{prox},\text{out}}^{\text{v}} C_{\text{p},\text{w}}^{\text{v}} + M_{\text{H}_2,\text{prox},\text{out}} C_{\text{p},\text{H}_2} + M_{\text{CO}_2,\text{prox},\text{out}} C_{\text{p},\text{CO}_2} \\ & + M_{\text{N}_2,\text{prox},\text{out}} C_{\text{p},\text{N}_2} + M_{\text{O}_2,\text{prox},\text{out}} C_{\text{p},\text{O}_2} + M_{\text{CO},\text{prox},\text{out}} C_{\text{p},\text{CO}}) (T_{\text{prox}} - T_{\text{ref}}) - \xi_3 \Delta h_{\text{rxn}3} \end{aligned} \quad (7.25)$$

where ξ_3 is the extent of reaction 7.23. In this work, it is assumed that the PROX reactor is operating perfectly, i.e. all CO is preferentially converted to CO₂. Thus, ξ_3 can be expressed as follows:

$$\xi_3 = M_{\text{CO},\text{wgs},\text{out}} \quad (7.26)$$

The assumption of a perfect reactor may be a source of modelling error because depending on the type of catalyst and operating conditions, combustion of H₂ present in the reformat gases may occur. Simplification such as this are common due to the lack of suitable data for selectivity. For example, Hawkes et al. [58] assumed that all CO is converted to CO₂ through the water gas shift reaction and hence did not consider further CO reduction in a preferential oxidation reactor. In addition, Pukrushpan et

al. [204] combined the water gas shift reactor and preferential oxidation reactor as one unit. Pukrushpan et al. modelled the lumped reactors in a simple manner by assuming a fixed percentage conversion of H_2 . The possible combustion of H_2 in the preferential oxidation reactor was also not considered in both works.

7.2.5 Further fuel processing

The reformat gases leaving the preferential oxidation reactor is hot and oversaturated with water. A phase change heat exchanger, hex2, is used to cool down the anode gases to the operating temperature of the fuel cell stack. In this study, the stack temperature is assumed to be operating at constant temperature of 80°C . Thus, some of the water vapour in the reformat gases may condense. The flow rates of water that has condensed and has remained in the vapour phase are given by equations 7.27 and 7.28, respectively.

$$M_{w,\text{hex2},\text{out}}^l = M_{w,\text{prox},\text{out}}^v - M_{w,\text{hex2},\text{out}}^v \quad (7.27)$$

$$M_{w,\text{hex2},\text{out}}^v = \frac{P_{w,\text{hex2}}^{\text{sat}} (M_{\text{CH}_4,\text{hex2},\text{out}} + M_{\text{H}_2,\text{hex2},\text{out}} + M_{\text{N}_2,\text{hex2},\text{out}} + M_{\text{CO}_2,\text{hex2},\text{out}})}{P_{\text{hex2}} - P_{w,\text{hex2}}^{\text{sat}}} \quad (7.28)$$

The liquid water is separated and collected in a water tank for use in the fuel processing subsystem or for water and thermal management of the PEFC. The heat recovered from the heat exchanger, Q_{hex2} , is taken to the thermal management subsystem.

$$\begin{aligned} Q_{\text{hex2}} = & (M_{\text{CH}_4,\text{prox},\text{out}} C_{p,\text{CH}_4} + M_{w,\text{prox},\text{out}}^v C_{p,w}^v + M_{\text{H}_2,\text{prox},\text{out}} C_{p,\text{H}_2} + M_{\text{CO}_2,\text{prox},\text{out}} C_{p,\text{CO}_2} \\ & + M_{\text{N}_2,\text{prox},\text{out}} C_{p,\text{N}_2}) (T_{\text{prox}} - T_{\text{ref}}) - (M_{\text{CH}_4,\text{hex2}} C_{p,\text{CH}_4} + M_{w,\text{hex2}}^v C_{p,w}^v + M_{w,\text{hex2}}^l C_{p,w}^l \\ & + M_{\text{H}_2,\text{hex2}} C_{p,\text{H}_2} + M_{\text{CO}_2,\text{hex2}} C_{p,\text{CO}_2} + M_{\text{N}_2,\text{hex2}} C_{p,\text{N}_2}) (T_{\text{hex2}} - T_{\text{ref}}) \end{aligned} \quad (7.29)$$

The reformat gases entering the anode of the fuel cell stack is saturated with water vapour and enters the anode at 100% relative humidity. Thus, the need for an anode humidifier is eliminated. On the other hand, the air supplied to the cathode of the stack passes through a humidifier and enters the cathode with at least 50% relative

humidity. The humidifier is operated at the temperature of the stack. The flow rate of water required for humidification, $M_{w,\text{hum},\text{in}}^V$, can be calculated from the energy balance around the humidifier.

$$M_{w,\text{hum},\text{in}}^V = \left[(M_{\text{O}_2,\text{hum},\text{out}} C_{p,\text{O}_2} + M_{\text{N}_2,\text{hum},\text{out}} C_{p,\text{N}_2} + M_{w,\text{hum},\text{out}}^V C_{p,w}^v) (T_{\text{hum}} - T_{\text{ref}}) - (M_{\text{O}_2,\text{hex4},\text{out}} C_{p,\text{O}_2} + M_{\text{N}_2,\text{hex4},\text{out}} C_{p,\text{N}_2}) (T_{\text{hex4}} - T_{\text{ref}}) \right] \frac{1}{C_{p,w}^v (T_{\text{hum},\text{in}} - T_{\text{ref}})} \quad (7.30)$$

7.3 Fuel cell subsystem

The fuel cell stack is the heart of the PEFC micro-cogeneration system. It transforms the chemical potential in the hydrogen gas mixture from the fuel processing subsystem into direct current electricity. The reactions that produce electricity take place at the electrodes are given in Eqs. 2.1-2.3.

The fuel cell stack model was used in Chapter 5 to investigate the trade-offs between the efficiency and the size of the system. The model takes into account the electrochemical reaction, the vapour-liquid equilibrium of water, the electro-osmotic drag transport of water, the back diffusion of water, and the chemical component balances. In Figure 7.1, a different set of components are entering the fuel cell stack, therefore, Eqs. 5.1 - 5.23 must be modified such that $i = \text{CH}_4, \text{H}_2\text{O}, \text{H}_2, \text{CO}_2,$ and N_2 for the anode and $i = \text{H}_2\text{O}, \text{O}_2,$ and N_2 for the cathode.

The molar flow rates of the component gases can be computed from the mass balances. In this work, it is supposed that only the H_2 in the gases entering the anode is electrochemically oxidised, similar to the assumption in Ref. [58]. In addition, only the water molecules can migrate across the membrane. Also, within the operating conditions considered in this study, only the water component of the gases can evaporate or condense. Thus, for a given current density, I , the component balances around the stack can be

expressed as

$$\begin{pmatrix} M_{\text{H}_2,\text{a},\text{out}} \\ M_{\text{w},\text{a},\text{out}}^{\text{v}} \\ M_{\text{CH}_4,\text{a},\text{out}} \\ M_{\text{CO}_2,\text{a},\text{out}} \\ M_{\text{N}_2,\text{a},\text{out}} \\ M_{\text{O}_2,\text{c},\text{out}} \\ M_{\text{w},\text{c},\text{out}}^{\text{v}} \\ M_{\text{N}_2,\text{c},\text{out}} \end{pmatrix} = \begin{pmatrix} M_{\text{H}_2,\text{hex2},\text{out}} \\ M_{\text{w},\text{hex2},\text{out}}^{\text{v}} \\ M_{\text{CH}_4,\text{hex2},\text{out}} \\ M_{\text{CO}_2,\text{hex2},\text{out}} \\ M_{\text{N}_2,\text{hex2},\text{out}} \\ M_{\text{O}_2,\text{hum},\text{out}} \\ M_{\text{w},\text{hum},\text{out}}^{\text{v}} \\ M_{\text{N}_2,\text{hum},\text{out}} \end{pmatrix} + \xi_4 \begin{pmatrix} -1 \\ 0 \\ 0 \\ 0 \\ 0 \\ -0.5 \\ 1 \\ 0 \end{pmatrix} + \begin{pmatrix} 0 \\ -\frac{A\alpha I}{F} \\ 0 \\ 0 \\ 0 \\ 0 \\ \frac{A\alpha I}{F} \\ 0 \end{pmatrix} + \begin{pmatrix} 0 \\ M_{\text{w},\text{a},\text{out}}^{\text{l}} \\ 0 \\ 0 \\ 0 \\ 0 \\ M_{\text{w},\text{c},\text{out}}^{\text{l}} \\ 0 \end{pmatrix} \quad (7.31)$$

The second, third and fourth vectors on the right of equation 7.31 represent the changes in molar flow rates of the components due to the electrochemical reaction, the migration of water across the membrane, and the phase change, respectively. The extent of reaction, ξ_4 , is given by the rate of hydrogen consumption:

$$\xi_4 = \frac{AI}{2F} \quad (7.32)$$

The amount of heat generated by the stack, Q_{stack} , can be obtained from the energy balance around the stack, as presented in equation 7.33. This heat is captured and passed on to the thermal management subsystem.

$$Q_{\text{stack}} = n_{\text{cell}} \frac{AI}{2F} \Delta h_{\text{rxn4}} - n_{\text{cell}} AI V_{\text{cell}} + (M_{\text{w},\text{a}}^{\text{l}} + M_{\text{w},\text{c}}^{\text{l}}) \Delta H_{\text{vap}} \quad (7.33)$$

7.4 Thermal management subsystem

The major components of this subsystem are an afterburner, a phase change heat exchanger, and a heat storage tank. Thus, a PEFC micro-cogeneration system can be viewed as a condensing boiler that can generate electricity.

7.4.1 Afterburner

The gases leaving the anode and cathode of the fuel cell stack is taken to an afterburner, where combustion of unreacted H_2 and CH_4 takes place to obtain additional heat. It is supposed that the combustion reactions taking place in the afterburner proceed into completion. In this case, a certain level of excess air is needed to ensure complete combustion. Percent excess air is a term used to describe how much more air is used for combustion than necessary. In this study, it is assumed that at least 50% excess air is used.

The flow rate of air supplied to the afterburner can be computed from the theoretical oxygen, θ , which describes the flow rate of oxygen needed to completely consume all the fuel that is being fed to the afterburner.

$$\theta = 2M_{CH_4,a,out} + 0.5M_{H_2,a,out} + 2M_{CH_4,burn,in} \quad (7.34)$$

By denoting the excess air as χ , the flow rate of air supplied to the afterburner, $M_{O_2,burn,in}$, can be calculated as:

$$M_{O_2,burn,in} = (1 + \chi)\theta \quad (7.35)$$

$$M_{N_2,burn,in} = \frac{0.79}{0.21}M_{O_2,burn,in} \quad (7.36)$$

$$M_{air,burn,in} = M_{O_2,burn,in} + M_{N_2,burn,in} \quad (7.37)$$

The flow rate of gases leaving out of the afterburner can be determined from the mass balances. Equation 7.38 represents the overall mass balance and the C, H, O and N

elemental balances.

$$\begin{pmatrix} 1 & 1 & 1 & 1 \\ 1 & 0 & 0 & 0 \\ 0 & 2 & 0 & 0 \\ 2 & 1 & 2 & 0 \\ 0 & 0 & 0 & 2 \end{pmatrix} \begin{pmatrix} M_{\text{CO}_2,\text{burn},\text{out}} \\ M_{\text{w},\text{burn},\text{out}}^{\text{v}} \\ M_{\text{O}_2,\text{burn},\text{out}} \\ M_{\text{N}_2,\text{burn},\text{out}} \end{pmatrix} = \begin{pmatrix} 1 & 1 & 1 & 1 & 1 & 1 & 1 & 1 & 1 & 1 & 1 \\ 1 & 0 & 0 & 1 & 0 & 0 & 0 & 0 & 0 & 0 & 1 \\ 4 & 2 & 2 & 0 & 0 & 2 & 0 & 0 & 0 & 0 & 4 \\ 0 & 1 & 0 & 2 & 0 & 1 & 2 & 1 & 2 & 2 & 0 \\ 0 & 0 & 0 & 0 & 2 & 0 & 0 & 2 & 0 & 2 & 0 \end{pmatrix} \begin{pmatrix} M_{\text{CH}_4,\text{a},\text{out}} \\ M_{\text{w},\text{a},\text{out}}^{\text{v}} \\ M_{\text{H}_2,\text{a},\text{out}} \\ M_{\text{CO}_2,\text{a},\text{out}} \\ M_{\text{N}_2,\text{a},\text{out}} \\ M_{\text{w},\text{c},\text{out}}^{\text{v}} \\ M_{\text{O}_2,\text{c},\text{out}} \\ M_{\text{N}_2,\text{c},\text{out}} \\ M_{\text{O}_2,\text{burn},\text{in}} \\ M_{\text{N}_2,\text{burn},\text{in}} \\ M_{\text{CH}_4,\text{burn},\text{in}} \end{pmatrix} \quad (7.38)$$

The temperature of the the exhaust gases leaving the afterburner, T_{burn} , can be calculated from the energy balance around the afterburner:

$$\begin{aligned}
 & (M_{\text{CH}_4,\text{a},\text{out}} C_{\text{p},\text{CH}_4} + M_{\text{w},\text{a},\text{out}}^{\text{v}} C_{\text{p},\text{w}}^{\text{v}} + M_{\text{H}_2,\text{a},\text{out}} C_{\text{p},\text{H}_2} + M_{\text{CO}_2,\text{a},\text{out}} C_{\text{p},\text{CO}_2} \\
 & + M_{\text{N}_2,\text{a},\text{out}} C_{\text{p},\text{N}_2}) (T_{\text{a}} - T_{\text{ref}}) + (M_{\text{w},\text{c},\text{out}}^{\text{v}} C_{\text{p},\text{w}}^{\text{v}} + M_{\text{O}_2,\text{c},\text{out}} C_{\text{p},\text{O}_2} \\
 & + M_{\text{N}_2,\text{c},\text{out}} C_{\text{p},\text{N}_2}) (T_{\text{c}} - T_{\text{ref}}) + (M_{\text{O}_2,\text{burn},\text{in}} C_{\text{p},\text{O}_2} + M_{\text{N}_2,\text{burn},\text{in}} C_{\text{p},\text{N}_2}) (T_{\text{burn},\text{in}} - T_{\text{ref}}) \\
 & + M_{\text{CH}_4,\text{burn},\text{in}} C_{\text{p},\text{CH}_4} (T_{\text{CH}_4,\text{burn},\text{in}} - T_{\text{ref}}) = (M_{\text{w},\text{burn},\text{out}}^{\text{v}} C_{\text{p},\text{w}}^{\text{v}} + M_{\text{CO}_2,\text{burn},\text{out}} C_{\text{p},\text{CO}_2} \\
 & + M_{\text{O}_2,\text{burn},\text{out}} C_{\text{p},\text{O}_2} + M_{\text{N}_2,\text{burn},\text{out}} C_{\text{p},\text{N}_2}) (T_{\text{burn}} - T_{\text{ref}}) - (M_{\text{CH}_4,\text{burn},\text{in}} + M_{\text{CH}_4,\text{a},\text{out}}) \Delta H_{\text{LHV},\text{CH}_4} \\
 & - M_{\text{H}_2,\text{a},\text{out}} \Delta H_{\text{LHV},\text{H}_2} \quad (7.39)
 \end{aligned}$$

7.4.2 Phase change heat exchanger

The heat from the high-temperature combustion gases leaving the afterburner is extracted using a phase change heat exchanger, hex5. The heat comes from the cooling of the exhaust gases, but the majority of the heat recovered is from the condensation

of the water vapour in the exhaust gases. The flow rates of water that has condensed and has remained in the vapour phase are given by equations 7.40 and 7.41, respectively. The condensed water is collected in a water tank for use in the fuel processing subsystem or for water and thermal management of the PEFC.

$$M_{w,hex5}^l = M_{w,burn,out}^v - M_{w,hex5,out}^v \quad (7.40)$$

$$M_{w,hex5,out}^v = \frac{P_{w,hex5}^{sat} (M_{CO_2,hex5,out} + M_{O_2,hex5,out} + M_{N_2,hex5,out})}{P_{hex5} - P_{w,hex5}^{sat}} \quad (7.41)$$

The heat recovered from the condenser can be calculated from the energy balance:

$$\begin{aligned} Q_{hex5} = & (M_{w,burn,out}^v C_{p,w}^v + M_{CO_2,burn,out} C_{p,CO_2} + M_{O_2,burn,out} C_{p,O_2} \\ & + M_{N_2,burn,out} C_{p,N_2}) (T_{burn} - T_{ref}) - M_{w,hex5,out}^l C_{p,w}^l (T_{hex5} - T_{ref}) \\ & - (M_{w,hex5,out}^v C_{p,w}^v + M_{CO_2,hex5,out} C_{p,CO_2} + M_{O_2,hex5,out} C_{p,O_2} \\ & + M_{N_2,hex5,out} C_{p,N_2}) (T_{hex5} - T_{ref}) + M_{w,hex5,out}^l \Delta H_{vap} \end{aligned} \quad (7.42)$$

7.4.3 Heat storage

A hot water tank stores the heat recovered from the system. The major sources of heat are the fuel cell stack and heat exchangers used to cool down the afterburner exhaust gases and hot reformat gases:

$$Q_{rec} = Q_{stack} + Q_{hex5} + Q_{hex2} \quad (7.43)$$

where Q_{rec} is the total heat that can be recovered from the system. The heat retrieved from the stack, Q_{stack} , is given by Equation 7.33, whilst the heat captured from the heat exchangers, Q_{hex5} and Q_{hex2} , are presented in Equations 7.42 and 7.29.

Part of the recovered heat is returned to the system to provide the heat needed by the

steam reformer, the steam generation, and the pre-heating of the reactant gases.

$$Q_{\text{prs}} = Q_{\text{sr}} + Q_{\text{hex1}} + Q_{\text{hex3}} + Q_{\text{hex4}} \quad (7.44)$$

where Q_{prs} is the parasitic heat. The heat required for steam reforming, Q_{sr} , is given by equation 7.17, for steam generation, Q_{hex1} , by equation 7.6, and for reactants pre-heating, Q_{hex3} and Q_{hex4} , by equations 7.3 and 7.4.

It is supposed that a certain percentage of the net heat recovered, $(1 - \eta_{\text{hs}})$, is lost to the surroundings. The net thermal output, Q_{del} , is used for water and space heating.

$$Q_{\text{del}} = \eta_{\text{hs}} (Q_{\text{rec}} - Q_{\text{prs}}) \quad (7.45)$$

7.5 Power management subsystem

The power management subsystem coordinates the electric power produced by the fuel cell with that drawn from or exported to the grid. At times of excess electricity production it can be exported to the grid, and imported at times of high electrical load.

The power output of the fuel cell stack given by equation ?? is a DC electric power. A DC/AC inverter converts the DC electric power into alternating current (AC) appropriate for electrical appliances and for export to the grid. In this work, the efficiency of the inverter, η_{inv} , is assumed to be 95% [103]. Part of the generated AC electric power is used for the parasitic loads such as the air compressor and the water pump. Therefore, the net power output of the system is:

$$W_{\text{del}} = \eta_{\text{inv}} W_{\text{stack}} - W_{\text{prs}} \quad (7.46)$$

where W_{prs} is the parasitic power, which includes the power consumption of the water

pump, W_{pump} , and the air compressor, W_{comp} :

$$W_{\text{prs}} = W_{\text{pump}} + W_{\text{comp}} \quad (7.47)$$

$$W_{\text{pump}} = \frac{64.8 \times \text{Head} \times \text{SG}}{367\eta_{\text{pump}}} M_{\text{w,pump,in}}^l \quad (7.48)$$

$$W_{\text{comp}} = \frac{cc \times T_{\text{air,in}}}{\eta_c \eta_m} \left[\left(\frac{P}{P_{\text{in}}} \right)^{0.286} - 1 \right] m_{\text{air}} \quad (7.49)$$

7.6 System efficiencies

The performance of a system is usually evaluated using the efficiency. For a micro-cogeneration system, efficiency is defined as the fraction of the input fuel that can be recovered as power and heat. There are three primary efficiencies associated with a micro-cogeneration system. These are the electrical efficiency, the thermal efficiency, and the overall efficiency:

$$\eta_{\text{elec}} = \frac{W_{\text{del}}}{W_{\text{fuel}}} \quad (7.50)$$

$$\eta_{\text{thermal}} = \frac{Q_{\text{del}}}{W_{\text{fuel}}} \quad (7.51)$$

$$\eta_{\text{overall}} = \frac{W_{\text{del}} + Q_{\text{del}}}{W_{\text{fuel}}} = \eta_{\text{elec}} + \eta_{\text{thermal}} \quad (7.52)$$

where W_{del} is the net power output or the delivered power (equation 7.46), Q_{del} is the net thermal output or the delivered heat (equation 7.45), and W_{fuel} is the power inherent in the fuel used (equation 7.53). The fuel consumption is given by the following equation:

$$W_{\text{fuel}} = M_{\text{CH}_4,\text{in}} \Delta H_{\text{LHV},\text{CH}_4} \quad (7.53)$$

For the energy balances in the model, the dependence of the heat capacity of each component, i , on temperature is given by Eq. 7.54 [205]. The values of the coefficients in Eq. 7.54 are presented in Table 7.1. The heat of vapourisation of water as a function

of temperature is expressed by Eq. 7.55 [148].

$$C_{p,i} = R \left(a_i + b_i T + c_i T^2 + \frac{d_i}{T^2} \right) \quad (7.54)$$

$$H_{\text{vap}} = 45070 - 41.94 (T - 273) + 3.44 \times 10^{-3} (T - 273)^2 \\ + 2.54810 \times 10^{-6} (T - 273)^3 - 8.98 \times 10^{-10} (T - 273)^4 \quad (7.55)$$

Table 7.1: Heat capacities of gases [205].

Component	a	$b \times 10^3$	$c \times 10^6$	$d \times 10^{-5}$
CH ₄	1.702	9.081	-2.164	0
H ₂	3.249	0.422	0	0.083
O ₂	3.639	0.506	0	-0.227
N ₂	3.280	0.593	0	0.040
H ₂ O(v)	3.470	1.450	0	0.121
H ₂ O(l)	8.712	1.250	-0.180	0
CO ₂	5.457	1.045	0	-1.157

Table 7.2 gives the values of the constant parameters used in the PEFC micro-cogeneration system model.

Table 7.2: Parametric constants in the PEFC micro-cogeneration system model.

Parameter	Value	Ref.
<i>Afterburner</i>		
Lower heating value of hydrogen ($\Delta H_{\text{LHV,H}_2}$)	$241 \times 10^3 \text{ J mol}^{-1}$	[48]
Lower heating value of methane ($\Delta H_{\text{LHV,CH}_4}$)	$800 \times 10^3 \text{ J mol}^{-1}$	[2]
<i>Compressor</i>		
Connecting efficiency (η_c)	0.85	[152]
Entry air temperature (T_e)	288 K	
Inlet pressure (P_{in})	1 atm	
Motor efficiency (η_{mt})	0.85	
Specific heat constant of air (c_p)	$1004 \text{ J K}^{-1}\text{kg}^{-1}$	
<i>Fuel cell stack</i>		
Amplification constant (β)	$0.085 \text{ V}(\text{cm}^2\text{A}^{-1})^k$	[28, 151]
Diffusion coefficient of water in membrane (D°)	$5.5 \times 10^{-7} \text{ cm}^2 \text{ s}^{-1}$	[125]
Dimensionless power in the amplification term (k)	1.1	[28, 151]
Dry density of the membrane ($\rho_{\text{m,dry}}$)	2.0 g cm^{-3}	[125]
Dry equivalent weight of the membrane ($M_{\text{m,dry}}$)	1100 g mol^{-1}	[125]
Heat of electrochemical reaction (Δh_{fc})	$-241 \times 10^3 \text{ J mol}^{-1}$	[171]
Limiting current density (I_L)	1.4 A cm^{-2}	[28]
Oxygen exchange current density (I_0)	0.01 A cm^{-2}	[149]
Reversible open-circuit potential (V_{oc})	1.1 V	[149]
Thickness of the membrane (t_m)	$5 \times 10^{-3} \text{ cm}$ (50 μm)	
<i>Preferential oxidation reactor</i>		
Heat of reaction (Δh_{prox})	$-279.5 \times 10^3 \text{ J mol}^{-1}$	[2]
<i>Pump</i>		
Efficiency (η_{pump})	0.75	[?]
Head (difference between height of suction and discharge)	1 m	
Specific gravity of water (SG)	1	
<i>Steam reformer</i>		
Heat of reaction (Δh_{sr})	$206 \times 10^3 \text{ J mol}^{-1}$	[187]
<i>Water-gas-shift</i>		
Heat of reaction (Δh_{wgs})	$-41 \times 10^3 \text{ J mol}^{-1}$	[2]

7.7 Case study: Trade-off between power output and fuel consumption of a fuel cell micro-cogeneration plant

There is a trade-off between the net electrical power output and the fuel consumption of a fuel cell micro-cogeneration system. Ideally, the system is operated at high power output and low fuel consumption, thus, the optimisation problem will involve maximisation of power output and minimisation of fuel consumption. These are conflicting because more fuel is needed to produce additional power. Also, in some cases, electricity in excess of the site requirements is generated which can be sold to the grid. However, exported electricity has a lower value compared to the electricity used on site. Deciding which of the two objectives - power output or fuel consumption - is more important depends on the cost of the fuel and electricity and the buyback rate of electricity exported to the grid. The inherent variability in the cost introduces difficulty in deciding which operating point is most beneficial economically. Thus, information that shows the compromise between the power output and the fuel consumption is an important tool in identifying the most suitable operating design for a given thermal and electrical demands.

7.7.1 Multi-objective optimisation

The multi-objective optimisation problem is formulated using the weighting method as

$$\begin{aligned} \min z &= -\omega W_{\text{del}} + (1 - \omega) W_{\text{fuel}} && (7.56) \\ \text{w.r.t.} & \text{ design parameters and operating conditions} \\ \text{subject to} & \text{ mass and energy balances} \\ & \text{electrochemical model} \\ & \text{equilibrium relations} \\ & \vdots \\ & \text{physical constraints} \\ & \text{bounds on some of the design variables} \end{aligned}$$

where W_{del} is the net power output in kW, W_{fuel} is the fuel consumption in kW, z is the weighted sum of the objectives, and $\omega \in [0, 1]$ represents the weighting factors. The negative sign preceding the net power output objective denotes a maximisation problem. Single-objective optimisation problems, i.e., minimisation of the fuel consumption and maximisation of the net power output, are represented at the extreme points $\omega = 0$ and $\omega = 1$, respectively. Evaluating the optimisation problem for any $\omega \in (0, 1)$ will produce solutions between these extremes where both objectives are simultaneously considered. The value of ω gives the relative importance of each objective.

The optimisation problem is subject to the constraints imposed by the mass and energy balances, the electrochemical model, the equilibrium relations, the transport equations, physical constraints and bounds on the design variables. The model was implemented in the GAMS [160] modelling language and was solved using LINDOGlobal. LINDOGlobal uses the branch-and-cut method to break a nonlinear programming (NLP) model down into a list of subproblems [161]. A discussion of the branch-and-cut method is given in Ref. [162].

7.8 Results and discussion

Figure 7.2 gives the trade-off solutions for fuel consumption *vs.* power output of a fuel cell micro-cogeneration plant at a thermal power rating of 9 kW_{th}. The highest point is the optimal solution for the single-objective maximisation of the net electrical power output without taking the fuel consumption into account. Conversely, the lowest point is the optimal solution for the single-objective minimisation of the fuel consumption regardless of the power output. The results indicate that the lowest fuel consumption occurs when the system is operating in “boiler only” mode, *i.e.*, the net electrical power output is zero. In this case, the system is still generating some electrical power but all of this is used to service the parasitic loads such as the blower and the water pump.

It can also be observed from Figure 7.2 that at power output below 7 kW_e, the power output trades almost linearly with the fuel consumption. In this region, roughly 0.85 W_e additional power is produced for every W of extra fuel. At power output above 7 kW_e, it is not economically practical to operate the system because there are no significant gains in power output with increase in fuel consumption. The limit on the maximum attainable net power output can be attributed to the fixed size of the fuel cell. In this study, the total active area of the membrane electrode assembly is considered to be 1.6 m² (*e.g.*, 40 cells, each with active area of 20×20 cm²).

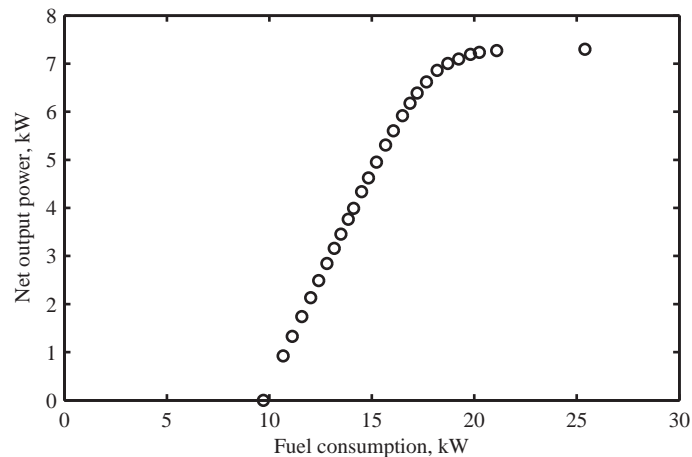


Figure 7.2: Pareto set showing the trade-offs between the net electrical power output (W_{del}) and fuel consumption (W_{fuel}).

Figure 7.3 shows the overall efficiency plotted against the fuel consumption. The figure indicates that placing more importance on the net power output as an objective leads to a decrease in the overall efficiency. Furthermore, the micro-cogeneration system can achieve an overall efficiency as high as 93%. The lowest overall efficiency is about 65% which is still higher than the 50-60% overall efficiency of a modern combined cycle power plant [98].

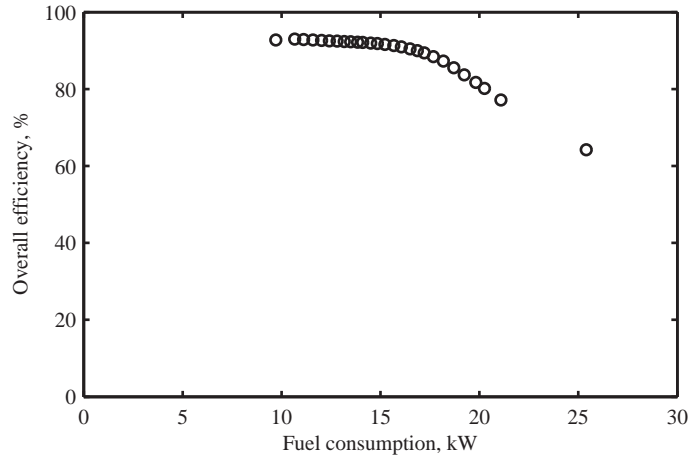
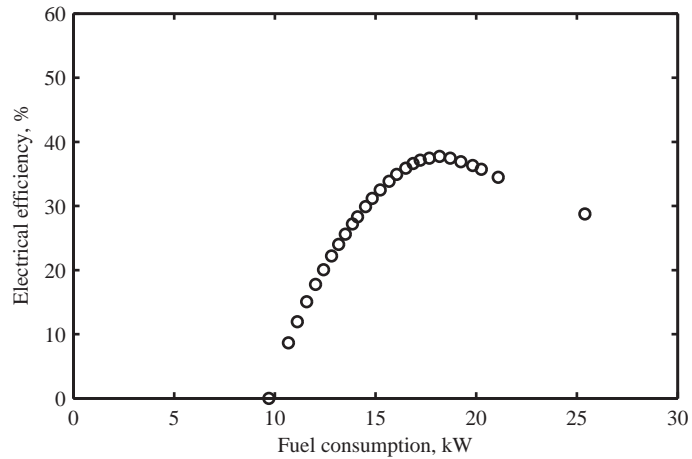
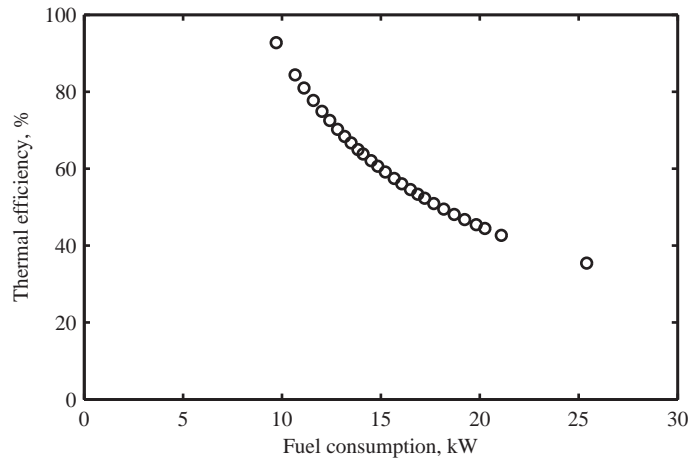


Figure 7.3: Values of the overall efficiency corresponding to the Pareto set in Figure 7.2.

Figure 7.4 shows the values of the electrical and thermal efficiencies corresponding to the Pareto set in Figure 7.2. It can be observed that a maximum value of the electrical efficiency occurs for a particular value of the weighting factor. Interestingly, the solution of the single-objective maximisation of the power output does not necessarily result in a maximum electrical efficiency. Finally, there is a trade-off between the thermal efficiency and the electrical efficiency. At high thermal efficiency, the electrical efficiency is low and *vice versa*. This clearly demonstrates the ability of the fuel cell to operate with a variable heat to power ratio.



(a)



(b)

Figure 7.4: Values of the individual efficiencies, (a) electrical efficiency and (b) thermal efficiency, corresponding to the Pareto set in Figure 7.2.

7.9 Conclusions

A system-level mathematical model for a system, which builds up on the PEFC model, suitable for multi-objective optimisation is presented. Sub-systems, such as the fuel cell stack, the fuel processing, the thermal and the power management, necessary to operate the system as a residential heat and power generator are modelled. There is a trade-off between the net power output and the fuel consumption when the system is operated in a heat-led manner to deliver a particular thermal demand. For the net power output below 7 kW, the net power output trades almost linearly with the fuel consumption, specifically ~ 0.85 Watt additional net power output is produced for every Watt of

extra fuel. For some values of the weighting factors, a surplus or a shortage in the net power output may result. Economic factors such as costs of natural gas and electricity and the buy-back rate of electricity exported to the grid determines whether this power is exported to or imported from the grid.

Chapter 8

Model application: investigation of the effectiveness of different fuel cell micro-cogeneration operating strategies

This chapter illustrates the use of the fuel cell micro-cogeneration system model developed in Chapter 7 in informing manufacturers and designers as to the relative benefit of three of the various operating strategies: constant-output mode, restricted-output mode and continuous-output mode. The effects of the different operating modes are investigated by using the gas and electricity consumption data of UK households recorded on a five-minute interval throughout a representative day.

This chapter does not investigate the total investment cost of a fuel cell micro-cogeneration system. The capital cost of the plant is deliberately not included to maintain the focus on the operating cost of each strategy. Therefore, this is not an investigation into the overall economy of a fuel cell micro-cogeneration investment, and only relates to how the system is to be operated. Some works that considered the total system cost and performance include Refs. [58, 206–208]. Also, in this chapter no attempt was made to sim-

ulate the transient performance (*e.g.*, during startup, shutdown or part-load/overload) of the fuel cell micro-cogeneration system. In practice, however, micro-cogeneration systems will be subjected to heat and power requirements that emerge in real time and this will have a considerable effect on the operating mode and controllability (*e.g.*, on/off/turndown decisions) of a micro-cogeneration system.

8.1 Energy demands

Accurate and detailed demand data for electricity and heat are necessary to appropriately investigate the effectiveness of the different operating strategies a fuel cell micro-cogeneration system. This section and the next describe the key characteristics of the electrical and thermal demands occurring within UK dwellings.

In the UK domestic sector, average annual heat and power demands amount to approximately 17 MWh_t and 4.6 MWh_e, respectively [102]. The total energy consumption per dwelling per unit time changes significantly, and depends on a broad range of factors such as geographical location, building design, the efficiency of the space heating systems, the stock of domestic appliances, occupancy patterns, attitudes towards energy use and disposable income [169, 209]. For these reasons, , it is difficult to correlate the house size and the heating demand. Therefore, defining a “typical home” for investigation is not a trivial task, nor determining an optimal micro-cogeneration design for UK homes in general.

The energy demand data collected by the IEA Energy Conservation in Buildings and Community Systems [198] was employed. The database consists of daily electricity and gas consumption data ¹, which were recorded on a 5 minute time base for 69 detached dwellings in the UK. Analyses of this database indicated that the average electrical load of each home was in the range 0.3–1.0 kW_e and that the daily peak electrical loads varied from 0.6–15 kW_e. The database was searched to find representative daily demand

¹The gas consumption data applies only to central-heating boilers and excludes gas fires and gas cookers.

profiles. The focus was placed on households employing mainly electrical appliances and a gas-fired central-heating system (for meeting both space and water heating needs); homes with electric space heating systems were not considered. Similarly, no attempt was made to analyse the influence of future trends in domestic energy usage.

A household's thermal demand may be considered to consist of three components:

1. Space heating

This depends to a great extent on the season/weather, house design, and occupancy pattern. If all occupants are absent during the day the heating system tends to be employed only in the morning and evening; but if not, space heating may be required for one relatively long period, for example, from morning to midnight [168].

2. Domestic hot water

This is usually met by the central heating boiler, but may be satisfied by electricity. Excluding those who use an off-peak electricity tariff, about 12% of households utilise electric immersion heaters throughout the year, while approximately 20% do so in summer [168]. In general, hot water is used irregularly in wide-ranging amounts for several different purposes. However, unlike requirements for space heating and electricity, the hot water load can be decoupled from the demand in most homes by means of the conventional hot water storage tank.

3. Cooking

This may be fuelled by gas, electricity, oil, or solid fuel. Micro-cogeneration design solutions do not usually extend to utilising the recovered heat to satisfy the thermal load due to cooking, because (unlike domestic hot water and space heating), cooking is characterised by requirements for small heat inputs at high temperatures for relatively short durations. However, if the thermal loads due to cooking are met by electricity (which applies for approximately half of UK

homes and significantly greater proportions in most other EU nations [210]), relatively large fluctuations in the electrical demand profile tend to occur during peak periods. Households that prefer non-electric cooking and a traditional kettle (i.e., gas heated) will place a much smoother electrical demand profile on a micro-cogeneration system [209].

8.2 Transient demand characteristics of an individual dwelling

From the dataset of houses that were monitored for one year, one house was randomly identified for detailed investigation. The total annual electricity and gas consumptions for this detached house were 8.5 MWh_e and 20.9 MWh_t, respectively. Individual days exhibited significant variations in both the thermal and electrical demand, but a moving average shows that the daily electricity consumption over the year is fairly consistent, whilst the heat requirement exhibits considerable seasonal variation, with much higher daily consumption during winter (Figure 8.1). For this home, the minimum and maximum daily electricity consumptions were 6.98 kWh_e on a Thursday in July and 43.46 kWh_e on a Saturday in January, respectively. The minimum and maximum daily thermal demands were 0 kWh_t on a Tuesday in August, and 178.48 kWh_t on a Wednesday in December. Approximately 15 kWh_t per day is almost always present throughout the year and this represents domestic water heating (that is, the base load), whilst the space heating load dominates during the winter season.

A simple classification of days may be derived from the distribution of daily thermal demand across the year (Figure 8.2): (A) days with thermal demand of 10 kWh_t and (B) days with thermal demand 80 of kWh_t. Type A days amounted to 36% of the sample with an average thermal demand of 10.9 kWh_t, whilst the remainder were characterised by an average of 79.60 kWh_t. On an annual basis the variations in the daily thermal and electrical demands were large, having coefficients of variation (COV) of 80% and

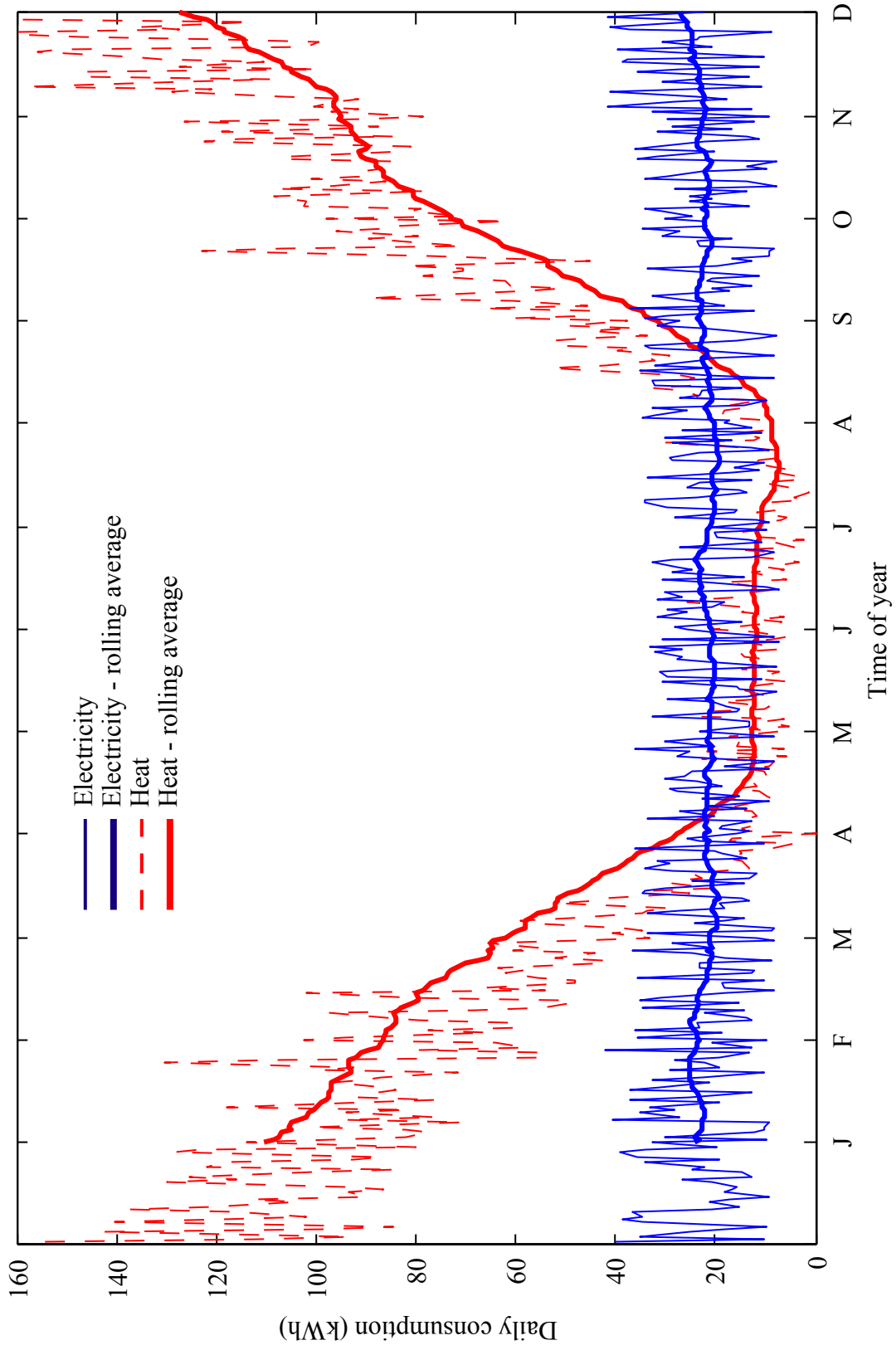


Figure 8.1: Trends in the daily and 30-day rolling average heat and power demands for a single house from January and December.

40%, respectively. The spread of thermal demand in summer ($\text{COV} = 39\%$ for A days) is lower than that of the heating season ($\text{COV} = 44\%$ for B days). This indicates that the daily electrical demand fluctuates but exhibits little seasonal change, while thermal requirements tend towards a minimum value of 36% for the year.

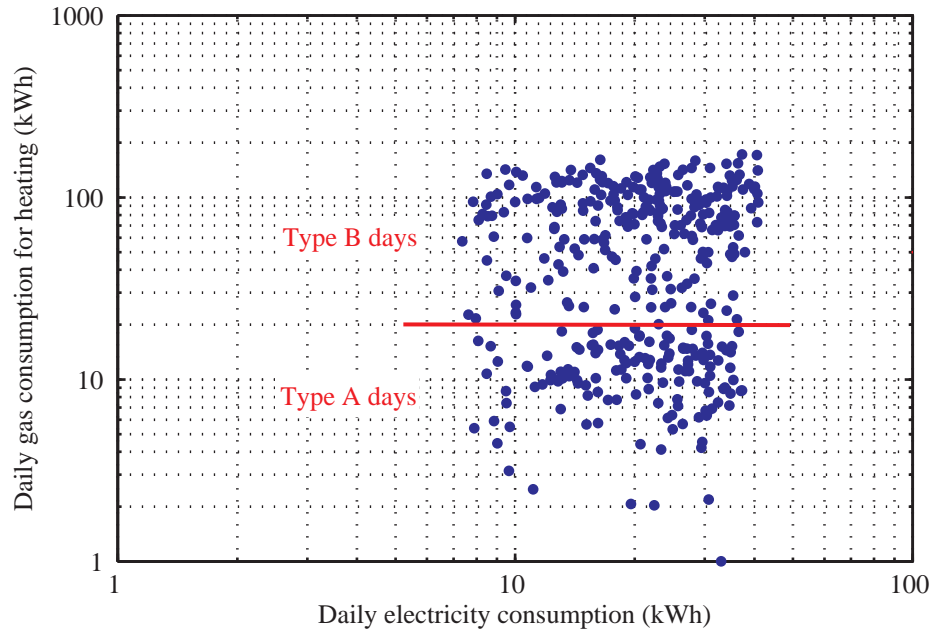


Figure 8.2: The daily thermal vs. electrical demand values on a log-log scale for the household with demand shown in Figure 8.1.

The daily electrical demand profile demonstrates a base load of about 100 W_e , irrespective of season. Some contributors to the base load include refrigeration appliances and other items on standby, most of which have a low power requirement. The remaining components of the demand profile tend to be of varying magnitude and may be categorised loosely as irregular, elective, or biased [209]. Biased loads are those that likely to happen on most days at similar times, or a reasonably predictable time, for instance, use of lighting and televisions. The majority of appliances in a household may be classified as elective loads as they are operated mainly at the user’s discretion (such as an electric kettle, washing machine, or lawn mower); predicting when these demands will occur is very difficult to ascertain [211]. Large cyclic loads such as immersion heaters and tumble dryers may be considered irregular, although they may be biased by a timeswitch to take advantage of off-peak electricity tariffs [209]. Different combinations of these

loads exist throughout any given day, but a relatively high degree of coincidence occurs during peak period(s). Much of a day’s electricity consumption occurs when the use of lighting and domestic appliances coincides, resulting in noticeable fluctuations in the demand profile from $\sim 100\text{ W}_e$ to several kilowatts. A representative electrical demand profile (for a day in January 2008) for this home was selected for assessing prospective micro-cogeneration systems (Figure 8.3).

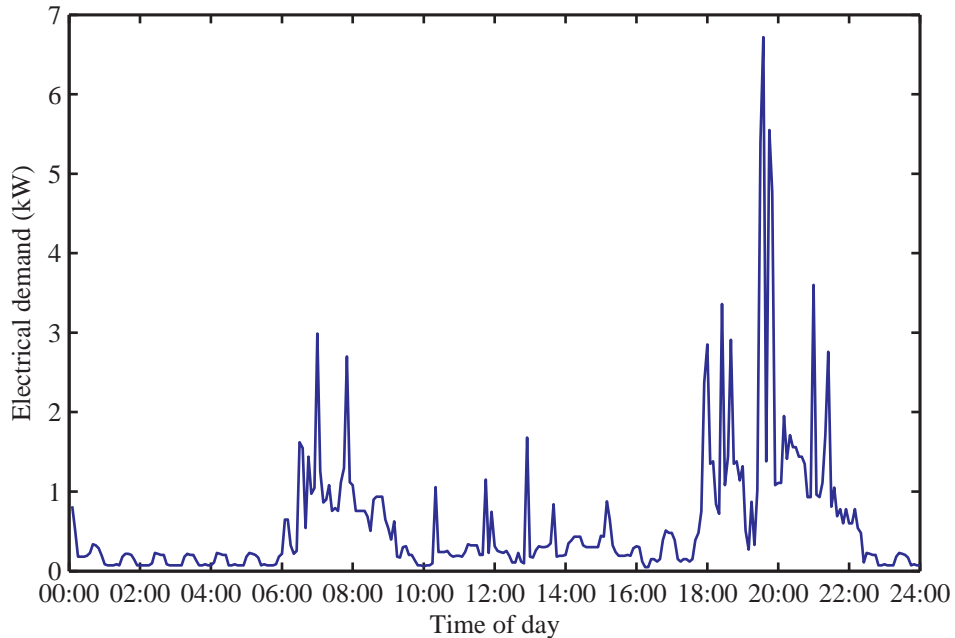


Figure 8.3: The daily electrical demand profile employed for simulation purposes.

The heat-to-power ratio of a micro-cogeneration system needs to agree with the household’s heat-to-power demand ratio. A household’s heat-to-power demand ratio changes markedly during a 24 hour period, displaying numerous sudden increases and decreases. Analysis of daily profiles of the heat-to-power ratio when time-averaged month of the year, indicates that values can easily reach 50:1, while daily averages lie mainly in the range 2:1 to 8:1 [211, 212]. Thus, matching the output of a micro-cogeneration system to this demand characteristic throughout the year is very challenging without relying on network electricity and supplementary heating, and/or appropriately sized energy-storage facilities.

Matching the size and operation of a micro-cogeneration unit to the demand charac-

teristics of an individual household is important both for the system designer and the operator. Table 8.1 considers different combinations of daily heat and power demands. Similarly there are several behavioural factors that occur on a short-time base, which will influence the heat and power demands that can be captured by a micro-cogeneration system on a given day. For instance, the thermal demand during the early part of a winter's day may be very high whilst the electrical demand is low (due to the inactivity of the occupants), and although two successive days may have similar total electricity consumptions the patterns of electricity use may differ significantly [169]. Such factors serve to complicate the estimation of the cost savings for a given micro-cogeneration system design.

The currently accepted parameters for the successful adoption of a micro-cogeneration system include the requirement for heat-to-power ratio of approximately 4:1, and a consistent electrical base load for about 17 hours per day [213]. Given the irregular demand characteristics of an individual dwelling, it is challenging to reconcile this general objective with the requirements for supplying a single home. Amongst the many design problems are the following: What micro-cogeneration size will be best? What efficiency is desirable? What cost saving might be achieved for a micro-cogeneration implementation? How much electricity/heat will be required to supplement the micro-cogeneration system? To investigate these issues, the model developed in Chapter 7 was used to predict the cost savings associated with a micro-cogeneration system at different prospective operating modes.

The model described in Chapter 7, which was implemented in the GAMS modelling language, was used to minimise the operating cost for a given micro-cogeneration system capacity specified according to the operating mode being considered. The results were subsequently applied to a 5-minute daily demand profile such as the one presented in Figure 8.3. The designated operating period of the micro-cogeneration system and the unit energy prices are specified. No attempt was made to simulate transient performance (*e.g.*, during startup, shutdown or part-load/overload performance). In practice,

Table 8.1: General influences of transient heat and power demand variations upon the design of micro-cogeneration systems.

Daily electrical demand	Daily thermal demand	Possible implications
Very low (<i>e.g.</i> , due to house being unoccupied for 24 hours or longer)	None	Not an important factor unless number of unoccupied days per year is high. Electrochemical and thermal stores will be useful, depending on intermittency of occupation.
Low (<i>e.g.</i> , a day of low activity or prolonged absence)	Low	Small savings can be achieved. Electrochemical and thermal stores will be useful.
High (<i>i.e.</i> , a day of high activity and/or prolonged occupancy)	High	Supplementary heat source may be required. Potentially large savings may be realised.
High (<i>i.e.</i> , a day of high activity and/or prolonged occupancy)	Low	Potentially large saving associated with high electrical demand cannot be achieved. Operation at high electrical efficiency is desirable.
High (<i>i.e.</i> , a day of high activity and/or prolonged occupancy)	High	Grid electricity and supplementary heat source may be required. Large savings may be realised.

micro-cogeneration systems will be subjected to heat and power requirements that unfold in real time, so the operating mode and controllability of a micro-cogeneration system (*e.g.*, on/off/turndown decisions) will have a considerable effect on savings.

8.3 Operating modes

To frame the analysis, the following six modes of operation are discussed (modes 1, 2, and 3 being associated with network-connected systems, and modes 4, 5, and 6 with autonomous variants):

1. Constant-output mode

A fuel cell micro-cogeneration system operates at a steady electrical power output for a single period per day, exporting excess electricity to the network when demand is less than the micro-cogeneration output and importing it when demand exceeds output.

2. Restricted running-time mode

The fuel cell micro-cogeneration system operates at a constant output for a small number of periods per day as a function of the household's requirements (*e.g.*, breakfast time and evening). This mode makes no attempt to capture all of the household's energy demand; it would tend to have a prime mover of greater electrical capacity than that of a constant-output system.

3. Continuous-output mode

A simple system operating continuously at a steady output, which is sized to supply only a modest electrical load, with all other electrical requirements being met by network electricity. The prime mover will be of smaller electrical capacity than those associated with the other modes.

4. Load-following mode

An ideal system that effectively follows the electrical demand, the rationale being to avoid exporting or importing electricity. By implication, an imperfect load-following system would capture a high proportion of the electrical demand, but require imports during high peaks and make exports during deep valleys.

5. Autonomous mode

A fuel cell micro-cogeneration system that operates at a steady output, usually for one or two periods per day, with the electrical output being used to charge a large battery store. All of the household's electrical demand is satisfied by the battery store via an inverter. The thermal demand is met mainly by heat recovered from the micro-cogeneration unit. The micro-cogeneration system will have a significantly greater electrical capacity than those associated with the other modes.

6. Energy-diverting mode

A fuel cell micro-cogeneration system, which operates at a steady output, with the electrical output being used primarily to supply the electrical demand, whilst any excess electricity is diverted to suitable energy-storage loads (rather than exported) [211]. Thermal stores (*e.g.*, an electrical heater in a hot water tank) and electrochemical stores (*e.g.*, a battery bank) may be employed, but these must be designed to meet at least the daily variation if importing is to be avoided.

At present, it appears that modes 1, 2, and 3 are considered for the potential mass market in the UK. Mode 5 may be most appropriate for households in rural and remote areas where security of supply and the absence of mains gas are important factors. The energy diverting system (mode 6) has been proposed for engineering development [169] and the load-following system (mode 4) is included here simply as a reference (*i.e.*, it is an idealised rather than a practical arrangement).

8.4 Network interaction

To investigate the interaction between micro-cogeneration operating modes 1, 2, and 3 and the electricity network, a preliminary analysis was performed. A representative daily profile for a house was selected from the database and Figure 8.4 shows a simple illustration of the operating modes as might be applied to the demand profile shown in Figure 8.3. It was assumed that the household's thermal demand on the considered day exceeded the heat output of the micro-cogeneration system (*i.e.*, operation was not inhibited by a heat limit). Also, this example is based on superimposing periods of operation onto a daily profile with the objective of achieving a reasonable supply/demand match. Although no attempt was made to optimise the periods of operation, it may well prove difficult in practice for a micro-cogeneration system to realise an optimal (start and stop) match with an unknown profile (*i.e.*, one that is emerging in real time).

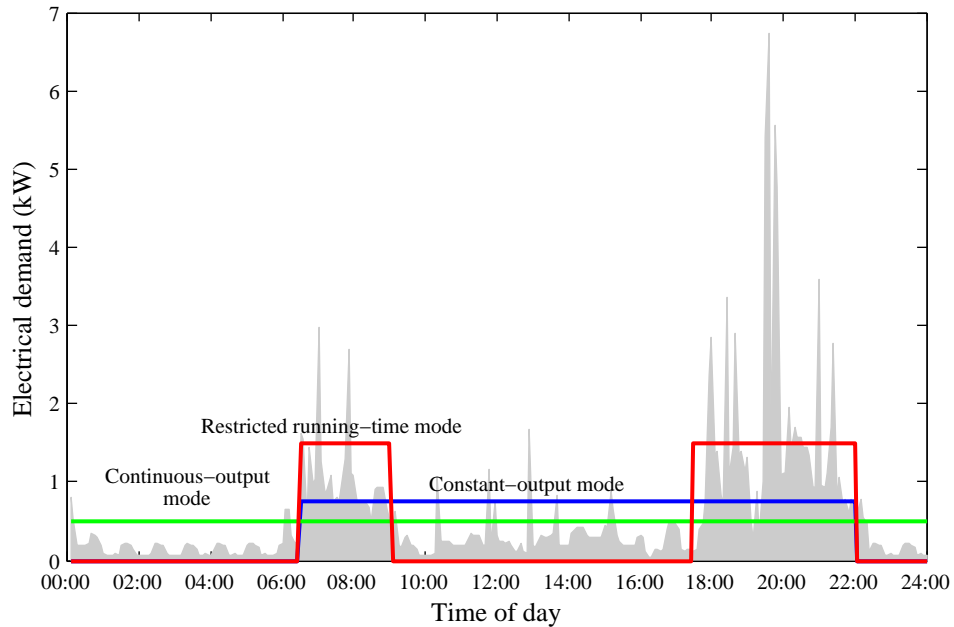


Figure 8.4: Example of applying the considered operating strategies for a micro-cogeneration system (as specified in Table 8.2) to a daily electrical demand profile.

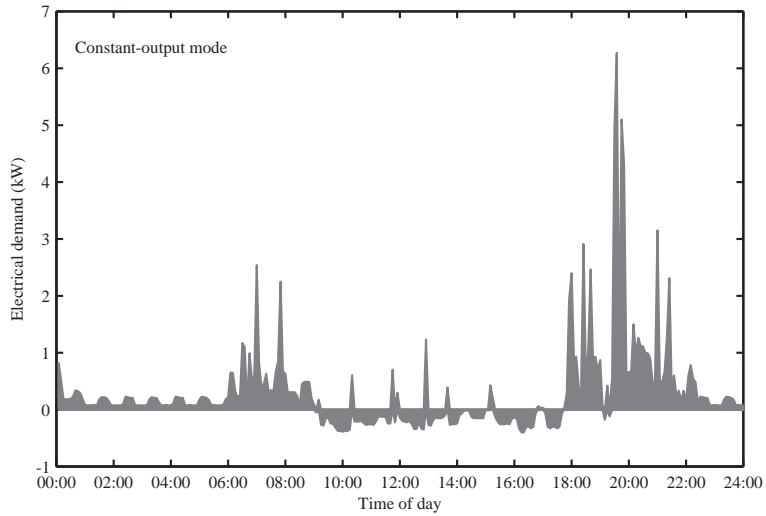
The characteristics of the considered operating modes are shown in Table 8.2. The constant-output, restricted running time and continuous modes capture approximately

50% of the electrical demand, and clearly fall far short of the idealised load-following system. They also require a portion of the generated electricity to be exported (*i.e.*, 7–13% of the demand). An increase in the proportion of demand satisfied by the micro-generation system likely results in increased exports. Amongst the three strategies, the continuous-output mode has the highest electrical generation, which despite this still imports a substantial amount of electricity from the grid. The constant-output mode, on the other hand, generates the least electrical power, and thus requires the greatest amount of import from the electricity network.

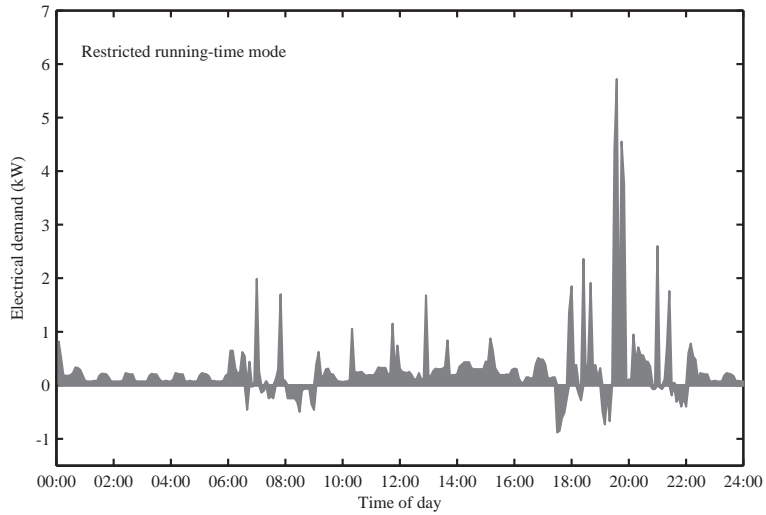
The export and import profiles for each of the considered strategy differ considerably (Figure 8.5). The constant-output mode meets significant proportions of the morning and evening demand, but exports electricity for much of the daytime. The restricted running-time mode satisfies higher proportions of the morning and evening demands, whilst avoiding export during the daytime and exporting some quantities at useful times in the morning and in the evening. The continuous-output mode effectively takes away the base load from the electricity network and focuses the household's import requirements into two distinct periods per day.

Table 8.2: The electricity generation and utilisation characteristics of some micro-cogeneration operating modes as shown in Figure 8.4.

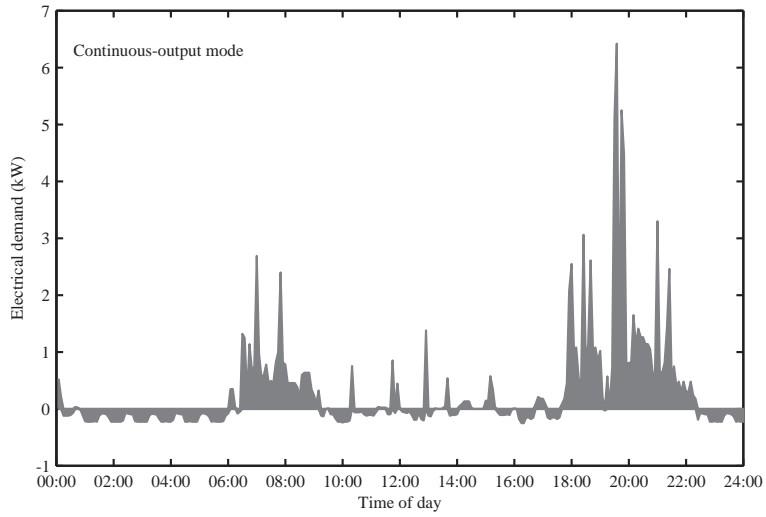
Operating mode	Size of the micro-cogeneration unit, kW _e	Period of operation	Electricity generated, kWh	Electricity imported, kWh	Electricity exported, kWh (% of demand)	Proportion of daily electrical demand met by micro-cogeneration, %
Constant-output	0.45	06:30-22:00	7.01	8.66	1.72 (12.34)	50.27
Restricted running-time	1.00	06:30-9:00 and 17:30-22:00	7.17	7.77	0.99 (7.09)	51.37
Continuous-output	0.30	-	7.20	8.63	1.88 (13.46)	51.61
Load-following	5.7 (max)	-	13.95	0	0 (0)	100



(a)



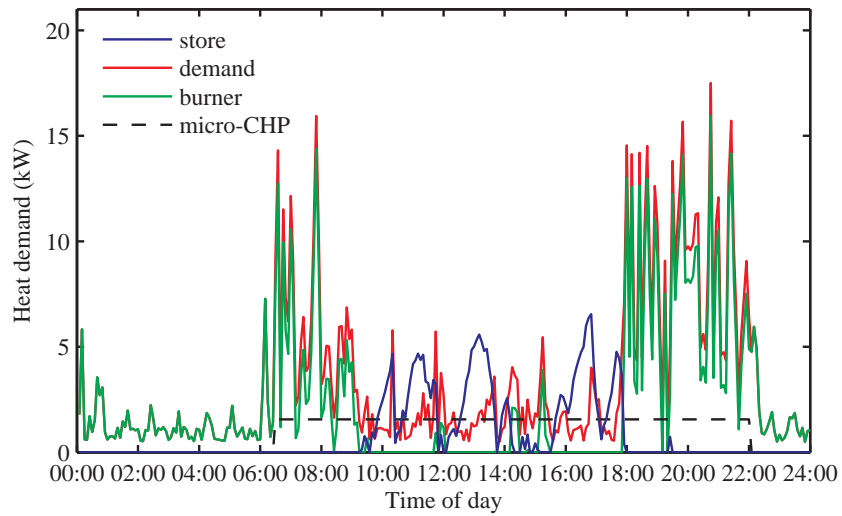
(b)



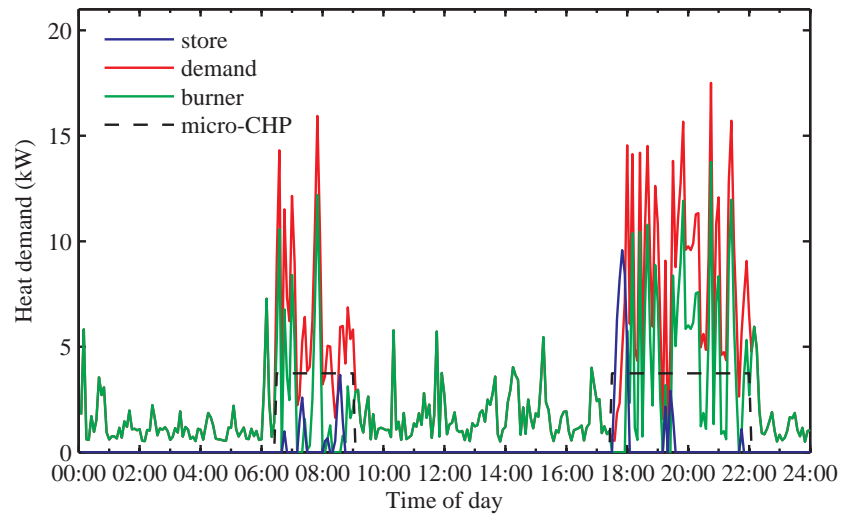
(c)

Figure 8.5: The import and export profiles (shown above and below the time-axis, respectively) for the three operating modes defined in Figure 8.4 and Table 8.2: (a) constant-output mode, (b) restricted running-time mode and (c) continuous-output mode.

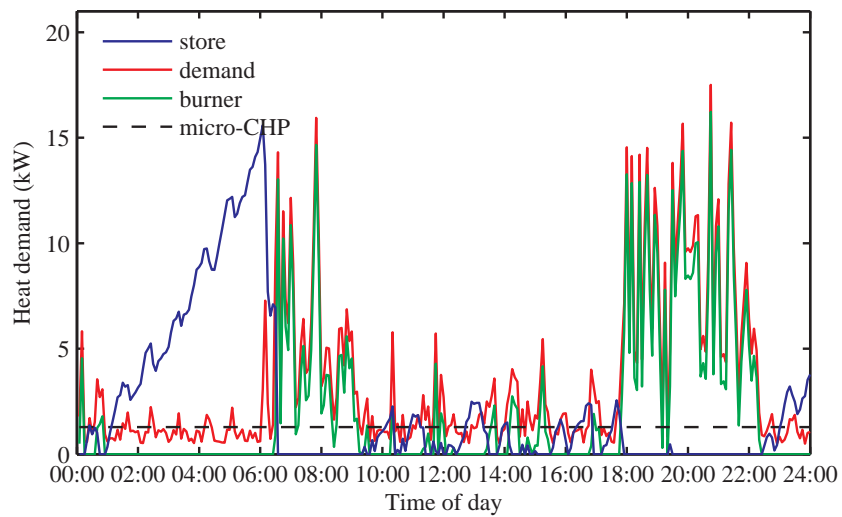
Figure 8.6 shows the resulting heat profiles for the three dispatch strategies considered in this chapter. The blue line represents the amount of energy in the thermal store, the red line corresponds to the heat demand, the green line indicates the heat generated by the supplementary boiler and the dashed grey line shows the heat output of the micro-generation system. For all the considered strategies, 62–70% of the daily heat demand is met by the supplementary boiler; the remaining heat demand is met by the micro-cogeneration unit. In the constant-output mode, shown in Figure 8.6 (a), the majority of the heat demand during the peak periods in the morning and evening is supplied by the supplementary boiler. The heat generated by the micro-cogeneration unit at times of low demand during the day goes to a thermal store, which is subsequently used up in the early evening. In the restricted running-time mode, presented in Figure 8.6 (b), the heat produced by the micro-cogeneration unit supplies a significant portion of the required heat during the high demand periods. The supplementary boiler fulfills the low heat requirement when the micro-cogeneration is not operating during most times in the day. In the continuous-output mode, given in Figure 8.6 (c), the micro-cogeneration system meets the low heat demand during the day whilst the supplementary boiler satisfies the high heat requirement in the morning and evening.



(a)



(b)



(c)

Figure 8.6: The heat profiles for the three operating modes defined in Figure 8.4 and Table 8.2: (a) constant-output mode, (b) restricted running-time mode and (c) continuous-output mode.

The characteristics of the considered micro-cogeneration operating modes with regards to heat utilisation and generation are given in Table 8.4. The performance of the three considered micro-cogeneration operating strategies are comparable with respect to the electrical and thermal efficiencies. The constant-output mode has the lowest heat-to-power ratio, followed by the restricted running-time mode and continuous-output mode. The thermal efficiency of all three considered strategies are high, having values between 72 and 75%. Correspondingly, the electrical efficiency drops from 21 to 18%, but overall, the total efficiency is very high at roughly 92.5% in all cases. The heat satisfied by the micro-cogeneration is between 30 and 38% so it is not probably not feasible to satisfy all of the demand. Furthermore, it is interesting that the restricted running-time mode operates for fewer hours but satisfies more of the demand. This may be because it operates when it is most needed. Amongst the three operating strategies, the continuous-output mode may require the largest thermal store, which is more than double the capacity of the constant-output mode. This can be attributed to the build-up of heat in the store overnight. Also, the spike in the blue curve in Figure 8.6 (b) is the cause of the need to have a large thermal store in the restricted running-time mode. Finally, the extra heat demand that is satisfied by the continuous-output mode is because it's allowed to run overnight. In the other two cases, the overnight heat demand is satisfied by the burner alone; in the continuous-output mode the burner is off most of the night.

8.5 Impact on operational economics

For the householder, it is the value of electricity generated that provides the potential economic benefits of micro-cogeneration. The electricity generated and used in the house reduces the electricity bought from the grid and hence can be valued at the normal retail price. For the results presented in Table 8.4, the retail price of gas is assumed to be 3p/kWh and the retail price of electricity is assumed to be 10p/kWh [102].

Table 8.3: The heat generation and utilisation characteristics of the considered micro-cogeneration operating modes shown in Figure 8.4.

	Constant-output	Restricted running-time	Continuous-output
Heat-to-power ratio of the micro-cogeneration system	3.46	3.74	4.28
Thermal efficiency, %	71.85	73.07	75.18
Electrical efficiency, %	20.79	19.52	17.57
Heat generated by the micro-cogeneration system, kWh (% of demand)	24.24(30.27)	26.83 (33.51)	30.81 (38.48)
Heat generated by the supplementary boiler, kWh (% of demand)	55.83(69.73)	53.24 (66.49)	49.26 (61.52)
Number of daily operating hours of the micro-cogeneration system	14.5	7	24
Number of daily operating hours of the supplementary boiler	16.5	22.33	10.42
Size of the thermal store	9.16	13.39	21.80

To date, export tariffs have not been widely available, although many energy suppliers are now offering these. Where available, such tariffs are currently thought to be worth up to a maximum equivalent to half of the retail price. Currently, some customers are rewarded for electricity which is exported to the grid whilst other householders receive nothing. The Carbon Trust, in their 2007 interim report [102], proposed three different export reward tariff options as follows:

- No export reward – the householder receives no payment for exported electricity,
- Half export reward – the householder receives half of the retail price (5p/kWh),
- Full export reward – the householder receives the full price (10p/kWh).

The operating costs and carbon savings potential at different export reward tariff options for various micro-cogeneration strategies considered in this chapter, applied to the electricity and heat demand profile shown in Figures 8.3 and 8.6, are summarised in Table 8.4. The daily energy savings is the difference between the daily cost of operating a condensing boiler and importing electricity from the grid to satisfy the electricity and heat demand, which is calculated to be £4.19 for the daily energy demand profile considered in this chapter, and the cost of running a micro-cogeneration unit using a specific strategy. Table 8.4 indicates that the constant-output mode is the most attractive strategy in terms of the daily savings. As expected, the daily savings increases as reward for export rises.

Finally, Table 8.5 presents a summary table for the comparison of the three considered operating strategies. It can be concluded that amongst the three considered strategies, the constant-output mode may be the most favourable strategy because it has the highest daily savings and requires the smallest thermal storage. The continuous-output mode may be the least attractive strategy for because it resulted in the highest operating cost and needs the largest thermal storage.

Table 8.4: Operating costs and carbon savings potential for different micro-cogeneration operating strategies.

	Daily operating cost (£)			Daily savings (£)		
	No export reward	Half export reward	Full export reward	No export reward	Half export reward	Full export reward
Constant-output	1.88	1.79	1.71	2.31	2.40	2.48
Restricted-running time	1.88	1.83	1.78	2.31	2.36	2.41
Continuous-output	2.09	2.00	1.90	2.10	2.19	2.29

Table 8.5: Summary table for the comparison of the three considered operating strategies.

	Highest	Lowest
Electricity generated	Continuous	Constant-output
Electricity imported	Constant-output	Restricted
Electricity exported	Continuous	Restricted
Heat-to-power ratio of the micro-cogeneration system	Constant-output	Continuous
Thermal efficiency	Continuous	Constant-output
Electrical efficiency	Constant-output	Continuous
Heat generated by the micro-cogeneration system	Continuous	Constant-output
Heat generated by the supplementary boiler	Constant-output	Continuous
Number of daily operating hours of the micro-cogeneration system	Continuous	Restricted
Number of daily operating hours of the supplementary boiler	Restricted	Continuous
Size of the thermal store	Continuous	Constant-output
Daily savings	Constant-output	Continuous

8.6 Implications of energy demand variation

The approach adopted here uses the model developed in the previous chapter to predict the performance of a specific operating strategy in satisfying the energy demands of one home on a representative day, and from this derive estimates of the cost savings. In reality, however, the exact pattern of energy use (*e.g.*, daily consumption, peak demand, heat-to-power ratio and duration of peaks/valleys) is very difficult to predict. Therefore, a micro-cogeneration system is subject to a considerable demand variation with time, variations in the concurrency of heat and power demands, and variations between households (which are due partly to user preferences with respect to type of cooker, washing machine, kettle, and water heater). For these reasons, the actual daily cost savings achieved by a micro-cogeneration system will be a strong function of the demand profiles that unfold in real time on a given day, and so savings will fluctuate

throughout the week/year.

On days when the thermal demand is particularly high (*e.g.*, during midwinter) the delivery of more heat per unit time will be necessary. This is not a substantial design problem as generating heat at high efficiency is relatively straightforward. The supplementary boiler integrated with the micro-cogeneration unit will serve the purpose in this situation. However, on days of moderate or low thermal demand (*e.g.*, during summer and mild spring/autumn days) the feasible operating period for a micro-cogeneration unit of a certain size will be restricted in relation to a household's emerging thermal demand. Once the thermal demand has been met, it may be disadvantageous to continue energy generation unless the electrical efficiency of the system is greater than that of grid electricity, (*e.g.*, $> 40\%$). Note that the electrical efficiency of the three operating strategies considered in this chapter have values between 18 and 21%, so on days of moderate or low thermal demand it may be beneficial to use network electricity in satisfying the electrical demand. In general, operating a micro-cogeneration system to meet the electrical demand on a summer day may not be economical because of this '*heat limit*' effect. A micro-cogeneration system will therefore save less money in summer than in winter. This also has implications on the control, reliability and maintenance of the system which is related to the run times and number of starts/stops .

8.7 Conclusions

The fuel cell micro-cogeneration model developed in Chapter 7 can be used to make informed predictions and obtain valuable information for the improvement of the design and operation of the system. This chapter presents an example of how the model can be applied to evaluate three of the various micro-cogeneration operating strategies, namely: constant-output mode, restricted-output mode and continuous-output mode. In principle, a successful design and operation of a micro-cogeneration system requires understanding of the energy consumption of a household, and so this chapter provides

a thorough discussion of the key characteristics of the electrical and thermal demands of UK dwellings. Using a representative daily energy demand profile, this chapter examines the interaction between the considered operating strategies and the electricity network.

In meeting about 50% of the daily electricity demands, the three strategies resulted in distinct import, export and heat characteristics. The results indicate that amongst the three considered operating strategies, the constant-output mode results in the highest daily savings and requires the smallest thermal storage. The continuous-output mode, on the other hand, gives the least daily savings and needs the largest thermal storage.

To reiterate, this chapter is an illustration of how the fuel cell micro-cogeneration model developed in Chapter 7 can be applied to investigate the effectiveness of the various operating modes. The results presented in this chapter may vary depending on the energy consumption profile of a household on a particular day.

Chapter 9

Conclusions and further work

This chapter summarises the work presented in this thesis and outlines some of the main conclusions that can be gained from the results. The final section discusses some area for improvement and some directions for future work.

9.1 Conclusions

This thesis illustrates the application of model-based design approaches in improving the design and operation of fuel cell systems by aiding the designer in making informed predictions and obtaining valuable information about the behaviour of the system. This thesis also highlights the use of modelling and optimisation in informing system design by generating different design alternatives, thus allowing design engineers to make decisions in a quantitative and rational way. Although the approach should be applicable to any type of fuel cell, polymer electrolyte fuel cells were particularly considered to demonstrate the procedure.

The design of a fuel cell system is a decision-making process, which involves identification of possible design alternatives and selection of the most suitable one. A good design is one that satisfies the design requirements and represents a trade-off amongst the different design objectives. In this thesis, the role of modelling and optimisation in

the design of fuel cell systems was examined. A typical fuel cell system design process was discussed and the use of modelling and optimisation in generating different design alternatives was demonstrated. Criteria for comparing these alternatives are necessary and identifying the important ones and those that can be disregarded is a critical step in the design. Therefore, some examples of application-specific criteria and design variations among applications were explored.

The existing models for portable, stationary and transportation applications were identified and characterised by approach, state, system boundary, spatial dimension, and complexity or detail. System-level models are necessary for the investigation of specific applications of fuel cells such as portable, stationary and transportation. A system-level model predicts the behaviour of a fuel cell system, which is composed of different subsystems such as fuel cell stack, fuel supply, oxidant supply, water management, heat management, power conditioning, instrumentation and controls, and in some cases, hybrid components. System-level models are also preferred for use in optimisation because individual components perform differently when operated as part of a system. To date, the majority of the available system-level fuel cell models are lumped, semi-empirical, steady-state and based on either PEFC or SOFC.

Three model-based design approaches commonly used in fuel cell systems design were discussed: parametric study, single-objective optimisation and multi-objective optimisation. In a parametric study, the design solutions are specific to the parameter combination used during the analysis, thus there is no guarantee that an optimal solution is obtained. Single-objective optimisation can identify an optimum value of a single objective but it cannot provide a set of alternative solutions that trade different objectives with each other. Multi-objective optimisation determines a set of trade-off optimal solutions that simultaneously considers conflicting design objectives, also known as a Pareto set.

A two-dimensional, non-isothermal mass and heat transfer model of a single-cell PEFC was first presented. The model describes the water transport across the membrane by

electro-osmosis and diffusion, heat transfer from the solid phase to the gas phase and latent heat associated with water evaporation and condensation in the flow channels. The model can be used to obtain essential information about appropriate water and heat management. An example that illustrates the use of the model to evaluate the effectiveness of a conventional humidification design was presented. This approach can be used to examine the effect of other humidification and heat removal designs on the performance of a PEFC.

The single-cell model was then extended to a fuel cell stack. This model was intended to use within a multi-objective optimisation framework, which requires evaluation of a large number of design alternatives with correspondingly high computational requirements. A reduced-order model was derived from the original two-dimensional problem. The reduced-order model has an acceptable accuracy and is complex enough to differentiate between design alternatives, whilst being simple enough to allow for repeated calculations during optimisation. The water balance was modified to correct the inconsistency of the model at saturation. A simulation of the model for a base case shows that for a given power output, a more efficient system is bigger and *vice versa*. The results of the multi-objective optimisation highlights the importance of formulating the problem as a multi-objective optimisation. Maximisation of the efficiency without taking the size into account will result to a possibly impractically large system. Conversely, a significantly small system but with very low efficiency will result if the only objective is size. This chapter presents a method of determining the PEFC stack optimal design such that for a particular application, a balance between efficiency and size is achieved.

A fuel cell micro-cogeneration model was developed by integrating the fuel cell stack model with the model for fuel processing subsystem, thermal management subsystem and power management subsystem. Similar to the problem encountered in the design of a fuel cell stack, the design of a micro-cogeneration system also involves conflicting objectives. The use of the model to investigate how fuel consumption trades with electrical power output was demonstrated. The results indicate that for power output

below 7 kW_e , the electrical power output trades almost linearly with the fuel consumption, specifically $\sim 0.85 \text{ W}_e$ additional power is produced for every Watt of extra fuel. For some values of the weighting factors, a surplus or a shortage in electrical power may result. Economic factors such as costs of natural gas and electricity and the buy-back rate of electricity exported to the grid determines whether this power is exported to or imported from the grid.

Additional examples of application of the fuel cell micro-cogeneration model in informing system design and operation were presented. Three operating strategies, namely constant-output mode, restricted-running time mode and continuous-output mode, were evaluated based on a representative energy consumption profile of a UK household. Overall, the three strategies resulted in distinct import, export and heat characteristics in meeting approximately 50% of the daily electricity demands,. Amongst the three operating strategies, the constant-output mode results in the highest daily savings and requires the smallest thermal storage. The continuous-output mode, on the other hand, gives the least daily savings and needs the largest thermal storage.

Finally, it is important to note that as with any models used in a decision-making process, it is important to ensure that the model correctly represents the behaviour of the actual fuel cell system. The design solutions are only useful within the limitations of the model assumptions, and their quality depends on how well the model has been formulated. When properly formulated and validated, modelling and optimisation are useful tools in fuel cell systems design as they provide means by which design engineers can obtain valuable information about the behaviour of the system, make informed decisions, generate different design alternatives and identify good designs.

9.2 Future directions

Despite the significant improvements in fuel cell systems modelling and optimisation, there are areas that need further study. For instance, most of the fuel cell system models

have not been fully validated against experimental data: only specific components of the system (e.g., a single fuel cell or a stack) were validated. More demonstration sites and experimental studies considering the entire fuel cell system are essential so that researchers can fully validate their model.

This thesis has also identified that the majority of the fuel cell system models are lumped, steady-state and semi-empirical. Further studies are required to assess the consequence of using lumped models, i.e. evaluate how realistic it is to treat a fuel cell system as a black box, especially when modelling phenomena such as mass and heat transport. More studies that compare lumped and distributed models for the same system are needed. Furthermore, there is a need for more dynamic models in order to explore the performance of the system under transient conditions (such as startup, shutdown and load changes) and evaluate control strategies. However, using distributed and dynamic models may prolong computational time. Hence, it is suggested that further trade-off studies be performed to find a model that exhibit a balance between accuracy and computational efficiency.

The models presented in this work provide the base on which to develop a full economic model which would allow one to estimate the payback period for the equipment and its installation in a typical domestic scenario. A full economic analysis, including both operating and capital costs, will be necessary for the selection of the best trade-off. Also, the models presented can be adapted for investigation of other conflicting design objectives such as cost savings versus environmental impact, cost savings versus safety cost, amongst others. Furthermore, the model for the PEFC stack can be extended to a vehicle fuel cell system, which can then be used for multi-objective optimisation (e.g., investigation of the trade-off between drivability and fuel economy).

Finally, by evaluating the uncertainty associated with a fuel cell system model, decision-makers are made aware of its limitations. The uncertainty in the model may be caused by imprecise knowledge of the parameter values (parameter uncertainty) or even of the phenomena governing the behaviour of the system (structural uncertainty). Therefore,

performing sensitivity and uncertainty analyses and developing models that can be used for design under uncertainty (or robust design) are amongst the future directions that can be taken in this area.

References

- [1] EG&G Technical Services, Inc. *Fuel Cell Handbook*. U.S. Department of Energy, Morgantown, West Virginia, 7th edition, 2004.
- [2] Frano Barbir. *PEM Fuel Cells: Theory and Practice*. Academic Press, 2005.
- [3] S. M. C. Ang, D. J. L. Brett, and E. S. Fraga. A multi-objective optimisation model for a general polymer electrolyte membrane fuel cell system. *Journal of Power Sources*, 195(9):2754–2763, 2010.
- [4] D.C. Dayton, M. Ratcliff, and R. Bain. Fuel cell integration - a study of the impacts of gas quality and impurities: Milestone completion report. Technical report, National Renewable Energy Laboratory, 2001.
- [5] T. R. Ralph and M. P. Hogarth. Catalysis for low temperature fuel cells. Part II. The anode challenges. *Platinum Metals Review*, 46(3):117–135, 2002.
- [6] W. Ruettinger, O. Ilinich, and R.J. Farrauto. A new generation of water gas shift catalysts for fuel cell applications. *Journal of Power Sources*, 118(1-2):61–65, 2003.
- [7] R. K. Ahluwalia, Q. Z. Zhang, D. J. Chmielewski, K. C. Lauzze, and M. A. Inbody. Performance of CO preferential oxidation reactor with noble-metal catalyst coated on ceramic monolith for on-board fuel processing applications. *Catalysis Today*, 99(3-4):271–283, 2005.

- [8] R. A. Dagle, Y. Wang, G. G. Xia, J. J. Strohm, J. Holladay, and D. R. Palo. Selective CO methanation catalysts for fuel processing applications. *Applied Catalysis A - General*, 326(2):213–218, 2007.
- [9] M. C. Duke, J. C. D. da Costa, G. Q. Lu, M. Petch, and P. Gray. Carbonised template molecular sieve silica membranes in fuel processing systems: permeation, hydrostability and regeneration. *Journal of Membrane Science*, 241(2):325–333, 2004.
- [10] Y. Wu and H. W. Gao. Optimization of fuel cell and supercapacitor for fuel-cell electric vehicles. *IEEE Transactions on Vehicular Technology*, 55(6):1748–1755, 2006.
- [11] K. Ahmed and K. Foger. Fuel processing for high-temperature high-efficiency fuel cells. *Industrial & Engineering Chemistry Research*, 49(16):7239–7256, 2010.
- [12] T. K. Yeh and C. H. Chen. Modeling and optimizing the performance of a passive direct methanol fuel cell. *Journal of Power Sources*, 175(1):353–362, 2008.
- [13] C. R. Liu and J. S. Lai. Low frequency current ripple reduction technique with active control in a fuel cell power system with inverter load. *2005 IEEE 36th Power Electronic Specialists Conference (PESC), Vols 1-3*, pages 2905–2911, 2005.
- [14] M. J. Vasallo, J. M. Andujar, C. Garcia, and J. J. Brey. A methodology for sizing backup fuel-cell/battery hybrid power systems. *IEEE Transactions on Industrial Electronics*, 57(6):1964–1975, 2010.
- [15] J. Lagorse, D. Paire, and A. Miraoui. Sizing optimization of a stand-alone street lighting system powered by a hybrid system using fuel cell, PV and battery. *Renewable Energy*, 34(3):683–691, 2009.
- [16] M. J. Kim and H. Peng. Power management and design optimization of fuel cell/battery hybrid vehicles. *Journal of Power Sources*, 165(2):819–832, 2007.

- [17] M. Kim, Y. J. Sohn, W. Y. Lee, and C. S. Kim. Fuzzy control based engine sizing optimization for a fuel cell/battery hybrid mini-bus. *Journal of Power Sources*, 178(2):706–710, 2008.
- [18] A. Schell, H. Peng, D. Tran, E. Stamos, C. C. Lin, and M. J. Kim. Modelling and control strategy development for fuel cell electric vehicles. *Annual Reviews in Control*, 29(1):159–168, 2005.
- [19] M. Burer, K. Tanaka, D. Favrat, and K. Yamada. Multi-criteria optimization of a district cogeneration plant integrating a solid oxide fuel cell-gas turbine combined cycle, heat pumps and chillers. *Energy*, 28(6):497–518, 2003.
- [20] F. Calise, M. D. d’Accadia, L. Vanoli, and M. R. von Spakovsky. Single-level optimization of a hybrid SOFC-GT power plant. *Journal of Power Sources*, 159(2):1169–1185, 2006.
- [21] F. Calise, M. D. d’Accadia, L. Vanoli, and M. R. von Spakovsky. Full load synthesis/design optimization of a hybrid SOFC-GT power plant. *Energy*, 32(4):446–458, 2007.
- [22] M. Koyama and S. Kraines. A flexible model integration approach for evaluating tradeoffs between CO₂ emissions and cost in solid oxide fuel cell-based building energy systems. *International Journal of Energy Research*, 29(14):1261–1278, 2005.
- [23] Y. F. Yi, A. D. Rao, J. Brouwer, and G. S. Samuelsen. Analysis and optimization of a solid oxide fuel cell and intercooled gas turbine (SOFC-ICGT) hybrid cycle. *Journal of Power Sources*, 132(1-2):77–85, 2004.
- [24] Y. Zhao, N. Shah, and N. Brandon. The development and application of a novel optimisation strategy for solid oxide fuel cell-gas turbine hybrid cycles. *Fuel Cells*, 10(1):181–193, 2010.

- [25] F. Marechal, F. Palazzi, J. Godat, and D. Favrat. Thermo-economic modelling and optimisation of fuel cell systems. *Fuel Cells*, 5(1):5–24, 2005.
- [26] K. Subramanyan, U. M. Diwekar, and A. Goyal. Multi-objective optimization for hybrid fuel cells power system under uncertainty. *Journal of Power Sources*, 132(1-2):99–112, 2004.
- [27] A. K. Kaviani, G. H. Riahy, and S. H. M. Kouhsari. Optimal design of a reliable hydrogen-based stand-alone wind/PV generating system, considering component outages. *Renewable Energy*, 34(11):2380–2390, 2009.
- [28] Colleen Spiegel. *PEM Fuel Cell Modeling and Simulation Using Matlab*. 2008.
- [29] S.M.C. Ang, D.J.L. Brett, and E.S. Fraga. *Fuel Cell Efficiency*, chapter Optimal design of fuel cell systems. Nova Science Publishers, Inc. New York, 2011.
- [30] S.M.C. Ang, D.J.L. Brett, I Staffell, A.D. Hawkes, E.S. Fraga, and N.P. Brandon. Design of fuel cell micro-cogeneration systems through modelling and optimisation. *Wiley Interdisciplinary Reviews*, 2011. Under Review.
- [31] S.M.C. Ang, E.S. Fraga, N.P. Brandon, N.J. Samsatli, and D.J.L. Brett. Fuel cell systems optimisation - methods and strategies. *International Journal of Hydrogen Energy*, 2011. In Press.
- [32] J. L. Zhuo, C. Chakrabarti, K. S. Lee, N. Chang, and S. Vrudhula. Maximizing the lifetime of embedded systems powered by fuel cell-battery hybrids. *IEEE Transactions On Very Large Scale Integration (VLSI) Systems*, 17(1):22–32, 2009.
- [33] D. Bhattacharyya and R. Rengaswamy. A review of solid oxide fuel cell (SOFC) dynamic models. *Industrial & Engineering Chemistry Research*, 48(13):6068–6086, 2009.
- [34] A. Biyikoglu. Review of proton exchange membrane fuel cell models. *International Journal of Hydrogen Energy*, 30(11):1181–1212, 2005.

- [35] D. Cheddie and N. Munroe. Review and comparison of approaches to proton exchange membrane fuel cell modeling. *Journal of Power Sources*, 147(1-2):72–84, 2005.
- [36] S. K. Das and A. S. Bansode. Heat and mass transport in proton exchange membrane fuel cells - a review. *Heat Transfer Engineering*, 30(9):691–719, 2009.
- [37] N. Djilali. Computational modelling of polymer electrolyte membrane (PEM) fuel cells: Challenges and opportunities. *Energy*, 32(4):269–280, 2007.
- [38] V. Gurau and J. A. Mann. A critical review of computational fluid dynamics multiphase models for proton exchange membrane fuel cells. *SIAM Journal on Applied Mathematics*, 70(2):410–454, 2009.
- [39] K. Haraldsson and K. Wipke. Evaluating PEM fuel cell system models. *Journal of Power Sources*, 126(1-2):88–97, 2004.
- [40] Q. A. Huang, R. Hui, B. W. Wang, and H. J. Zhang. A review of AC impedance modeling and validation in SOFC diagnosis. *Electrochimica Acta*, 52:8144–8164, 2007.
- [41] M. B. Ji and Z. D. Wei. A review of water management in polymer electrolyte membrane fuel cells. *Energies*, 2(4):1057–1106, 2009.
- [42] S. Kakac, A. Pramuanjaroenkij, and X. Y. Zhou. A review of numerical modeling of solid oxide fuel cells. *International Journal of Hydrogen Energy*, 32(7):761–786, 2007.
- [43] J. LaManna and S. G. Kandlikar. A critical review of water transport models in gas diffusion media of PEM fuel cell. *Proceedings of the 6th International Conference on Nanochannels, Microchannels, and Minichannels, Pts A and B*, pages 1305–1315, 2008.

- [44] C. Siegel. Review of computational heat and mass transfer modeling in polymer-electrolyte-membrane (PEM) fuel cells. *Energy*, 33(9):1331–1352, 2008.
- [45] H. Li, Y. H. Tang, Z. W. Wang, Z. Shi, S. H. Wu, D. T. Song, J. L. Zhang, K. Fatih, J. J. Zhang, H. J. Wang, Z. S. Liu, R. Abouatallah, and A. Mazza. A review of water flooding issues in the proton exchange membrane fuel cell. *Journal of Power Sources*, 178(1):103–117, 2008.
- [46] A. Faghri and Z. Guo. Challenges and opportunities of thermal management issues related to fuel cell technology and modeling. *International Journal of Heat and Mass Transfer*, 48(19-20):3891–3920, 2005.
- [47] V. Lawlor, S. Griesser, G. Buchinger, A. G. Olabi, S. Cordiner, and D. Meissner. Review of the micro-tubular solid oxide fuel cell. Part I. Stack design issues and research activities. *Journal of Power Sources*, 193(2):387–399, 2009.
- [48] C. A. Frangopoulos and L. G. Nakos. Development of a model for thermoeconomic design and operation optimization of a PEM fuel cell system. *Energy*, 31(10-11):1501–1519, 2006.
- [49] D. Xue and Z. Dong. Optimal fuel cell system design considering functional performance and production costs. *Journal of Power Sources*, 76(1):69–80, 1998.
- [50] C. N. Maxoulis, D. N. Tsinoglou, and G. C. Koltsakis. Modeling of automotive fuel cell operation in driving cycles. *Energy Conversion and Management*, 45(4):559–573, 2004.
- [51] J. Godat and F. Marechal. Optimization of a fuel cell system using process integration techniques. *Journal of Power Sources*, 118(1-2):411–423, 2003.
- [52] V. Tsourapas, A. Stefanopoulou, and J. Sun. Dynamics, optimization and control of a fuel cell based combined heat power (CHP) system for shipboard applications. *ACC: Proceedings of the 2005 American Control Conference, Vols 1-7*, pages 1993–1998, 2005.

- [53] C. Zamfirescu and I. Dincer. Thermodynamic performance analysis and optimization of a SOFC-H⁺ system. *Thermochimica Acta*, 486(1-2):32–40, 2009.
- [54] R. Chandrasekaran, W. Bi, and T. F. Fuller. Robust design of battery/fuel cell hybrid systems-methodology for surrogate models of Pt stability and mitigation through system controls. *Journal of Power Sources*, 182(2):546–557, 2008.
- [55] S. F. Au, S. J. McPhail, N. Woudstra, and K. Hemmes. The influence of operating temperature on the efficiency of a combined heat and power fuel cell plant. *Journal of Power Sources*, 122(1):37–46, 2003.
- [56] S. Gamou, R. Yokoyama, and K. Ito. Optimal unit sizing of cogeneration systems in consideration of uncertain energy demands as continuous random variables. *Energy Conversion and Management*, 43(9-12):1349–1361, 2002.
- [57] A. Hawkes and M. Leach. Impacts of temporal precision in optimisation modelling of micro-combined heat and power. *Energy*, 30(10):1759–1779, 2005.
- [58] A. D. Hawkes, P. Aguiar, C. A. Hernandez-Aramburo, M. A. Leach, N. P. Brandon, T. C. Green, and C. S. Adjiman. Techno-economic modelling of a solid oxide fuel cell stack for micro combined heat and power. *Journal of Power Sources*, 156(2):321–333, 2006.
- [59] F. Jurado and M. Valverde. Enhancing the electrical performance of a solid oxide fuel cell using multiobjective genetic algorithms. *Renewable Energy*, 30(6):881–902, 2005.
- [60] B. Oyarzabal, M. R. von Spakovsky, and M. W. Ellis. Optimal synthesis/design of a PEM fuel cell cogeneration system for multi-unit residential applications - application of a decomposition strategy. *Journal of Energy Resources Technology-Transactions of the ASME*, 126(1):30–39, 2004.
- [61] B. Oyarzabal, M. W. Ellis, and M. R. von Spakovsky. Development of thermodynamic, geometric, and economic models for use in the optimal synthesis/design

- of a PEM fuel, cell cogeneration system for multi-unit residential applications. *Journal of Energy Resources Technology-Transactions of the ASME*, 126(1):21–29, 2004.
- [62] F. Palazzi, N. Autissier, F. M. A. Marechal, and D. Favrat. A methodology for thermo-economic modeling and optimization of solid oxide fuel cell systems. *Applied Thermal Engineering*, 27(16):2703–2712, 2007.
- [63] N. Perdikaris, K. D. Panopoulos, L. Fryda, and E. Kakaras. Design and optimization of carbon-free power generation based on coal hydrogasification integrated with SOFC. *Fuel*, 88(8):1365–1375, 2009.
- [64] S. Petrescu, C. Petre, M. Costea, O. Malancioiu, N. Boriaru, A. Dobrovicescu, M. Feidt, and C. Harman. A methodology of computation, design and optimization of solar Stirling power plant using hydrogen/oxygen fuel cells. *Energy*, 35(2):729–739, 2010.
- [65] E. Riensche, E. Achenbach, D. Froning, M. R. Haines, W. K. Heidug, A. Lokurlu, and S. von Andrian. Clean combined-cycle SOFC power plant - cell modelling and process analysis. *Journal of Power Sources*, 86(1-2):404–410, 2000.
- [66] M. H. Saidi, M. A. Ehyaei, and A. Abbasi. Optimization of a combined heat and power PEFC by exergy analysis. *Journal of Power Sources*, 143(1-2):179–184, 2005.
- [67] V. Verda and F. Nicolin. Thermodynamic and economic optimization of a MCFC-based hybrid system for the combined production of electricity and hydrogen. *International Journal of Hydrogen Energy*, 35(2):794–806, 2010.
- [68] C. Wallmark and P. Alvfors. Design of stationary PEFC system configurations to meet heat and power demands. *Journal of Power Sources*, 106(1-2):83–92, 2002.
- [69] Adam Z. Weber and John Newman. Modeling transport in polymer-electrolyte fuel cells. *Chemical Reviews*, 104(10):4679–4726, 2004.

- [70] F. Baratto and U. M. Diwekar. Multi-objective trade-offs for fuel cell-based auxiliary power units: case study of South California Air Basin. *Journal of Power Sources*, 139(1-2):197–204, 2005.
- [71] B. Chachuat, A. Mitsos, and P. I. Barton. Optimal design and steady-state operation of micro power generation employing fuel cells. *Chemical Engineering Science*, 60(16):4535–4556, 2005.
- [72] A. Mitsos, B. Chachuat, and P. I. Barton. What is the design objective for portable power generation: efficiency or energy density? *Journal of Power Sources*, 164(2):678–687, 2007.
- [73] F. A. Mohamed and H. N. Koivo. System modelling and online optimal management of microgrid using mesh adaptive direct search. *International Journal of Electrical Power & Energy Systems*, 32(5):398–407, 2010.
- [74] P. Alotto, M. Guarnieri, and F. Moro. Optimal design of micro direct methanol fuel cells for low-power applications. *IEEE Transactions on Magnetics*, 45(3):1570–1573, 2009.
- [75] S. K. Mazumder, S. K. Pradhan, J. Hartvigsen, D. Rancruel, M. R. von Spakovsky, and M. Khaleel. A multidiscipline and multi-rate modeling framework for planar solid oxide fuel cell based power-conditioning system for vehicular APU. *Simulation-Transactions of the Society for Modeling and Simulation International*, 84(8-9):413–426, 2008.
- [76] S. Jemei, D. Hissel, M. C. Pera, and J. M. Kauffmann. A new modeling approach of embedded fuel-cell power generators based on artificial neural network. *IEEE Transactions on Industrial Electronics*, 55(1):437–447, 2008.
- [77] C. Weber, F. Marechal, D. Favrat, and S. Kraines. Optimization of an SOFC-based decentralized polygeneration system for providing energy services in an office-building in Tokyo. *Applied Thermal Engineering*, 26(13):1409–1419, 2006.

- [78] *COMSOL Multiphysics User's Guide*. [Online]. Available: <http://math.nju.edu.cn/help/mathhpc/doc/comsol/guide.pdf>.
- [79] *FemLab Version 2.0 Reference Manual*, September 2000.
- [80] *FLUENT 6.3 User's Guide*. [Online]. Available: <http://my.fit.edu/itresources/manuals/fluent6.3/>.
- [81] X. Cheng, Z. Shi, N. Glass, L. Zhang, J. J. Zhang, D. T. Song, Z. S. Liu, H. J. Wang, and J. Shen. A review of PEM hydrogen fuel cell contamination: Impacts, mechanisms, and mitigation. *Journal of Power Sources*, 165(2):739–756, 2007.
- [82] G. Hoogers. *Fuel cell technology handbook*, chapter Stationary power applications. CRC Press, Boca Raton, Florida, 2003.
- [83] Federal Energy Management Program. Fuel cells in backup power applications: clean power generators - an alternative to conventional backup power sources. Technical report, U.S. Department of Energy.
- [84] U.S. Department of Energy Hydrogen Program. Early markets: Fuel cells for backup power. Technical report, 2008.
- [85] J. Tolsma and P. I. Barton. DAEPACK: An open modeling environment for legacy models. *Industrial & Engineering Chemistry Research*, 39(6):1826–1839, 2000.
- [86] *Golden, CO: HOMER NREL*. [Online]. Available: <http://www.nrel.gov/homer>.
- [87] *Simulation System Simplorer 6.0 User Manual*.
- [88] T. Markel, M. Zolot, and K.B. Wipke. Energy storage system requirements for hybrid fuel cell vehicles. In *Proceedings of Advanced Automotive Battery Conference, Nice, France*, 2005.

- [89] S. G. Chalk and J. E. Miller. Key challenges and recent progress in batteries, fuel cells, and hydrogen storage for clean energy systems. *Journal of Power Sources*, 159(1):73–80, 2006.
- [90] K.B. Wipke, M.R. Cuddy, and S.D. Burch. ADVISOR 2.1: a user-friendly advanced powertrain simulation using a combined backward/forward approach. *Vehicle Technology, IEEE Transactions*, 48(6):1751–1761, 1999.
- [91] The MathWorks, Inc. *Simulink 7: User's Guide*. [Online]. Available: <http://www.mathworks.com/help/toolbox/simulink/>.
- [92] The MathWorks, Inc. *SimPowerSystems: For Use with Simulink. User's Guide*. [Online]. Available: www.math.carleton.ca/old/help/matlab/.../pdf.../powersys.pdf.
- [93] Process System Enterprise Ltd. *gPROMS ModelBuilder*. [Online]. Available: <http://www.psenterprise.com/gproms/modelbuilder.html>.
- [94] Process System Enterprise Ltd. *gO:Simulink. The gPROMS Object for Simulink*. [Online]. Available: www.psenterprise.com/gproms/objects/gosimulink.html.
- [95] M.G. Giesselmann. Averaged and cycle by cycle switching models for buck, boost, buck-boost and cuk converters with common average switch model. In *Energy Conversion Engineering Conference, 1997. IECEC-97., Proceedings of the 32nd Intersociety*, volume 1, pages 337–341 vol.1, 1997.
- [96] Aspen Technology, Inc. *Aspen Plus User Guide*. [Online]. <http://web.ist.utl.pt/ist11038/acad/Aspen/AspUserGuide10.pdf>.
- [97] K. Baba, R. Shibata, and M. Sibuya. Partial correlation and conditional correlation as measures of conditional independence. *Australian & New Zealand Journal of Statistics*, 46(4):657–664, 2004.

- [98] The Institution of Engineering and Technology. Combined heat and power (CHP). Technical report, July 2008.
- [99] A. Hawkes, D.J.L. Brett, and N.P. Brandon. The role of fuel cell based micro-cogeneration in low carbon heating. *Journal of Power and Energy, in press*, 2010.
- [100] A. Hawkes, D.J.L. Brett, and N.P. Brandon. Fuel cell micro-CHP technoeconomics. Part 1 - Model concept and formulation. *International Journal of Hydrogen Energy*, 34(23):9545–9557, 2009.
- [101] A. Hawkes, D.J.L. Brett, and N.P. Brandon. Fuel cell micro-CHP technoeconomics. Part 2 - Model application to consider the economic and environmental impact of stack degradation. *International Journal of Hydrogen Energy*, 34(23):9558–9569, 2009.
- [102] Carbon Trust. Micro-CHP Accelerator. Technical report, Carbon Trust, London, November 2007.
- [103] A. Hawkes, I. Staffell, D. J. L. Brett, and N. Brandon. Fuel cells for micro-combined heat and power generation. *Energy and Environmental Science*, 2:729 – 744, 2009.
- [104] K. Adamson. *Stationary Fuel Cells: An Overview*. Elsevier Ltd., 2007.
- [105] A.D. Rao, G.S. Samuelsen, F.L. Robson, B. Washom, and S.G. Berenyi. Advanced power plant development and analyses methodologies. Technical report, Advanced Power and Energy Program, University of California, 2006.
- [106] G.P. Rangaiah, editor. *Multi-objective Optimization: Techniques and Applications in Chemical Engineering*, volume Advances in Process Systems Engineering - Vol. 1. World Scientific Publishing Co. Pte. Ltd., 2009.
- [107] Panos Papalambros and Douglas Wilde. *Principles of Optimal Design*. Cambridge University Press, 2000.

- [108] L. T. Biegler and I. E. Grossmann. Retrospective on optimization. *Computers & Chemical Engineering*, 28(8):1169–1192, 2004.
- [109] I.E. Grossmann and L.T. Biegler. Part II. future perspective on optimization. *Computers & Chemical Engineering*, 28(8):1193–1218, 2004.
- [110] S. Rao. *Engineering Optimization*. John Wiley and Sons, Inc., fourth edition, 2009.
- [111] T. Lambert, P. Gilman, and P. Lilienthal. *Integration of Alternative Sources of Energy*, chapter Micropower system modeling with HOMER, pages 379–418. John Wiley and Sons, Inc., 2006.
- [112] Urmila Diwekar. *Introduction to Applied Optimization*. New York : Springer, 2008.
- [113] K. Miettinen. *Nonlinear Multiobjective Optimization*. Kluwer Academic Publishers, 1999.
- [114] K. A. Proos, G. P. Steven, O. M. Querin, and Y. M. Xie. Multicriterion evolutionary structural optimization using the weighting and the global criterion methods. *AIAA Journal*, 39(10):2006–2012, 2001.
- [115] A. Setamaa-Karkkainen, K. Miettinen, and J. Vuori. Best compromise solution for a new multiobjective scheduling problem. *Computers and Operations Research*, 33(8):2353–2368, 2006.
- [116] K. Miettinen. *Lecture Notes in Computer Science*, chapter Some Methods for Nonlinear Multi-objective Optimization, pages 1–20. Springer, 2001.
- [117] N. Srinivas and K. Deb. Multiobjective optimization using nondominated sorting in genetic algorithms. *Evolutionary Computation*, 2(3):221–248, 1994.

- [118] S. Bandyopadhyay, S. Saha, U Maulik, and K. Deb. A simulated annealing-based multiobjective optimization algorithm: Amosa. *IEEE Transactions on Evolutionary Computation*, 12(3):269 – 283, June 2008.
- [119] K. Deb. Non-linear goal programming using multi-objective genetic algorithms. *Journal of the Operational Research Society*, 1998.
- [120] M. Sakawa. Multiobjective optimization by the surrogate worth trade-off method. *Microelectronics Reliability*, 19(5-6):414 – 414, 1979.
- [121] K. Miettinen and M. M. Makela. Synchronous approach in interactive multiobjective optimization. *European Journal of Operational Research*, 170(3):909–922, 2006.
- [122] A. Abraham. *Evolutionary Multi-objective Optimization: Theoretical Advances and Applications*. Springer-Verlag London Ltd., 2005.
- [123] G. Leyland. *Multi-objective Optimization Applied to Industrial Energy Problems*. PhD thesis, EPFL, Lausanne, 2002.
- [124] Y. Cooren, A. Nakib, and P. Siarry. Image thresholding using TRIBES, a parameter-free particle swarm optimization algorithm. *Learning and Intelligent Optimization*, 5313:81–94, 2008.
- [125] T. V. Nguyen and R. E. White. A water and heat management model for proton-exchange-membrane fuel-cells. *Journal of the Electrochemical Society*, 140(8):2178–2186, August 1993.
- [126] T.E. Springer, T.A. Zawodzinski, and S. Gottesfeld. Polymer electrolyte fuel-cell model. *Journal of the Electrochemical Society*, 138(8):2334–2342, 1991.
- [127] J. T. Hinatsu, M. Mizuhata, and H. Takenaka. Water-uptake of perfluorosulfonic acid membranes from liquid water and water-vapor. *Journal of the Electrochemical Society*, 141:1493–1498, 1994.

- [128] U. Ascher and L. Petzold. *Computer Methods for Ordinary Differential Equations and Differential-Algebraic Equations*. SIAM, 1999.
- [129] K.E. Brenan, S.L. Campbell, and L.R. Petzold. *Numerical Solution of Initial Value Problems in Differential Algebraic Equations*. North Holland, 1989, republished by SIAM.
- [130] A. J. Hung, Y. H. Chen, L. Y. Sung, and C. C. Yu. Cost analysis of proton exchange membrane fuel cell systems. *AIChE Journal*, 54(7):1798–1810, 2008.
- [131] M.A.R.S. Al-Baghdadi and H.A.K.S. Al-Janabi. Parametric and optimization study of a PEM fuel cell performance using three-dimensional computational fluid dynamics model. *Renewable Energy*, 32(7):1077–1101, 2007.
- [132] A. M. Azmy and I. Erlich. Online optimal management of PEM fuel cells using neural networks. *IEEE Transactions on Power Delivery*, 20(2):1051–1058, 2005.
- [133] S. Chen, J. C. Ordonez, J. V. C. Vargas, J. E. F. Gardolinski, and M. A. B. Gomes. Transient operation and shape optimization of a single PEM fuel cell. *Journal of Power Sources*, 162(1):356–368, 2006.
- [134] P. K. Das, X. G. Li, and Z. S. Liu. Analytical approach to polymer electrolyte membrane fuel cell performance and optimization. *Journal of Electroanalytical Chemistry*, 604(2):72–90, 2007.
- [135] W. R. W. Daud, A. B. Mohamad, A. A. H. Kadhum, R. Chebbi, and S. E. Iyuke. Performance optimisation of PEM fuel cell during MEA fabrication. *Energy Conversion and Management*, 45(20):3239–3249, 2004.
- [136] A. J. J. Kadjo, P. Brault, A. Caillard, C. Coutanceau, J. P. Gamier, and S. Martemianov. Improvement of proton exchange membrane fuel cell electrical performance by optimization of operating parameters and electrodes preparation. *Journal of Power Sources*, 172:613–622, 2007.

- [137] G. Karimi, J. J. Baschuk, and X. Li. Performance analysis and optimization of PEM fuel cell stacks using flow network approach. *Journal of Power Sources*, 147(1-2):162–177, 2005.
- [138] J. Wishart, Z. Dong, and A. Secanell. Optimization of a PEM fuel cell system based on empirical data and a generalized electrochemical semi-empirical model. *Journal of Power Sources*, 161(2):1041–1055, 2006.
- [139] K. I. Chen, J. Winnick, and V. I. Manousiouthakis. Global optimization of a simple mathematical model for a proton exchange membrane fuel cell. *Computers & Chemical Engineering*, 30(8):1226–1234, 2006.
- [140] S. K. Kamarudin, W. R. W. Daud, A. M. Som, M. S. Takriff, and A. W. Mohammad. Synthesis and optimization of a PEM fuel cell system via reactor-separation network (RSN). *Journal of Power Sources*, 159(2):1194–1204, 2006.
- [141] S. E. Iyuke, A. B. Mohamad, A. A. H. Kadhum, W. R. W. Daud, and C. Rachid. Improved membrane and electrode assemblies for proton exchange membrane fuel cells. *Journal of Power Sources*, 114(2):195–202, 2003.
- [142] C. C. Boyer, R. G. Anthony, and A. J. Appleby. Design equations for optimized PEM fuel cell electrodes. *Journal of Applied Electrochemistry*, 30(7):777–786, 2000.
- [143] S. A. Grigoriev, A. A. Kalinnikov, V. N. Fateev, and A. A. Wragg. Numerical optimization of bipolar plates and gas diffusion layers for PEM fuel cells. *Journal of Applied Electrochemistry*, 36(9):991–996, 2006.
- [144] M. Grujicic, C. L. Zhao, K. M. Chittajallu, and J. M. Ochterbeck. Cathode and interdigitated air distributor geometry optimization in polymer electrolyte membrane (PEM) fuel cells. *Materials Science and Engineering B-Solid State Materials for Advanced Technology*, 108(3):241–252, 2004.

- [145] S. D. Yim, W. Y. Lee, Y. G. Yoon, Y. J. Sohn, G. G. Park, T. H. Yang, and C. S. Kim. Optimization of bifunctional electrocatalyst for PEM unitized regenerative fuel cell. *Electrochimica Acta*, 50(2-3):713–718, 2004.
- [146] W. Na and B. Gou. The efficient and economic design of PEM fuel cell systems by multi-objective optimization. *Journal of Power Sources*, 166(2):411–418, 2007.
- [147] F. Barbir and T. Gomez. Efficiency and economics of proton exchange membrane (PEM) fuel cells. *International Journal of Hydrogen Energy*, 22(10-11):1027–1037, 1997.
- [148] J. Golbert and D. R. Lewin. Model-based control of fuel cells: (1) regulatory control. *Journal of Power Sources*, 135(1-2):135–151, September 2004.
- [149] J. S. Yi and T. V. Nguyen. An along-the-channel model for proton exchange membrane fuel cells. *Journal of the Electrochemical Society*, 145(4):1149–1159, April 1998.
- [150] S. H. Ge and B. L. Yi. A mathematical model for PEMFC in different flow modes. *Journal of Power Sources*, 124(1):1–11, October 2003.
- [151] G. Squadrito, G. Maggio, E. Passalacqua, F. Lufrano, and A. Patti. An empirical equation for polymer electrolyte fuel cell (PEFC) behaviour. *Journal of Applied Electrochemistry*, 29(12):1449–1455, 1999.
- [152] P. C. Pei, W. Yang, and P. Li. Numerical prediction on an automotive fuel cell driving system. *International Journal of Hydrogen Energy*, 31(3):361–369, 2006.
- [153] Junbom Kim, Seong-Min Lee, Supramaniam Srinivasan, and Charles E. Chamberlin. Modeling of proton exchange membrane fuel cell performance with an empirical equation. *Journal of the Electrochemical Society*, 142:2670–2674, 1995.

- [154] L. Wang, A. Husar, T. H. Zhou, and H. T. Liu. A parametric study of PEM fuel cell performances. *International Journal of Hydrogen Energy*, 28(11):1263–1272, November 2003.
- [155] A. Kazim and P. Lund. Basic parametric study of a proton exchange membrane fuel cell. *Proceedings of the Institution of Mechanical Engineers Part A - Journal of Power and Energy*, 220(A8):847–853, December 2006.
- [156] A. Mughal and X. Li. Experimental diagnostics of PEM fuel cells. *International Journal of Environmental Studies*, 63(4):377–389, August 2006.
- [157] Q. G. Yan, H. Toghiani, and H. Causey. Steady state and dynamic performance of proton exchange membrane fuel cells (PEMFCs) under various operating conditions and load changes. *Journal of Power Sources*, 161(1):492–502, October 2006.
- [158] Y. Zhang and R. Pitchumani. Numerical studies on an air-breathing proton exchange membrane (PEM) fuel cell. *International Journal of Heat and Mass Transfer*, 50(23-24):4698–4712, November 2007.
- [159] P. Ngatchou, Anahita Z., and M.A. El-Sharkawi. Pareto multi objective optimization. pages 84–91, Nov. 2005.
- [160] Richard E. Rosenthal. *GAMS - A User's Guide*. [Online]. Available: <http://www.gams.com/dd/docs/bigdocs/GAMSUsersGuide.pdf>.
- [161] Lindo Systems, Inc. *LINDOGlobal*.
- [162] A. Lucena and J.E. Beasley. Branch and cut algorithms. pages 187–221, 1996.
- [163] S. Obara. *Distributed Energy Systems*. Nova Science Publishers, Inc. New York, 2009.
- [164] D. Parker. *Microgeneration: Low Energy Strategies for Larger Buildings*. Elsevier Ltd., 2009.

- [165] Directive 2004/8/EC of the European Parliament and of the Council of 11 February 2004 on the promotion of cogeneration based on useful heat demand in the internal energy market and amending Directive 92/42/EE. Technical report, European Union, Bruxelles, 2004.
- [166] J. Harrison. *Micro Energy Systems: Review of Technology, Issues of Scale and Integration*, chapter Micro Combined Heat & Power, pages 77–98. Wiley-Blackwell, 2004.
- [167] Department of Energy and Climate Change. Digest of UK Energy Statistics Annex, available from <http://www.decc.gov.uk>.
- [168] Office of Deputy Prime Minister. English house condition survey 1991. Technical report, HMSO, London, UK, 1996.
- [169] M. Newborough. Assessing the benefits of implementing micro-CHP systems in the uk. *Proceedings of the Institution of Mechanical Engineers Part A - Journal of Power And Energy*, 218(A4):203–218, 2004.
- [170] I. Staffell, J. Barton, R. Blanchard, F. Hill, C. Jardine, and D. Brett. UK micro-generation. Part II: Technology overviews. *Proceedings of the Institute of Civil Engineers : Energy*, 2009.
- [171] J. Larminie. *Fuel Cell Systems Explained*. 2nd edition, 2003.
- [172] N. Bergman, A. Hawkes, D. J. L. Brett, P. Baker, and J. Barton. UK microgeneration. part I: policy and behavioural aspects. In *Proceedings of the ICE - Energy*, volume 162, pages 23–36, 2009.
- [173] P. J. Mago, L. M. Chamra, and A. Hueffed. A review on energy, economical, and environmental benefits of the use of CHP systems for small commercial buildings for the North American climate. *International Journal of Energy Research*, 33(14):1252–1265, 2009.

- [174] C. E. Gibbs and M. C. F. Steel. European opportunities for fuel cell commercialization. *Journal of Power Sources*, 37(1-2):35–43, 1992.
- [175] M. V. Biezma and J. R. San Cristobal. Investment criteria for the selection of cogeneration plants - a state of the art review. *Applied Thermal Engineering*, 26(5-6):583–588, 2006.
- [176] V. Dorer, R. Weber, and A. Weber. Performance assessment of fuel cell micro-cogeneration systems for residential buildings. *Energy And Buildings*, 37(11):1132–1146, 2005.
- [177] N. Strachan and A. Farrell. Emissions from distributed vs. centralized generation: The importance of system performance. *Energy Policy*, 34(17):2677–2689, 2006.
- [178] M. De Paepe, P. D’Herdt, and D. Mertens. Micro-CHP systems for residential applications. *Energy Conversion and Management*, 47(18-19):3435–3446, 2006.
- [179] A. D. Hawkes and M. A. Leach. Cost-effective operating strategy for residential micro-combined heat and power. *Energy*, 32(5):711–723, 2007.
- [180] V. Dorer and A. Weber. Energy and CO₂ emissions performance assessment of residential micro-cogeneration systems with dynamic whole-building simulation programs. *Energy Conversion and Management*, 50(3):648–657, 2009.
- [181] A. D. Hawkes and M. A. Leach. The capacity credit of micro-combined heat and power. *Energy Policy*, 36(4):1457–1469, 2008.
- [182] W. Colella. Design options for achieving a rapidly variable heat-to-power ratio in a combined heat and power (CHP) fuel cell system (FCS). *Journal of Power Sources*, 106(1-2):388–396, 2002.
- [183] S. Giddey, F. T. Ciacchi, and S. P. S. Badwal. Fuel quality and operational issues for polymer electrolyte membrane (PEM) fuel cells. *Ionics*, 11(1-2):1–10, 2005.

- [184] G. Gigliucci, L. Petruzzi, E. Cerelli, A. Garzisi, and A. La Mendola. Demonstration of a residential CHP system based on PEM fuel cells. *Journal of Power Sources*, 131(1-2):62–68, 2004.
- [185] A. Abusoglu and M. Kanoglu. Exergoeconomic analysis and optimization of combined heat and power production: A review. *Renewable and Sustainable Energy Reviews*, 13(9):2295–2308, 2009.
- [186] S. Campanari, E. Macchi, and G. Manzolini. Innovative membrane reformer for hydrogen production applied to pem micro-cogeneration: Simulation model and thermodynamic analysis. *International Journal of Hydrogen Energy*, 33(4):1361–1373, 2008.
- [187] H. Jahn and W. Schroer. Dynamic simulation model of a steam reformer for a residential fuel cell power plant. *Journal of Power Sources*, 150:101–109, 2005.
- [188] J. Pukrushpan, A. Stefanopoulou, S. Varigonda, J. Eborn, and C. Haugstetter. Control-oriented model of fuel processor for hydrogen generation in fuel cell applications. *Control Engineering Practice*, 14(3):277–293, March 2006.
- [189] A. Ersoz. Investigation of hydrocarbon reforming processes for micro-cogeneration systems. *International Journal of Hydrogen Energy*, 33(23):7084–7094, 2008.
- [190] W. G. Colella. Design considerations for effective control of an afterburner subsystem in a combined heat and power (CHP) fuel cell system (FCS). *Journal of Power Sources*, 118(1-2):118–128, 2003.
- [191] N. Al-Azri, M. Al-Thubaiti, and M. El-Halwagi. An algorithmic approach to the optimization of process cogeneration. *Clean Technologies And Environmental Policy*, 11(3):329–338, 2009.
- [192] M. Y. El-Sharkh, M. Tanrioven, A. Rahman, and M. S. Alam. Cost related sensitivity analysis for optimal operation of a grid-parallel PEM fuel cell power plant. *Journal of Power Sources*, 161(2):1198–1207, 2006.

- [193] A. D. Hawkes and M. A. Leach. Modelling high level system design and unit commitment for a microgrid. *Applied Energy*, 86(7-8):1253–1265, 2009.
- [194] R. Inada, H. Sugihara, O. Saeki, and K. Tsuji. Evaluation of the introduction of a micro-cogeneration system into residential houses based on monitored daily-basis energy demand data. *Electrical Engineering In Japan*, 166(4):20–30, 2009.
- [195] M. A. Lozano, J. C. Ramos, M. Carvalho, and L. M. Serra. Structure optimization of energy supply systems in tertiary sector buildings. *Energy and Buildings*, 41(10):1063–1075, 2009.
- [196] I. Staffell. *Fuel cells for domestic heat and power: Are they worth it?* PhD thesis, Chemical Engineering, University of Birmingham, 2010.
- [197] The Energy Institute. Combined heat and power: selecting, installing and operating CHP, December 2003. URL: <http://www.energymanager.eu/getResource/10019/CHP.pdf>.
- [198] International Energy Agency (IEA). Energy conservation in buildings and community systems. annex 42. the simulation of buildings-integrated fuel cell and other cogeneration systems (COGEN-SIM), 2007. URL:<http://www.ecbcs.org/annexes/annex42.htm>.
- [199] N. Osaka, K. Nishizaki, M. Kawamura, K. Ito, N. Fujiwara, and Y. Nishizaka. Development of residential PEFC co-generation systems. Presented at Fuel Cell Seminar and Exposition, Palm Springs, California. 2005.
- [200] Y. Hamada, R. Goto, M. Nakamura, H. Kubota, and K. Ochifuji. Operating results and simulations on a fuel cell for residential energy systems. *Energy Conversion and Management*, 47(20):3562–3571, 2006.
- [201] Panasonic Corporation. Tokyo Gas and Panasonic to launch new improved "Ene-Farm" home fuel cell with world-highest power generation efficiency at more affordable price. Accessed July 2011 from:

<http://www.panasonic.co.jp/corp/news/official.data/data.dir/en110209-2/en110209-2.html>.

- [202] S.M.C. Ang, D.J.L. Brett, and E.S. Fraga. A model for the multi-objective optimisation of a polymer electrolyte fuel cell micro-combined heat and power system. In S. Pierucci and G. Buzzi Ferraris, editors, *20th European Symposium on Computer Aided Process Engineering*, volume Volume 28, pages 949–954. Elsevier, 2010.
- [203] Y. Choi and H. Stenger. Water gas shift reaction kinetics and reactor modeling for fuel cell grade hydrogen. *Journal of Power Sources*, 124(2):432 – 439, 2003.
- [204] J.T. Pukrushpan, Stefanopoulou A.G., and Peng H. *Control of fuel cell power systems: principles, modeling, analysis and feedback design*. Springer-Verlag London Ltd, 2004.
- [205] J. Smith, H. Van Ness, and M. Abbott. *Introduction to Chemical Engineering Thermodynamics*. McGraw-Hill, 6th edition edition, 2001.
- [206] A. Hawkes and M. Leach. Solid oxide fuel cell systems for residential micro-combined heat and power in the uk: Key economic drivers. *Journal of Power Sources*, 149:72–83, September 2005.
- [207] A.D. Hawkes and M.A. Leach. SOFC systems for the micro-CHP market - modelling key characteristics and sensitivities. In *In: Fuel cell seminar, San Antonio, TX, USA*, 2004.
- [208] A.D. Hawkes, G. Tiravanti, and M.A. Leach. Routes to energy efficiency: complementary energy service products in the UK residential sector. In *In: 2005 ECEEE Summer Study, , France*, 2005.
- [209] M. Newborough and P. Augood. Demand-side management opportunities for the uk domestic sector. *Proceedings IEEE Generation, Transmission and Distribution*, 146(3):283–293, 1999.

- [210] Kasanen, P. (Ed.). Efficient domestic ovens, final report SAVE II 4.1031//97-047. Technical report, 2000 (TTS-Institute, Helsinki).
- [211] W.R. Agar and M. Newborough. Implementing micro-CHP systems in the UK residential sector. *Journal of the Institute of Energy*, 71:178–189, 1998.
- [212] J. Tennet. Micro CHP: demand-side analysis. Master’s thesis, Cranfield University, Bedford, 2001.
- [213] Combined Heat & Power Association. Good practice guide 1: Guidance notes for the implementation of small scale packaged combined heat and power. Technical report, 1989 (CHPA, London).